Fall 2011

Geochemistry, Geothermobarometry and Geochronology of High-Pressure Granulites and Implications for the Exhumation History of Ultrahigh-Pressure Terranes: Dulan, Western China

Benjamin David Joseph Christensen
Central Washington University

GEOCHEMISTRY, GEOTHERMOBAROMETRY AND GEOCHRONOLOGY OF HIGH-PRESSURE GRANULITES AND IMPLICATIONS FOR THE EXHUMATION HISTORY OF ULTRAHIGH-PRESSURE TERRANES: DULAN, WESTERN CHINA

A Thesis

Presented to

The Graduate Faculty

Central Washington University

In Partial Fulfillment

of the Requirements for the Degree

Master of Science

Geological Sciences

---

by

Benjamin David Joseph Christensen

September 2011

CENTRAL WASHINGTON UNIVERSITY

Graduate Studies

We hereby approve the thesis of

Benjamin David Joseph Christensen

Candidate for the degree of Master of Science

APPROVED FOR THE GRADUATE FACULTY

_____ _____
Dr. Chris Mattinson, Committee Chair

_____ _____
Dr. Audrey Huerta

_____ _____
Dr. Jeff Lee

_____ _____
Dean of Graduate Studies

ABSTRACT

GEOCHEMISTRY, GEOTHERMOBAROMETRY AND GEOCHRONOLOGY OF HIGH-PRESSURE GRANULITES AND IMPLICATIONS FOR THE EXHUMATION HISTORY OF ULTRAHIGH-PRESSURE TERRANES: DULAN, WESTERN CHINA

by

Benjamin David Joseph Christensen

The Dulan ultrahigh-pressure (UHP) rocks of the North Qaidam terrane, Western China, represent continental crust that has been subducted ~100 km during continental collision. Adjacent granulites representing burial to ~50 km could either be overprinted eclogites or a separate high-pressure-high-temperature (HP-HT) granulite unit. Overprinted eclogites and HP-HT granulites imply different P-T-t paths for UHP rocks. Metamorphic conditions for the granulites are 750–880 ˚C and 14–17 kbar. Zircon U-Pb geochronology, REE patterns and Ti-in-zircon thermometry indicate an increase in temperature from ~800 ˚C (449 Ma) to ~900 ˚C (418 Ma). This temperature increase could explain the presence of granulite leucosomes and tonalites (419 Ma) interpreted to represent partial melts. The temperature increase coincides with the end of UHP metamorphism and may be related to exhumation of UHP rocks. These granulites represent a separate HP-HT unit from the thickened overriding crust in a continental collision zone, above subducting UHP rocks.

ACKNOWLEDGMENTS

There are many people deserving of thanks for their help in this research. To begin with there is my advisor Dr. Chris Mattinson. Towards the end of my senior year at Gustavus I received an email from Chris asking if I wanted to work as his graduate student, a position that included traveling to China for field work that very summer. The trip was an amazing experience for me not just professionally but also personally. Since then Chris has been indescribably helpful during my stay at CWU and I have learned more from him than I probably realize. I must also thank all the people I met on that trip: Dr. Jianxing Zhang, Dr. Carrie Menold, Dr. Emily Walsh, and Shengyao Yu. All of them helped a very young, inexperienced student with his first field research experience.

I also need to thank my two other committee members: Dr. Jeff Lee and Dr. Audrey Huerta. In their classes I have learned a lot of material that has offered me a broader understanding of my research topic. They have also been very helpful with the more bureaucratic aspects of my thesis, such as not complaining when I suddenly appear in their door for a last minute signature or questions on their quarter schedules.

This research was funded by a National Science Foundation grant (NSF-EAR0710927) and a CWU Masters Research Grant. I also received support from both the CWU graduate office and the Geological Society of America several times in order to travel and present my research at GSA conferences. The funding paid for the travel and the use of the instruments for this study, but I must also thank those who run the various instruments labs: Joe Wooden and Brad Ito at the Stanford/USGS SHRIMP-RG lab,

Michael Rowe at the Washington State University electron microprobe lab, and all from the Washington State University X-ray Fluorescence Lab.

All the CWU geology graduate students deserve some degree of thanks for their help through the last few years. But I wish to extend extra thanks to Aaron Mayfield and Rachel Hunt for their help critiquing my presentations and sharing research woes. I also wish to thank Zoe Weis, Zoe Futornick and Holly Rotman for keeping me sane with Sci-Fi shows when I was not working. I would also like to extend a great many thanks to Kurtis Oduber, a recent undergraduate at CWU who helped with the electron microprobe data.

Finally I'd like to extend thanks to my family and friends (especially my girlfriend Maria) for their support during my stay at Central. They did not always understand my rants and explanations about my research, but they listened anyway.

TABLE OF CONTENTS

TABLE OF CONTENTS (continued)

Chapter Page

LIST OF TABLES

LIST OF TABLES (continued)

LIST OF FIGURES

LIST OF FIGURES (continued)

LIST OF FIGURES (continued)

CHAPTER I

INTRODUCTION

High-pressure (HP) granulites and ultrahigh-pressure (UHP) eclogites form under very different P-T conditions, but are often found together in continental subduction and collision zones (Chopin, 2003; Indares et al., 2003; O'Brien and Rötzler, 2003). The mineral textures, whole rock chemistry, mineral chemistry and age of the HP-granulites discern whether the HP-granulites represent a separate unit from UHP eclogites, or if they represent overprinted UHP rocks. The presence of overprinted eclogites in UHP terranes relates to the rate of UHP exhumation. Therefore the specific origin and timing of HP-granulite metamorphism is needed to understand the exhumation rate of the UHP rocks.

High-pressure granulites are defined by the mineral assemblage garnet + clinopyroxene + plagioclase in mafic or intermediate compositions. The disappearance of orthopyroxene in mafic compositions marks the lower pressure limit of the HP-granulites facies. The upper pressure limit is marked by the disappearance of plagioclase (Fig. 1; O'Brien and Rötzler, 2003; Pattison, 2003). Ultrahigh-pressure conditions are defined by the transition from quartz to coesite and mark burial to >80 km (Chopin, 2003). The transition from quartz to coesite occurs from about 27–28 kbar at 650–750 ˚C, which is >11 kbar higher than HP granulite pressures at the same temperatures. This pressure difference corresponds to a ~50 km difference in burial depth between UHP rocks and HP granulites. High-pressure granulites form under two conditions: within the thickened crust of collision zones, or as eclogites that have passed through the HP-granulite facies (O'Brien and Rötzler, 2003). The two different HP-granulite

origins imply a different P-T-t path for the nearby UHP rocks, therefore understanding the P-T-t path for HP-granulites can indicate how the granulites became associated with the UHP rocks (Fig. 1).

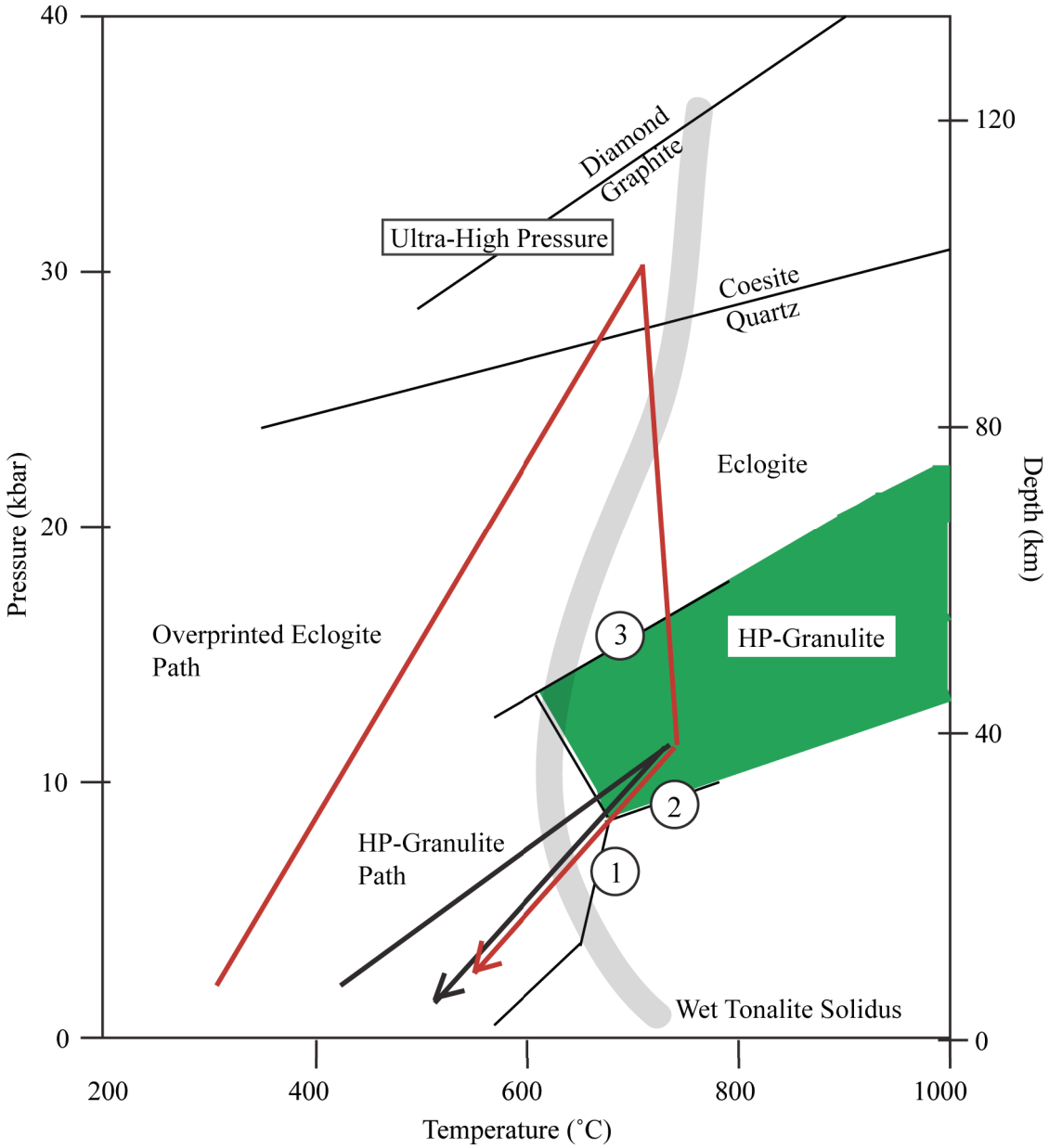

Figure 1. Summary view of HP-Granulite and UHP P-T regions. Boundaries are amphibolite-granulite (1), MP-granulite-HP-granulite (2), and HP-granulite-eclogite (3). Paths indicate a general trend for overprinted eclogites (red line-which passes though the HP-granulite facies after HP/UHP conditions), and HP-HT granulites (black line-which only reaches the HP-granulite facies). Modified after Liou et al. (1998), wet tonalite solidus (thick grey line) from Lambert and Wyllie (1974).

High-pressure granulites that form within the thickened crust of continental collision zones are characterized by the assemblage garnet + clinopyroxene + plagioclase growing in equilibrium with each other. These minerals can coexist with kyanite and, in more intermediate compositions, quartz. Clinopyroxene has a high calcium-tschermak (CaTs) and a non-omphacitic jadeite composition (<20% jadeite). Symplectite after HP-granulite Cpx is generally low Na-Cpx + Pl or Amp + Pl (O'Brien and Rötzler, 2003; see Table 1 for definitions of abbreviations). Overprinted eclogites have a peak assemblage of Grt + Omp (Jd>20%), and HP-granulite minerals are secondary to this, replacing the peak assemblage. Non-omphacitic Cpx and Pl are only found as symplectites after Omp (O'Brien and Rötzler, 2003). If the eclogite had experienced UHP conditions, coesite pseudomorphs consisting of polycrystalline Qtz can sometimes be found within Grt or Omp.

TABLE 1. LIST OF MINERAL ABBREVIATIONS USED

Abbreviation	Mineral	Abbreviation	Mineral	Abbreviation	Mineral
Alm	Almandine	Ep	Epidote	Phl	Phlogopite
Amp	Amphibole	Grs	Grossular	Pl	Plagioclase
An	Anorthite	Grt	Garnet	Prp	Pyrope
Ap	Apatite	Hd	Hedenbergite	Qtz	Quartz
Bt	Biotite	Jd	Jadeite	Rt	Rutile
Chl	Chlorite	Kfs	K-feldspar	Sa	Sanidine
Cpx	Clinopyroxene	Ky	Kyanite	Scp	Scapolite
Czo	Clinozoisite	Ms	Muscovite	Ser	Sericite
Di	Diopside	Omp	Omphacite	Sph	Sphene
East	Eastonite	Opq	Opaques	Zrn	Zircon

Note: All abbreviations after Kretz, 1983 except Amp, Opq, and East.

The North Qaidam terrane contains UHP rocks and HP granulites, indicating a complex history involving rocks from very different P-T conditions within the same terrane. Coesite has been reported in the North Qaidam rocks, confirming that these rocks have experienced UHP conditions (Fig. 2; Song et al., 2003a, 2003b; Yang et al.,

2001, 2002). High-pressure granulites have also been reported from the North Qaidam terrane, and previous study on granulites from several parts of the North Qaidam by Zhang et al., (Xitieshan, Lüliangshan, and South Altyn; 2005a, 2008a, 2009a) and Song et al. (Dulan; 2003a, 2003b) concluded they represent overprinted eclogites as described by O'Brien and Rötzler (2003).

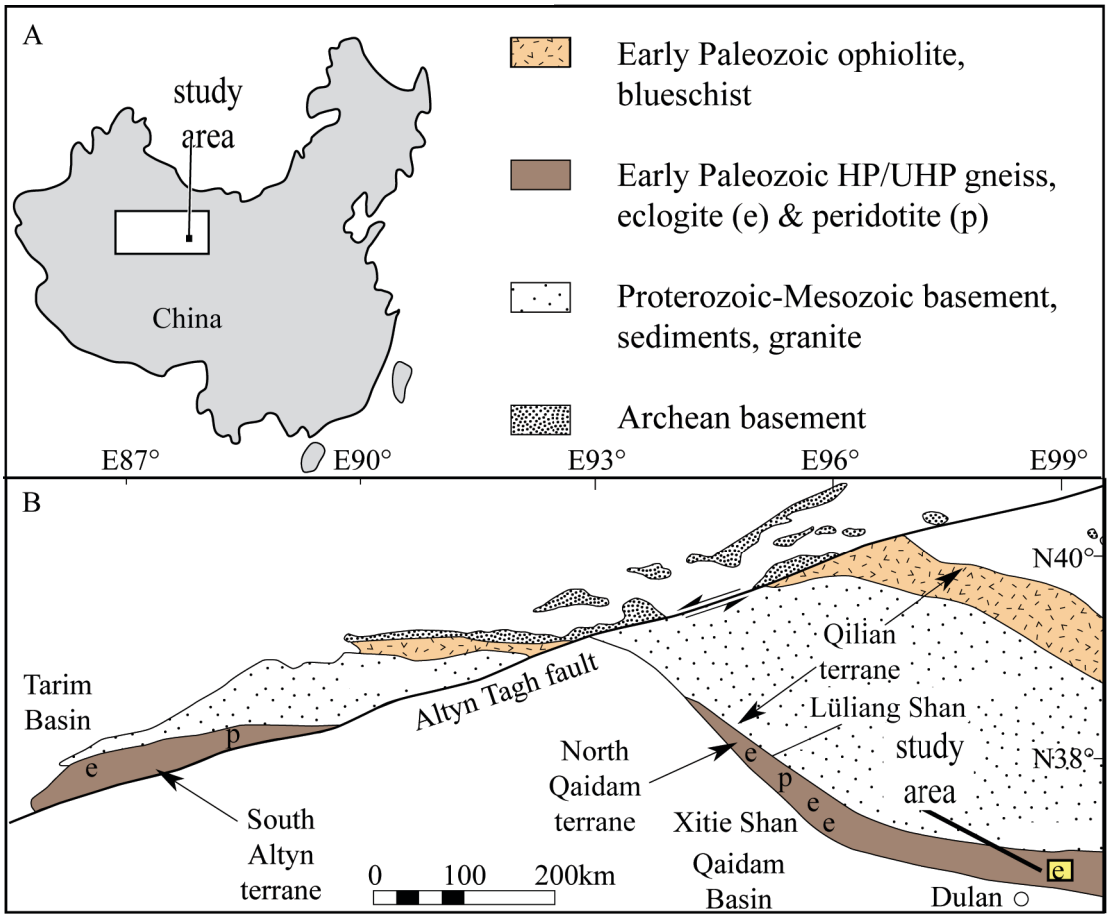

Figure 2. Map of China showing the location of the North Qaidam Terrane (A). Below (B) is a schematic map of the Qaidam-Qilian-Altyn terranes showing major units and locations of eclogite and peridotite. The yellow box marks the Dulan UHP exposure and study area.

Recently a HP granulite unit was identified in the SE North Qaidam, within the Dulan UHP exposure. Previously, the HP-granulites from Dulan were interpreted as overprinted eclogites (Song et al., 2003a, 2003b). Preliminary petrography and

geochronology on the newly discovered granulite unit suggest they are not overprinted eclogites (Zhang et al., 2009c). Pressure-temperature calculations by Yu et al. (2010) confirmed peak conditions within the HP-granulite facies, and concluded that the textural relationship between Grt-Cpx-Pl and inclusions in Grt do not support previous HP or UHP conditions. There has been no detailed geochronological study on the HP-granulites to determine the timing of HP-granulite metamorphism. The previous interpretation for the granulites suggests slow exhumation for the Dulan UHP rocks (Song et al., 2003a, 2003b). If the Dulan granulites do not represent overprinted eclogites, the exhumation rate for the UHP rocks is called into question. Therefore the goals of this study are to further examine samples from the Dulan granulite area in order to: 1) determine the timing of HP-granulite metamorphism relative to UHP metamorphism; 2) estimate P-T conditions from both mafic granulites and an associated Grt-Ky paragneiss; 3) use zircon U-Pb and trace-element analysis to link calculated P-T conditions to a metamorphic age (Rubatto, 2002); 4) study the role of partial melting in the Dulan granulites; and 5) test the two models for HP-granulite formation in the Dulan unit as described by O'Brien and Rötzler (2003).

CHAPTER II

BACKGROUND

Geologic Setting

The Dulan UHP and HP exposure is located in the North Qaidam metamorphic belt in North Western China. The North Qaidam terrane extends NW-SE for 350 miles (Fig. 2). This belt is located on the northern edge of the Tibetan Plateau and is bounded by the Qilian Terrane to the north, the Qaidam Basin to the south, the Altyn-Tagh Fault to the west, and by the Wenquan fault to the east. The basement rock of the North Qaidam is composed primarily of paragneiss and orthogneiss along with marble, granulite, quartzite, amphibolite, eclogite and ultramafic rocks. The orthogneiss and paragneiss host rocks are part of a larger group of Proterozoic basement rocks collectively known as the Dakendaban group gneiss. The Dakendaban gneiss is not limited to the North Qaidam, and though it includes HP/UHP rocks it also encompasses rocks with no HP/UHP history (e.g. the Quanji block, Chen et al., 2009). Because of the wide range of possible rock types associated with the Dakendaban gneiss, for clarity "UHP gneiss" will be used when referring to the HP/UHP host gneiss of the North Qaidam terrane. Included in the UHP gneiss are eclogite, ultramafic rocks, marble, quartzite, and amphibolite (representing retrogressed eclogite). Paleozoic metasediments are in depositional contact with the UHP rocks, and Paleozoic granites crosscut the UHP foliation (Mattinson et al., 2007). There are three locations of reported HP/UHP exposures within the North Qaidam terrane: the Lüliangshan, Xitieshan, and Dulan (Fig. 2).

The Dulan UHP exposure, named for the town of Dulan located to the southwest, contains eclogites and ultramafic rocks within the UHP gneiss (Fig. 3). Eclogite occurs as boudins or layers in both the para- and orthogneiss and are up to 10s of meters in size. A tight to isoclinaly folded amphibolite-facies foliation in the gneiss strikes northwest and dips to the northeast. A locally developed northwest plunging lineation trends northwest, and is identified mainly by stretched Kfs grains in the UHP orthogneiss (appendix A).

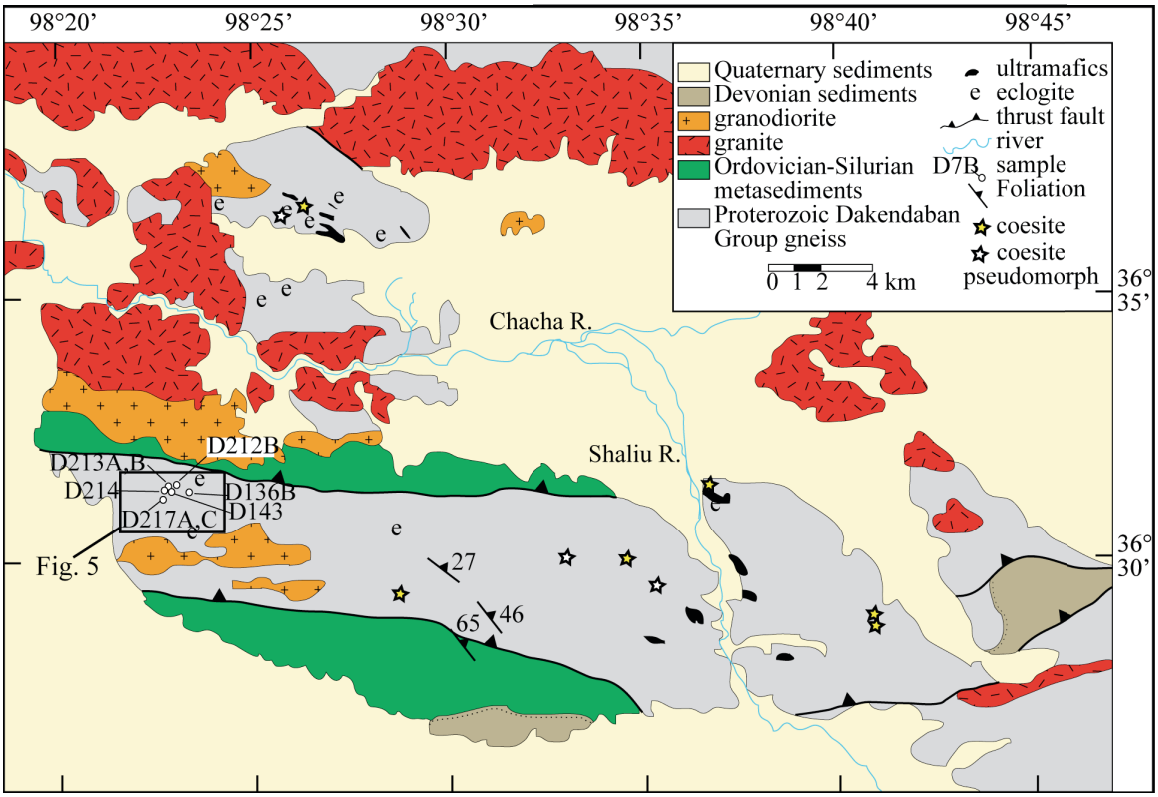

Figure 3. Geologic map of the Dulan UHP exposure. The town of Dulan is located ~30 km SW of the map area. Samples from this study are labeled and the surrounding box indicates the approximate area covered in Fig. 5.

Previous Work on the Dulan HP/UHP Rocks

Ultrahigh-pressure conditions in the Dulan HP/UHP exposure were first confirmed by Yang et al. (2001, 2002) and Song et al. (2003a, 2003b, 2006) based on the

presence of coesite in zircon from pelitic gneiss enclosing eclogite, and P-T calculations from the eclogite. This suggested both the gneiss and the enclosed eclogite were buried to UHP conditions above the quartz-coesite transition. More recent discoveries of coesite within garnet and omphacite from eclogite further support that both the pelitic gneiss and the eclogite experienced UHP conditions (Zhang et al., 2009b, 2009d, 2010).

Peak-stage UHP conditions are represented by a mineral assemblage of Grt + Omp + Rt ± Qtz ± Ep ± Phe ± Ky in the Dulan eclogites. Pressure-temperature conditions for the UHP rocks are estimated at 610–830 ˚C, 26–35 kbar (Fig. 4; Song et al., 2003a, 2003b; Yang et al., 2001; Zhang et al., 2008b, 2009b, 2009d, 2010).

Reported ages based on zircon U/Pb and Grt-Omp-WR Sm/Nd geochronology for the Dulan eclogite range from 422-459 Ma (Song et al., 2003a, 2003b; Mattinson et al., 2006; Zhang et al, 2008b, 2009b, 2009d, 2010). These ages are interpreted to represent metamorphic growth, indicating eclogite facies conditions appear to span a 35+ m.y. range (Mattinson et al., 2006; Zhang et al., 2010). Recent dating on coesite eclogites from the Dulan UHP rocks yielded an age range of 446-430 Ma, indicating UHP conditions persisted for at least ~16 Ma (Zhang et al., 2009d, 2010).

Previous Work on the Dulan HP-Granulites

High-pressure granulites have only been reported in the southern portion of the Dulan UHP exposure (south of N36˚32', see Fig. 3). This occurrence has led some to classify the north and south areas of the Dulan UHP rocks as the North Dulan Belt (NDB) and the South Dulan Belt (SDB; Song et al., 2003a, 2003b; Yang et al., 2001, 2002). Reported inclusions of omphacite in kyanite from the HP-granulites led Song et al.

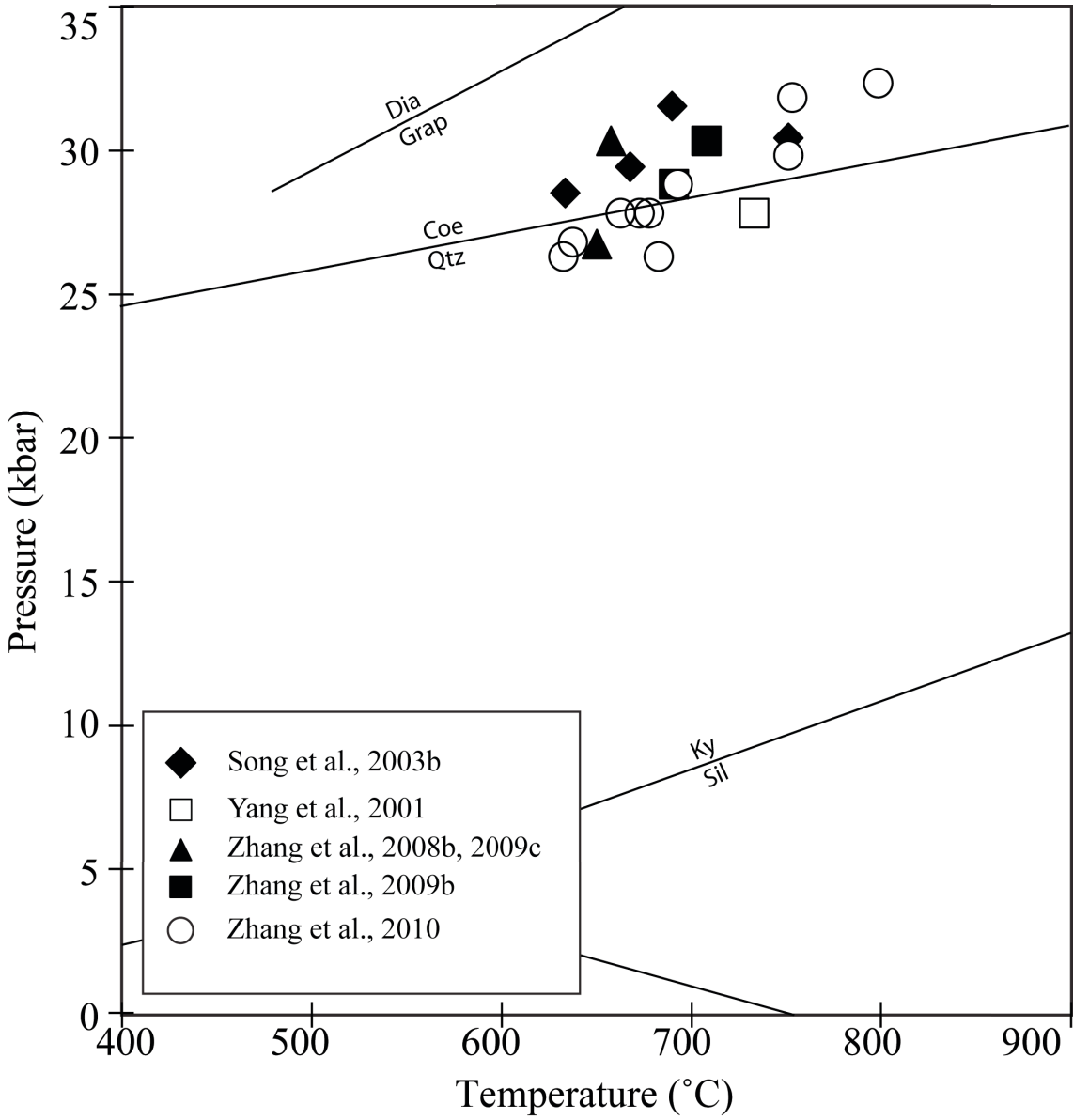

Figure 4. Summary of previous P-T calculations for the Dulan HP/UHP eclogites. Points represent averages of reported HP/UHP conditions by the listed authors and span a complete range of 610–830 ˚C, 26–35 kbar. Chart modified from Liou et al. (1998).

(2003a, 2003b) to conclude that the HP-granulites were overprinted UHP rocks. Song et al. (2003a) also reported differences in the whole rock chemistry of eclogites from the NDB and SDB. The chemical differences and the lack of any reported granulite facies in the NDB led to the hypothesis that the NDB and SDB represent two distinct UHP units with different P-T-t histories. The conclusion was that both units experienced UHP

conditions (subduction down to ~100 km), but their retrograde history is different due to different exhumation rates. The NDB unit exhumed to the surface quickly and preserved its UHP history with only a low to medium pressure amphibolite overprint. The SDB unit exhumed slower than the NDB, and during decompression received a HP-granulite overprint before returning to the surface.

Recent petrographic and P-T studies on the HP-granulites by Yu et al. (2010) reported that peak conditions for the granulites never reached the UHP eclogite facies. Continued U-Pb SHRIMP geochronology of UHP eclogites from both the SDB and NDB indicate both belts share the same P-T-t history, with no recorded granulite facies seen in eclogite zircons from both the SDB and NDB (Zhang et al., 2010). These results suggest the HP granulites are a separate unit that has been incorporated within the UHP gneiss. This would change the previous conclusion on the different exhumation rates between the NDB and SDB. This study is meant to test the hypothesis that the HP-granulites are a separate unit, as well as provide more information on the timing of HP-granulite metamorphism, and determine what the presence of these granulites indicates about the exhumation rate of the Dulan UHP rocks. This hypothesis was tested using field observations, whole rock chemistry, mineral chemistry, and zircon U-Pb and trace element analysis.

CHAPTER III

SAMPLE DESCRIPTIONS

Field Relations

The Dulan HP-granulites have only been identified in the western portion of the SDB, and so far have only been identified in a few canyons ~2 km in length (Fig. 5). The contact between the UHP gneiss and the granulites has yet to be mapped but is presumed to be a fault contact based on the significant P-T differences between the HP-granulite and UHP units; limited field investigation has shown eclogites exposed only to the east of the presumed contact and granulites only to the west.

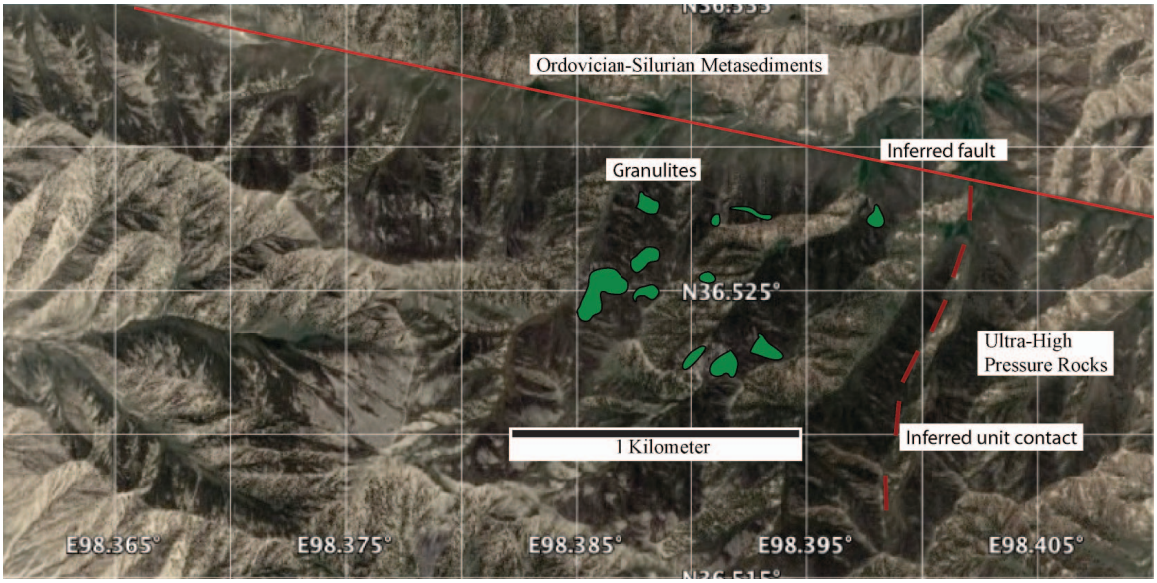

Figure 5. Close-up Google Earth image of the Dulan HP-granulite exposure. Green spots indicate locations of HP-granulite outcrop. Red line is an inferred fault contact, and the red dashed line is the inferred contact between the HP-granulites and UHP rocks. The map area corresponds to the box in Fig. 3.

High-pressure granulite occurs as layers 10s to 100s of meters in length within kyanite rich paragneiss in the southwestern portion of the Dulan UHP gneiss (Fig. 3,

sample locations; Fig. 6). The contact between the HP-granulite and Grt-Ky gneiss is sharp, but it is not clear if the contact is tectonic, intrusive or depositional (Fig. 6). The granulite layers range from mafic to felsic compositions, with mafic-intermediate compositions being most common. Felsic granulite is only found interlayered with mafic-intermediate granulite (Fig. 6). Tonalities cross cut both the granulites and the Grt-Ky host gneiss. Minor amounts of amphibolite and calc-silicate rocks are in contact with the granulites and host gneiss. Forty-one granulite, paragneiss, amphibolite, and calc-silicate samples were collected during two field seasons. Five granulite samples that best preserved the HP-granulite assemblage were chosen for detailed petrographic analysis, zircon U-Pb analysis, and zircon trace-element analysis. For pressure-temperature calculation, samples were also selected based on the presence of kyanite in the mineral assemblage. Also chosen for detailed study were two cross cutting tonalite samples and a Grt-Ky gneiss sample.

Petrographic Descriptions

Mafic Granulite D212B

Mafic granulite sample D212B has a mineral assemblage of Grt + Cpx + Pl + Czo + Ky + Qtz + Rt + Ap (Table 2; Fig. 7A). The sample has a foliation defined by Cpx + Czo + Ky, with Czo forming thick, oriented clusters throughout the sample. The sample shows compositional variation with alternating bands of Grt + Cpx + Pl and Czo + Ky ± Cpx (Fig. 7B). Larger garnets have inclusion rich cores and inclusion poor rims (Fig. 7C). Inclusions of Czo + Qtz + Pl are found in the garnet cores and Czo + Qtz + Pl + Rt are found in the garnet rims. Garnet rims also contain fined-grained Ser + Czo

pseudomorphs after kyanite (Fig. 7D). Smaller garnets in the sample resemble the rims of larger garnets in both composition and in inclusion content (Fig. 7E; see results).

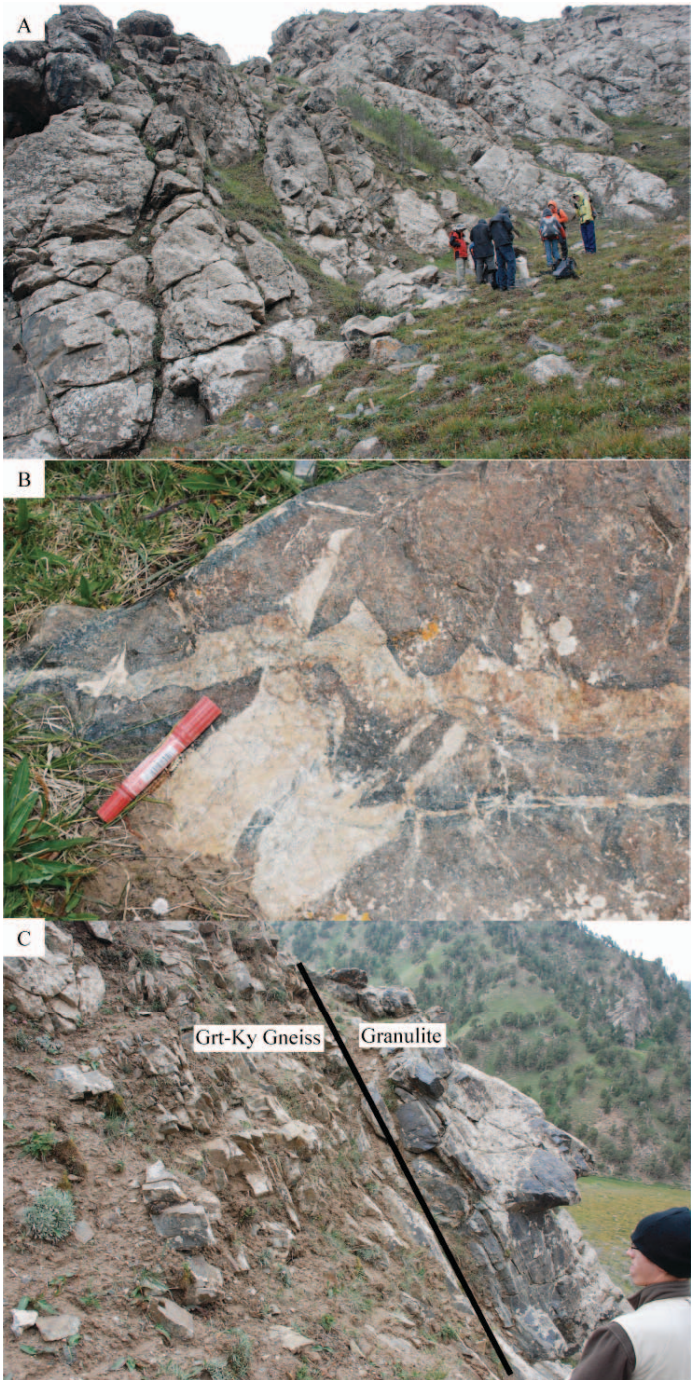

Figure 6. Field photographs of the Dulan HP-granulite exposure. A) Outcrop of mafic-intermediate granulite (people in the foreground for scale). B) Relationship between felsic granulites and mafic/intermediate granulites. C) Grt-Ky gneiss contact with intermediate granulite.

TABLE 2. MODAL ABUNDANCES OF STUDIED SAMPLES, NORTH QAIDAM TERRANE, WESTERN CHINA

Sample	Rock Name	Grt* (%)	Cpx (%)	Pl (%)	Kfs (%)	Czo (%)	Bt (%)	Ky (%)	Qtz (%)	Rt (%)	Amp (%)	Other	Localities
D136B	Granulite leucosome	15	<5	<1	-	20-25	-	3-5	50-55	<1	~1	Ap,Opq, Ser	N36°31.440' E98°23.460'
D143	Banded Grt-granulite	20	5-10	15-20	-	<1	<1	1-3	30-35	<1	5-10	Ap,Chl†	N36°31.500' E98°23.100'
D211C	Grt-clinopyroxenite	25	60	-	-	2-5	-	-	-	-	10	-	N36°31.489' E98°23.076'
D212B	Mafic Granulite	30	15-20	10	-	30-35	-	1-2	2-5	1-2	5	Ap,Opq, Ep,Ser	N36°31.558' E98°23.120'
D213A	Tonalite	-	-	50-55	-	-	-	-	45-50	-	-	Zr,Ep, Chl,Ser	N36°31.549' E98°23.107'
D213B	Intermediate Granulite	30-35	20-25	5-10	-	<1	-	1-3	25-30	1	2-5	Ap,Opq, Ep,Chl	N36°31.549' E98°23.107'
D214	Intermediate Granulite	25	15-20	15-20	-	5	-	1-2	20-25	1	2-3	Ap,Opq, Ep	N36°31.534' E98°23.098'
D217A	Grt-Ky mica schist	15-20	-	15	20-25	-	10	3-5	25-30	~1	-	Ap,Opq, Ms	N36°31.360' E98°23.090'
D217C	Rt bearing tonalite	-	-	50-55	-	-	trace	-	45-50	~1	<1	Ap,Ep, Chl,Ser	N36°31.360' E98°23.090'

Note: Abundances are based on visual estimation.

*Abbreviations are after Kretz (1983) except Amp (amphibole) and Opq (opaques).

†Epidote and chlorite in granulite samples D143, D212B, D213B and D214 is secondary, and occurs along mineral veins.

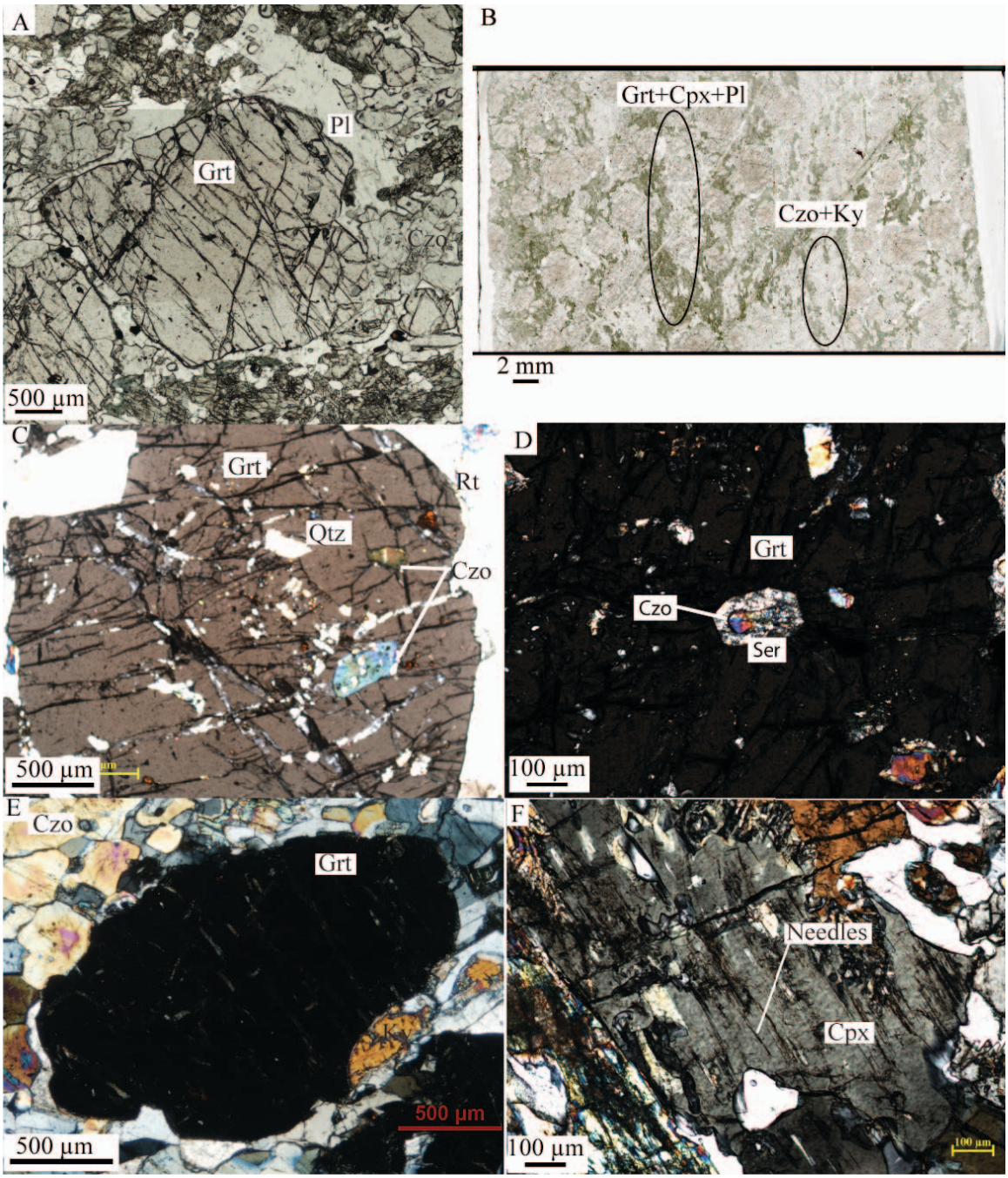

Figure 7. Photomicrographs of mafic granulite sample D212B. A) Plain polar (PP) overview of HP granulite mineral assemblage Grt + Cpx + Pl + Czo + Ky. B) Scan of thin section showing variations between Czo + Ky and Grt + Cpx + Pl bands. C) PP view of inclusions of Czo, Rt and Qtz in Grt. D) Cross-polar (XP) view of Ser + Czo inclusions in Grt that may represent former Ky. E) XP image of smaller Grt with similar inclusion poor nature to larger Grt rims. F) XP image of Cpx grain with thin, oriented needles along the long axis.

Clinopyroxene is relatively inclusion free and contains elongate needles oriented along the long axis of the grain (Fig. 7F). These needles are visible in plain and cross polars, and show low relief and low-order yellow or grey birefringence, indicating that they are possibly quartz. The presence of apparently exsolved Qtz needles in Cpx has previously been interpreted as being caused by decompression of high-silica content Cpx thought to only be stable at UHP conditions. However, Cpx with a hi-silica content has been shown to be stable within the Qtz stability field (prior to the quartz-coesite transition), indicating the presence of exsolve Qtz needles in Cpx from the Dulan HP-granulites does not necessarily indicate previous UHP conditions (Page et al., 2005). Kyanite is rimed by sericite, with some grains completely replaced. The sample has fine-grained Amp + Pl symplectite after Cpx and amphibole rims around Grt. The amount of this amphibole replacement varies throughout the sample (<5% total) and is stronger near epidote rich veins.

Intermediate Granulite D213B

Intermediate granulite sample D213B has a mineral assemblage of Grt + Cpx + Pl + Qtz + Ky + Czo + Rt + Ap (Table 2; Fig. 8A). A weak foliation is defined by Cpx + Ky (Fig. 8B). Inclusions of Czo + Qtz + Pl within the cores of the larger garnets show an older foliation at an angle to the matrix foliation (Fig. 8A and 8C). Several features in this sample are similar to D212B. Garnets have inclusion rich cores and inclusion poor rims. Inclusions in both cores and rims include Czo + Qtz + Pl (+ Rt in the rims). Smaller garnets are similar to the rims of larger garnets in composition and inclusion content. Clinopyroxene contains elongate needles oriented along the long axis. Clinopyroxene grain boundaries are irregular and commonly enclose Pl and/or Ky (Fig.

8D). This sample has less Amp + Pl symplectite than mafic granulite sample D212B. Symplectite after Cpx and amphibole rims around Grt are more common near epidote rich veins, where both Grt and Cpx are completely replaced by Ep + Chl + Amp.

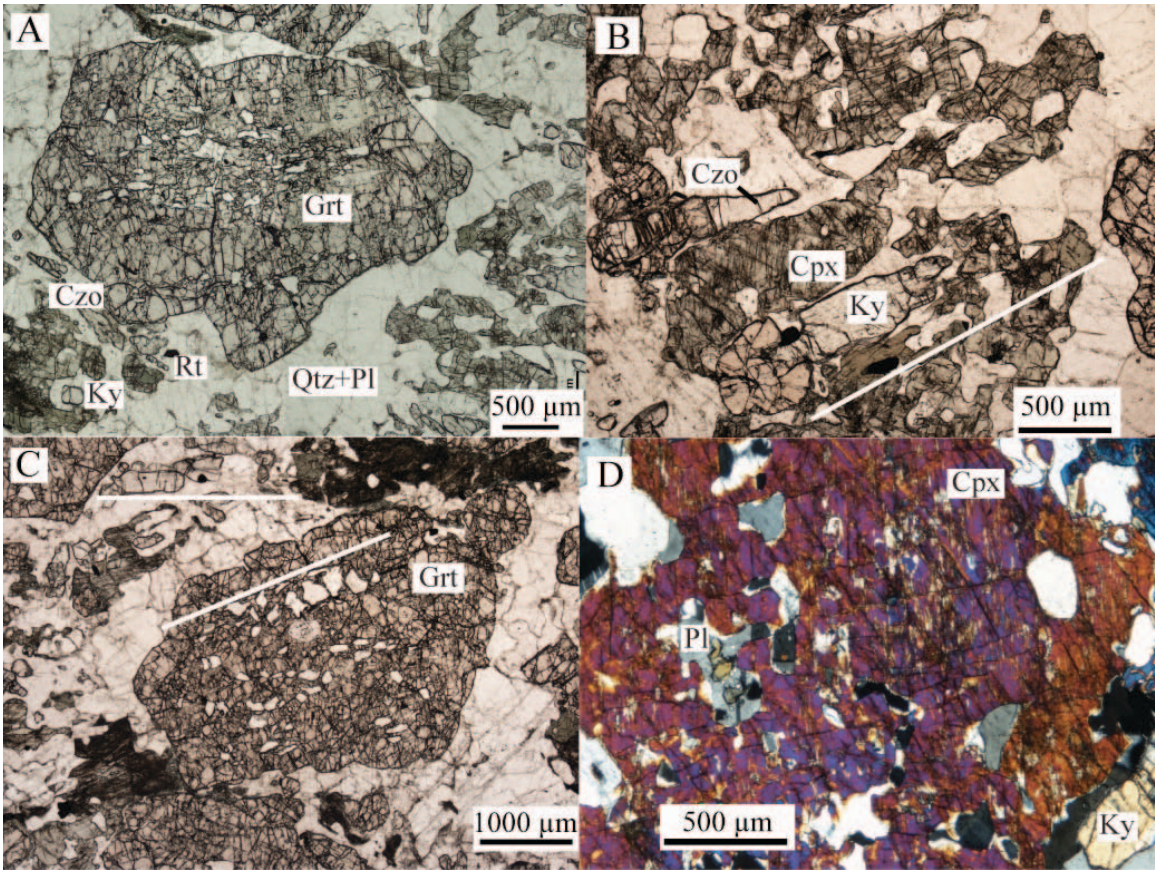

Figure 8. Photomicrographs of intermediate granulite sample D213B. A) PP overview of HP mineral assemblage Grt + Cpx + Pl + Qtz +Ky + Czo + Rt. B) PP view of foliation defined by Cpx + Ky + Czo (white line indicates approximate direction of foliation). C) PP view of internal foliation marked by inclusions in Grt, White lines indicate direction of matrix foliation and Grt foliation (see also Fig. 17). D) XP image of Cpx enclosing Pl with a nearby Ky, also visible are the oriented needles similar to those described in sample D212B (see text).

Intermediate Granulite D214

Intermediate granulite sample D214 has a mineral assemblage of Grt + Cpx + Pl + Qtz + Czo + Ky + Rt (Table 2, Fig. 9A). A foliation is defined by Cpx + Czo + Ky. Quartz inclusions in some Grt cores show an older foliation at an angle to the matrix

foliation. Inclusions in both cores and rims of Grt include Czo + Qtz + Pl (+Rt in the rims). Quartz inclusions are generally concentrated in one zone between the cores and rims of Grt grains (Fig. 9B). This sample has more Czo than intermediate granulite sample D213B, with elongate Czo grains forming a common part (~5% modal

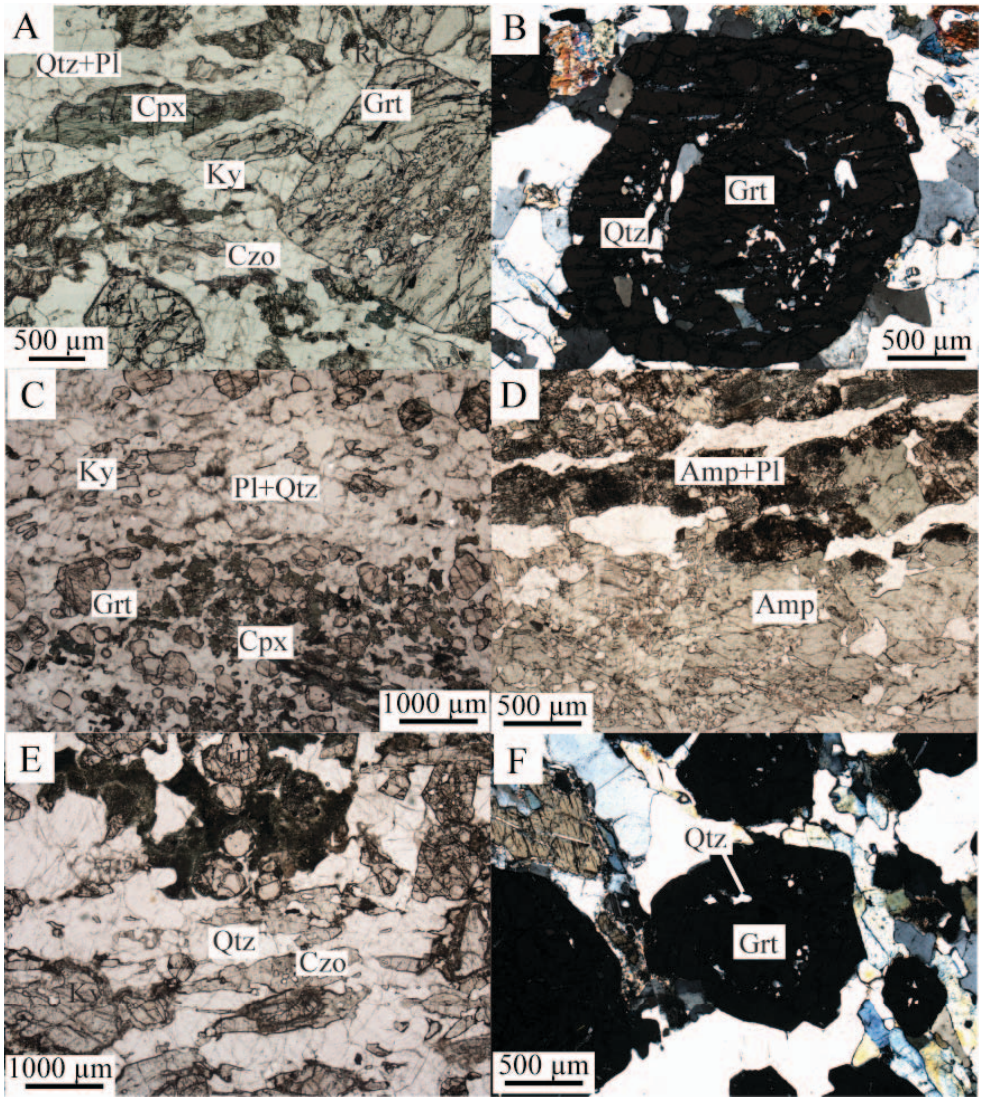

Figure 9. Photomicrographs of granulite samples D214, D143 and D136B. A) PP overview of sample D214 showing HP granulite assemblage of Grt + Cpx + Pl + Ky + Czo + Qtz + Rt. B) XP image of circular inclusion pattern of Qtz in Grt for sample D214. C) PP image of bands of Grt + Cpx and Pl + Qtz + Ky seen in granulite sample D143. D) PP image of Amp veins running through sample D143. E) Oriented Qtz + Czo + Ky grains in granulite leucosome sample D136B. F) XP view of Qtz inclusions in Grt for sample D136B.

abundance) of the matrix. Amphibole rims and Amp + Pl symplectites are similar to the other granulite samples.

Banded Granulite D143

Sample D143 is a felsic granulite with a mineral assemblage of Grt + Cpx + Pl + Qtz + Ky + Rt + Czo (Table 2). The sample has alternating bands of Cpx + Grt and Pl + Qtz + Ky (Fig. 9C). Clinopyroxene is strongly replaced by amphibole and amphibole + plagioclase symplectite. Bands of coarse-grained amphibole are parallel to the foliation defined by Cpx + Ky (Fig. 9D). Garnet is small and relatively inclusion free.

Granulite leucosome D136B

Sample D136B is a felsic granulite with a mineral assemblage of Grt + Cpx + Pl + Qtz + Czo + Ky + Rt (Table 2). Clinopyroxene, clinozoisite, kyanite and quartz are strongly oriented (Fig. 9E). Clinopyroxene is scarce and replaced by amphibole and amphibole + plagioclase symplectite. The freshest Cpx contains elongate needles oriented along the long axis. Garnet is small (<0.5 mm) and contains quartz inclusions (Fig. 9F). Clinozoisite is present throughout the sample (20-25%) as thin, elongate grains. Kyanite is abundant (3-5%), coarse-grained, and generally rimmed by sericite.

Garnet-kyanite paragneiss D217A

Sample D217A is a Grt-Ky paragneiss containing 15-20% garnet and 3-5% kyanite (Table 2). The sample alternates between bands of Qtz + Kfs + Pl and bands of Grt + Ky + Bt + Rt + Opq (Fig. 10A and 10B). Inclusions in garnet are Pl + Kfs + Qtz + Bt + Ms (Fig. 10C). Muscovite was identified as an inclusion in one garnet, but is not present as part of the matrix mineral assemblage (Fig. 10D).

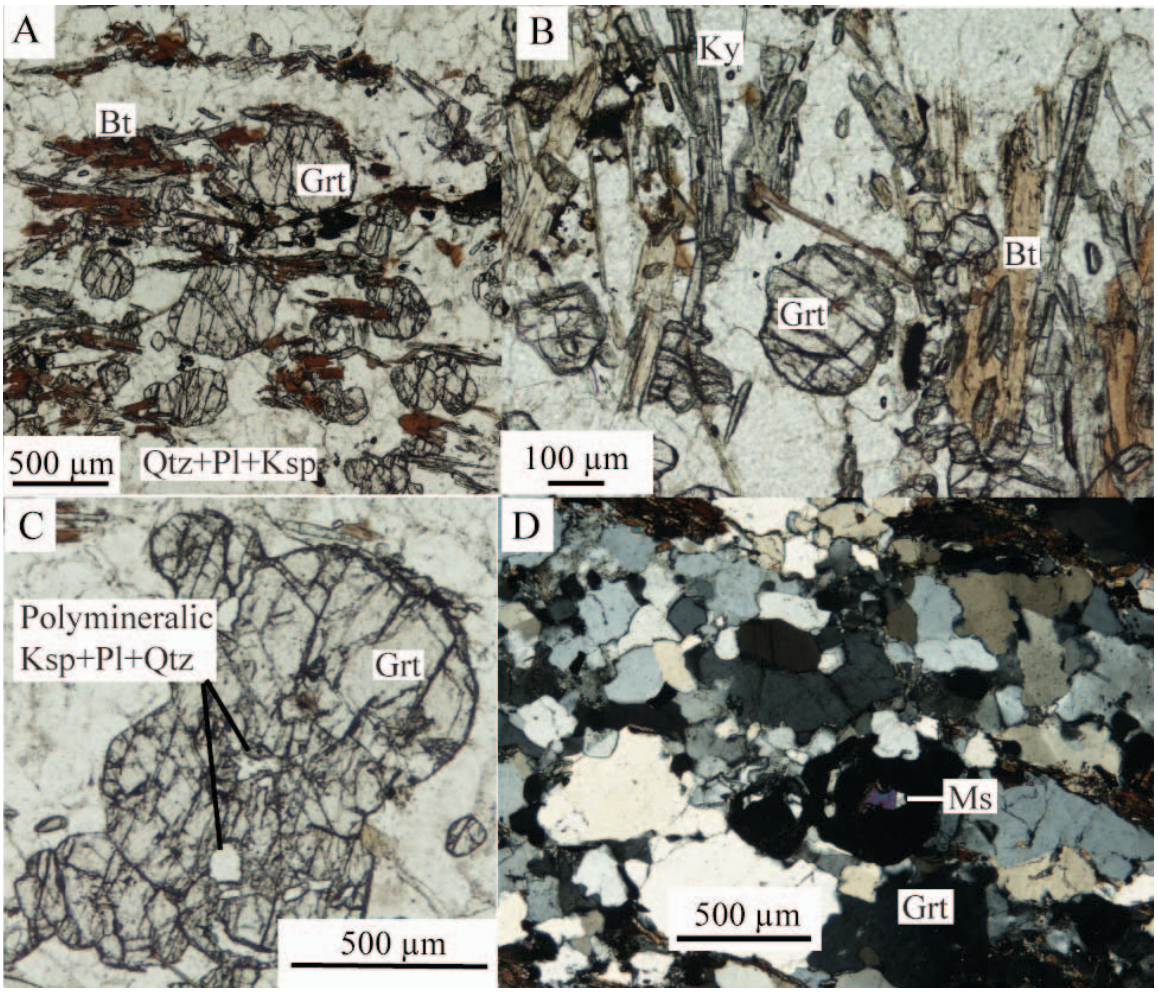

Figure 10. Photomicrographs of Grt-Ky gneiss D217A. A) PP overview of alternating bands of Qtz + Pl + Kfs and Grt + Bt + Ky. B) PP close up of Grt + Bt + Ky bands. C) Polymineralic inclusions of Qtz + Pl + Kfs in Grt. D) XP image of Ms inclusion in Grt.

Tonalite D213A

Tonalite sample D213A (Table 2, Fig. 11A) contains coarse-grained plagioclase (some > 4 mm), quartz (1-2 mm) and minor (<1%) chlorite and epidote. Plagioclase is partially to completely sericitized. Chlorite forms small clusters of several grains around a single elongate grain (Fig. 11B). All grains are chlorite and these clusters are interpreted to represent pseudomorphs after Bt. Epidote is present in the Chl clusters and in veins.

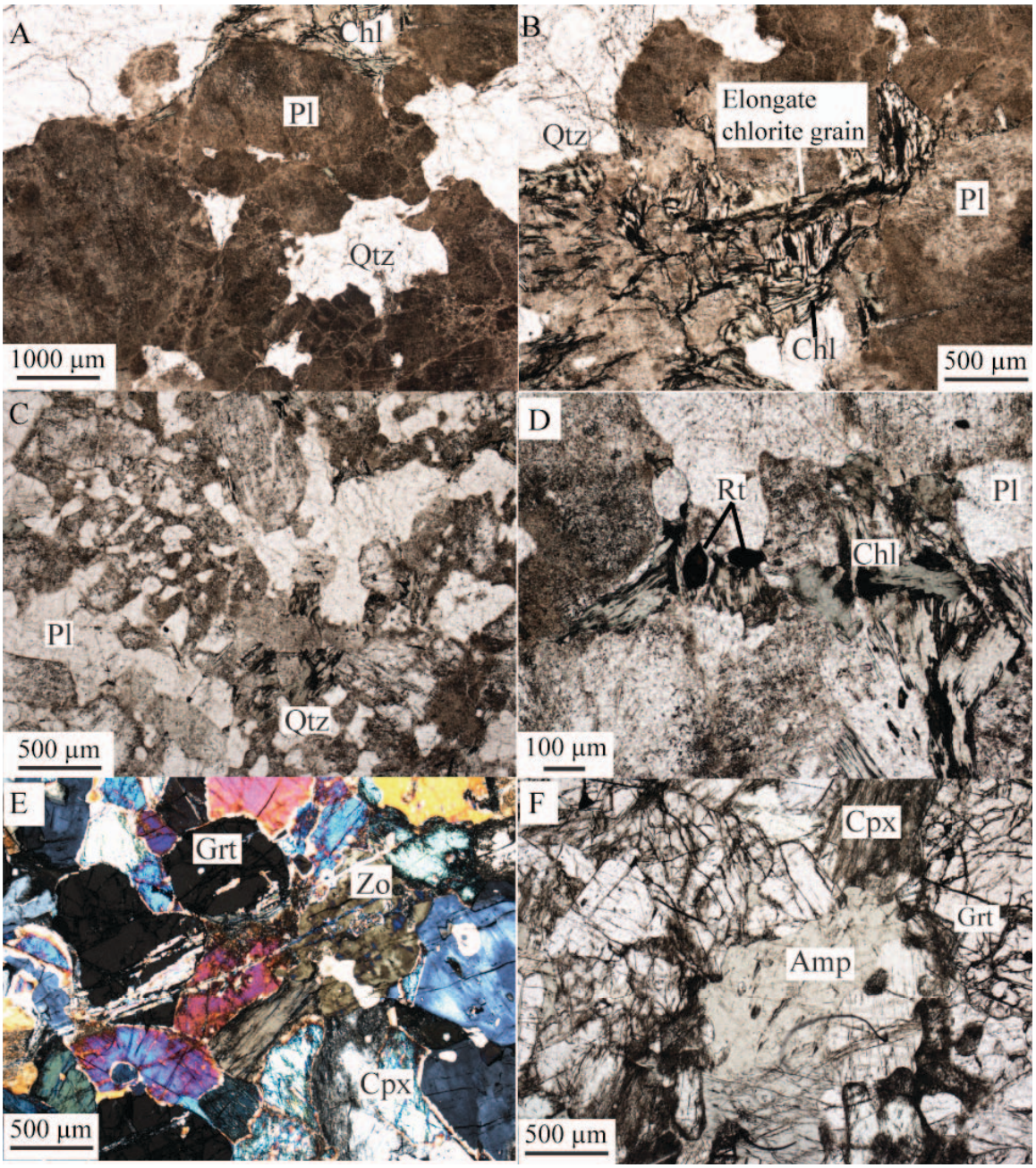

Figure 11. Photomicrographs of samples 213A, D217C and D211C. A) PP view of coarse-grained Pl and Qtz in tonalite sample D213A. B) PP view of Chl cluster from D213A centered around one elongate grain. C) PP overview of Pl + Qtz in Rt-bearing tonalite D217C. D) PP close-up of Chl + Rt cluster in sample D217C. E) XP view of Grt-clinopyroxenite D211C showing assemblage of Grt + Cpx + Zo. F) PP image of minor, coarse grained Amp from sample D211C.

Rutile-bearing tonalite D217C

Sample D217C is a tonalite with a similar abundance of plagioclase, quartz, chlorite, and epidote to D213A (Table 2, Fig. 11C). This sample also contains a small amount (<1%) of rutile, generally associated with Chl + Ep (Fig. 11D). This Chl + Rt combination is interpreted to be the product of high-Ti biotite breakdown.

Garnet Clinopyroxenite D211C

Sample D211C contains a mineral assemblage of Cpx + Grt + Zo (Table 2, Fig. 11E). Amphibole does not appear as halos around Grt or Cpx as in the granulites and instead is present as coarse-grains about the same size as Cpx. It is not clear whether the Amp is part of the peak assemblage (Fig. 11F). No plagioclase was found in this sample. Garnets are smaller (0.5-1 mm) than in the granulite samples and are mostly inclusion free. Clinopyroxene is replaced by fine-grained symplectite similar to that seen in HP-granulite samples. It would appear to be an eclogite; however, there is no mineral chemistry data for this sample so it cannot be confirmed whether or not the Cpx is Omp (see results). For the purposes of this study it will be referred to as a garnet clinopyroxenite.

CHAPTER IV

METHODS

Whole Rock Analysis

Samples were sent to Washington State University (WSU) for whole rock X-ray fluorescence (XRF) analysis using a ThermoARL XRF. Samples were analyzed for 29 major and trace elements using the methods of Johnson et al. (1999). For a complete list of the elements analyzed see appendix B.

Geochronology and Trace Elements

Zircon U-Pb geochronology and trace element analysis were performed using the Stanford/USGS SHRIMP-RG (sensitive high resolution ion micro-probe reverse geometry) facility using the methods of Mattinson et al. (2006, 2009). Zircon grains separated from the samples were mounted with zircon age standard R33 (419 Ma; Black et al., 2004) in 2.54 cm epoxy discs polished to expose the interior of the grains. Cathodoluminescence (CL) and reflected light images of the polished grains were collected to document their locations on the mount and to map their internal structures. Cathodoluminescence images were collected using a JEOL 5600LV scanning electron microscope located at the Stanford/USGS SHRIMP-RG lab. Locations for SHRIMP spot analyses were chosen to avoid cracks, pits, and inclusions based on both CL and reflected light images. The samples were Au-coated and placed under high vacuum for 24 hours prior to analysis.

Samples were first analyzed for U-Pb and 11 trace elements. The analytical routine for U-Pb geochronology followed Williams (1998), and age calculations were

performed using Isoplot and Squid programs (Ludwig, 2001, 2003) and IUGS recommended decay constants (Steiger and Jäger, 1977). Samples were analyzed using a beam diameter of ~23 μm. The concentration of U was calibrated using zircon trace element standard MAD and the Pb/U ratio was calibrated using zircon age standard R33 (419 Ma; Black et al., 2004). Estimates of common-Pb compositions use the two-stage Pb evolution model of Stacey and Kramers (1975). Individual ages reported are $^{206}Pb/^{238}U$ ages corrected for common-Pb using ^{207}Pb. For ages >1 Ga $^{207}Pb/^{206}Pb$ ages are reported and corrected for common-Pb using ^{204}Pb (Williams, 1998). Ages calculated from multiple analyses are expressed as either weighted mean or intercept ages and errors are given at 95% confidence.

Samples selected for detailed trace element analysis were lightly re-polished and a new Au coating was added. This expanded trace element analysis consisted of 35 elements and used a smaller spot size (~17 μm) and in some cases, multiple spots were analyzed on individual zircon grains.

Based on analyses of the zircon trace element standard MAD, standard deviations of P, Y, Hf, Th, and U are 3-10%, and the REE are 3-12%, except La (34%) which has extremely low abundance, providing a conservative estimate of the uncertainty of the trace element analyses (Grimes et al., 2009; Mattinson et al., 2006). The consistency of the REE patterns suggests that part of this variability reflects true heterogeneity in the MAD standard. The agreement between U concentrations measured during U-Pb analysis and trace element analysis indicates that the trace element measurements may be applied to the interpretation of the U-Pb measurements for most analyses (see results; appendix C).

Some trace element analyses contain elevated Al, Ca, Fe, and/or Mn, and are considered unrepresentative of igneous or metamorphic growth compositions (see results). These elements are normally very low in crystalline, inclusion-free zircon, suggesting that the elevated LREE and Ti (see results) of these analyses are related to mineral or fluid micro-inclusions, or post-crystallization introduction of these elements into radiation-damaged zones in the zircons (Grimes et al., 2009).

Ti-in-zircon thermometry (Ferry and Watson, 2007) assumes TiO_2 and SiO_2 activities = 1.0, which is appropriate for the rutile and quartz bearing metamorphic assemblages observed the studied samples. Temperatures were calculated using a calibration pressure of 10 kbar and may underestimate true values by 50 ˚C per 10 kbar above that pressure (Ferry and Watson, 2007).

Mineral Chemistry

Mineral compositions were measured using the WSU JEOL 8500F field emission electron microprobe. X-ray maps were first collected for Ca, Fe, Mg, Mn, and Na and were used to select the best representative cross-sections for microprobe transects across mineral grains. Transects took spots every ~50 μm, but the very edges of the garnet rims took spots every 2–3 μm. Samples were analyzed for up to 13 elements using natural and synthetic standards. Samples were run at 15 or 30 nA beam current, and 1-10 μm spot size depending on the mineral sample being analyzed (see appendix B).

Zircon mounts from the previous SHRIMP-RG work were also analyzed for mineral inclusions identified by reflected light and CL images. Most inclusions were too small for quantitative analysis without interference from surrounding zircon but all were

analyzed by energy dispersive x-ray spectroscopy (EDS, same instrument) to provide a qualitative inclusion composition used to infer mineral identity.

Pressure-Temperature Estimates

The mineral assemblage from the granulite and paragneiss samples allows for the use of several geothermobarometers to estimate pressure and temperature: the Fe-Mg exchange thermometer (Grt-Cpx and Grt-Bt), garnet-plagioclase-quartz-aluminosilicate barometer (GASP), garnet-plagioclase-clinopyroxene-quartz barometer (GADS), and the Ab-Jd-Qtz barometer. Exchange reactions such as the Grt-Cpx (Eq. 1) and Grt-Bt (Eq. 2) thermometers involve a very small change in volume. This means a pressure independent reaction, providing a good geothermometer.

$$(1/3)Mg_3Al_2Si_3O_{12} + CaFeSi_2O_6 = (1/3)Fe_3Al_2Si_3O_{12} + CaMgSi_2O_6 \quad (1)$$

$$Mg_3Al_2Si_3O_{12} + KFe_3AlSi_3O_{10}(OH)_2 = Fe_3Al_2Si_3O_{12} + KMg_3AlSi_3O_{10}(OH)_2 \quad (2)$$

Net transfer reactions, such as GASP (Eq. 3), GADS (Eq. 4), and Ab-Jd-Qtz (Eq. 5) are useful for pressure calculations due to the consumption of mineral phases causing a large change in volume, which is pressure sensitive.

$$Ca_3Al_2Si_3O_{12} + 2Al_2SiO_5 + SiO_2 = 3CaAl_2Si_2O_8 \quad (3)$$

$$CaAl_2Si_2O_8 + CaMgSi_2O_6 = (2/3)Ca_3Al_2Si_3O_{12} + (1/3)Mg_3Al_2Si_3O_{12} + SiO_2 \quad (4)$$

$$NaAlSi_2O_6 + SiO_2 = NaAlSi_3O_8 \quad (5)$$

The intersection of a geobarometer and a geothermometer provides a P-T estimate.

There are several problems associated with Fe-Mg exchange thermometers in HT rocks. Because of the high-temperatures associated with granulite conditions, diffusion during cooling could cause exchange reactions to reset, therefore calculated P-T conditions may not represent peak conditions. Iron content also has an effect because

ferric iron affects the final temperature in Fe-Mg exchange thermometers. It is not possible, however, to differentiate between Fe^{3+} and Fe^{2+} in EMP analysis. Therefore a representative Fe^{3+} composition must be calculated, but there are large uncertainties in these calculations. Any uncertainty in this Fe^{3+} calculation is added to any temperature estimate. Different calculations of Fe^{3+} can span a final temperature range of ~100 ˚C, suggesting individual T estimates using the Fe-Mg exchange system should include error brackets of at least ±100 ˚C in order to fully account for error in Fe^{3+} estimation (Krogh Ravna and Paquin, 2003).

Calibrations of the geothermobarometers used in this study were chosen because they are considered internally consistent, i.e., thermometer(s) and barometer(s) do not make contradictory calculations or assumptions. An internally consistent set of calibrations either uses the same thermodynamic dataset or activity model, or is calibrated against the same empirical data. Pressure-temperature estimates of granulites using the Grt-Cpx thermometer of Pattison and Newton (1989) and GADS barometer of Newton and Perkins (1982) are internally consistent because both models are calibrated against the Grt-Pl-Hbl-Qtz barometer of Kohn and Spear (1990; Spear, 1995). The Grt-Bt thermometer and GASP barometer from Hodges and Spear (1982) used for the Grt-Ky gneiss sample are internally consistent because both are calibrated using the same empirical dataset. The granulite samples contained kyanite and quartz, therefore the GASP barometer of Hodges and Spear (1982) as well as the Ab-Jd-Qtz barometer of Holland (1980) could also be used on these samples.

Pressure-temperature calculations were performed with the program GTB v2.1 (Spear and Kohn, 1999) using mineral compositions interpreted to represent peak

conditions. Average values of Grt rims were chosen to represent peak metamorphic conditions based on inclusions of Czo + Qtz + Pl + Rt ± Ky pseudomorphs interpreted as representing the peak metamorphic assemblage (see results). Magnesium in Cpx is an important element in geothermobarometry for these samples (see above equations), therefore Cpx compositions were chosen based on minimum, maximum and average Mg content. Compositions for Pl, Czo, Bt and Kfs were chosen in a similar manner using Na, Fe, Mg and K content respectively (minimum, maximum and average values). If peak conditions are truly being represented, results using combinations of minimum, maximum, and average compositions should be similar. The potential spread in P-T results will also give a measurement of the true P-T uncertainty, with outliers suggesting a composition not representing peak conditions. Average compositions used for P-T estimates are listed in Tables 3 and 4, and a complete listing of compositions used for P-T estimates can be found in appendix D.

The mineral compositions input into the program GTB were also input into the program THERMOCALC v.3.33 (Holland and Powell, 1998). The program THERMOCALC uses an internally consistent dataset and inputs mineral end-member activities to calculate an independent set of equations used to calculate an average P-T, including errors and error correlations (see appendix D). Reactions involving clinozoisite are temperature dependant reactions replacing the Fe-Mg exchange reactions from GTB. One example is:

$2Czo = Grs + An + H_2O + Ky$ (equation 2, see appendix B)

TABLE 3. AVERAGE COMPOSITIONS FOR MINERALS USED IN P-T ESTIMATES OF GRANULITE SAMPLES

Sample	D212B						D213B						
No.	Grt1A	Grt1B	Cpx1	Cpx2	Pl1	Czo1	Grt1A	Grt1B	Cpx1	Cpx2	Pl1	Pl2	Czo1
SiO_2	39.28	38.04	50.50	49.53	61.45	38.05	39.30	38.70	50.72	50.35	61.35	61.68	38.13
TiO_2	0.09	0.06	0.54	0.64	0.01	0.12	0.05	0.05	0.52	0.54	0.01	0.00	0.17
Al_2O_3	22.96	22.03	9.57	10.08	24.11	27.82	22.64	22.30	9.63	9.49	24.1	23.91	27.64
Cr_2O_3	0.00	0.01	0.00	0.00	0.00	0.01	0.03	0.01	0.02	0.03	0.00	0.00	0.02
FeO*	21.25	21.73	6.84	7.26	0.07	6.43	19.19	19.54	6.48	6.57	0.05	0.09	6.84
MnO	0.43	0.50	0.03	0.06	0.00	0.02	0.36	0.33	0.02	0.02	0.00	0.00	0.06
MgO	7.77	7.14	10.07	9.69	0.01	0.21	10.71	10.63	10.46	10.49	0.00	0.01	0.29
CaO	9.02	9.57	18.57	18.70	5.78	23.08	7.31	7.36	18.27	18.4	5.87	5.68	22.89
Na_2O	0.03	0.06	3.04	2.82	8.24	0.01	0.04	0.01	3.08	2.96	8.11	8.19	0.02
K_2O	0.00	0.02	0.00	0.01	0.05	0.00	0.00	0.00	0.01	0.00	0.08	0.09	0.00
Totals	100.83	99.16	99.16	98.79	99.73	96.46	99.63	98.93	99.21	98.85	99.58	99.66	96.81
Oxygens	12	12	6	6	8	12.5	12	12	6	6	8	8	12.5
Si	2.969	2.935	1.858	1.835	2.733	2.999	2.958	2.937	1.860	1.855	2.733	2.744	2.998
Ti	0.005	0.003	0.015	0.018	0.000	0.007	0.003	0.003	0.014	0.015	0.000	0.000	0.010
Al	2.046	2.004	0.415	0.440	1.264	2.585	2.009	1.995	0.416	0.412	1.266	1.254	2.562
Cr	0.000	0.001	0.000	0.000	0.000	0.001	0.002	0.001	0.001	0.001	0.000	0.000	0.001
Fe^{3+}	0.011	0.130	0.056	0.057	0.003	0.420	0.073	0.125	0.054	0.058	0.002	0.003	0.445
Fe^{2+}	1.332	1.272	0.154	0.167	0.000	0.004	1.135	1.115	0.145	0.144	0.000	0.000	0.004
Mn	0.028	0.033	0.001	0.002	0.000	0.001	0.023	0.021	0.001	0.001	0.000	0.000	0.004
Mg	0.875	0.821	0.552	0.535	0.001	0.025	1.201	1.202	0.572	0.576	0.000	0.001	0.034
Ca	0.730	0.791	0.732	0.742	0.275	1.949	0.590	0.599	0.718	0.726	0.280	0.271	1.928
Na	0.004	0.009	0.217	0.203	0.711	0.002	0.006	0.001	0.219	0.211	0.700	0.706	0.003
K	0.000	0.002	0.000	0.000	0.003	0.000	0.000	0.000	0.000	0.000	0.005	0.005	0.000
Sum	8.000	8.000	4.000	4.000	4.990	7.992	8.000	8.000	4.000	4.000	4.986	4.984	7.990

Note: FeO* assumes all iron is FeO.

TABLE 4. AVERAGE COMPOSITIONS FOR MINERALS
USED IN P-T ESTIMATES FOR GRT-KY GNEISS

Sample	D217A							
No.	Grt1rimavg	Grt2rimavg	Bt1avg	Bt2avg	Bt3avg	Pl1avg	Pl2avg	Ksp1avg
SiO_2	37.90	37.79	36.89	36.90	37.04	62.95	63.04	64.74
TiO_2	0.05	0.06	3.72	3.84	3.84	0.01	0.00	0.01
Al_2O_3	22.34	22.06	18.22	18.18	18.36	22.67	22.73	18.50
Cr_2O_3	0.02	0.02	0.00	0.00	0.00	0.00	0.00	0.00
FeO*	27.92	26.98	14.67	14.69	14.15	0.08	0.05	0.07
MnO	0.53	0.49	0.02	0.03	0.03	0.00	0.00	0.00
MgO	5.15	5.56	12.77	12.64	12.72	0.01	0.03	0.02
CaO	6.18	6.69	0.15	0.16	0.13	4.43	4.46	0.23
Na_2O	0.03	0.03	0.12	0.12	0.15	8.66	8.60	1.07
K2O	0.02	0.01	9.11	9.45	9.34	0.28	0.32	14.99
Totals	100.14	99.69	95.68	96.02	95.77	99.1	99.24	99.65
Oxygens	12	12	11	11	11	8	8	8
Si	2.959	2.953	2.723	2.721	2.727	2.806	2.806	2.991
Ti	0.003	0.004	0.207	0.213	0.213	0.000	0.000	0.000
Al	2.056	2.033	1.586	1.580	1.594	1.192	1.193	1.008
Cr	0.001	0.001	0.000	0.000	0.000	0.000	0.000	0.000
Fe^{3+}	0.025	0.058	0.000	0.000	0.000	0.003	0.002	0.003
Fe^{2+}	1.798	1.706	0.906	0.906	0.871	0.000	0.000	0.000
Mn	0.035	0.032	0.001	0.002	0.002	0.000	0.000	0.000
Mg	0.599	0.648	1.405	1.389	1.396	0.001	0.002	0.001
Ca	0.517	0.560	0.012	0.013	0.010	0.212	0.213	0.011
Na	0.005	0.005	0.017	0.017	0.021	0.749	0.742	0.096
K	0.002	0.001	0.858	0.889	0.877	0.016	0.018	0.883
Sum	8.000	8.000	7.715	7.730	7.713	4.978	4.976	4.994

Note: FeO* = all Fe calculated as FeO.

Mineral end-member activities were calculated using the program a-X (Holland and Powell, 1998) using an input P-T (initial input using the GTB results). Quartz, kyanite, and H_2O activities were assumed to be 1.0. Calculated activities were input into the average P-T calculation of the program THERMOCALC. The P-T output from THERMOCALC was then input back into the program a-X and the process repeated until the resulting P-T calculations did not change. Because Czo and Bt both include water in their structure at least one independent equation used in the P-T calculation would

include H_2O as an end-member. Therefore several trials were run with decreasing H_2O activity (from 1.0 down to 0.7) to see if there was any effect on the final results. Results were evaluated based on the significance of fit provided by the THERMOCALC program.

CHAPTER V

RESULTS

Whole Rock and Mineral Chemistry

Whole Rock Chemistry All Samples

Granulite samples differ from the Dulan eclogites and span a SiO_2 range of 43–73 wt% (Table 5; Fig. 12A). TiO_2 concentrations in all granulite samples are low compared to the Dulan eclogites, less than 1.0 wt% (Fig. 12B). Zirconium concentrations in the granulite samples are all relatively low. Mafic and intermediate granulite samples (D212B, D213B, and D214) contain <10 ppm Zr, and the felsic samples (D136B and D143) contain <50 ppm Zr, this explains the low zircon yields during sample preparation.

The two felsic granulite samples have chemical properties different from the other granulites. Banded granulite sample, D143 has a high Na_2O content (5.4 wt%) compared to the other granulites, which range from 1.7-3.1 wt%. Granulite leucosome, D136B, has very low MgO, Na_2O, and K_2O (0.6, 0.31 and 0.09 wt% respectively) compared to the other four granulite samples (Fig. 12A).

The Grt clinopyroxenite, D211C, contains ~47 wt% SiO_2 and <0.1 wt% TiO_2, similar to the granulites in this study (Table 5; Fig. 12). The sample has higher MgO and CaO than other samples: ~10 wt% and ~17 wt%. Using the whole rock Na_2O concentration of 1.63 wt% and a modal abundance of ~60% Cpx a rough estimate of the sodium concentration in pyroxene for this sample can be estimated. This estimates ~2.7 wt% Na_2O in clinopyroxene for this sample, which is slightly lower than the EMP results from the Cpx analyzed from granulites D212B and D213B. Similar Cpx compositions to the granulites suggests sample D211C experienced similar HP-granulite conditions.

TABLE 5. WHOLE ROCK ANALYSIS RESULTS, XRF, NORTH QAIDAM, WESTERN CHINA

Sample	D66B	D136B	D143	D211C	D212B
Rock type	Eclogite	Granulite leucosome	Banded granulite	Grt-clinopyroxenite	Mafic granulite
Major element oxide (wt%)					
SiO_2	45.75	73.72	61.42	47.42	43.48
TiO_2	1.441	0.144	0.167	0.195	0.936
Al_2O_3	16.00	11.73	17.04	14.95	19.33
FeO*	13.53	3.43	4.32	7.24	15.52
MnO	0.265	0.121	0.066	0.159	0.298
MgO	8.62	0.62	4.16	10.54	6.21
CaO	12.28	8.40	6.19	17.31	10.86
Na_2O	1.80	0.31	5.43	1.63	1.67
K_2O	0.26	0.09	0.31	0.24	0.13
P_2O_5	0.013	0.037	0.062	0.020	0.208
Sum	99.96	98.61	99.17	99.70	98.64
LOI	0.79	0.80	0.45	0.85	1.21
Trace element (ppm)					
Ni	99	1	25	48	6
Cr	342	6	74	150	2
Sc	50	10	17	68	51
V	348	144	143	192	440
Ba	28	21	149	50	21
Rb	12	5	4	10	7
Sr	67	1321	638	365	556
Zr	68	33	43	5	10
Y	25	3	3	6	24
Nb	5.4	1.8	1.0	0.4	2.3
Ga	16	16	18	12	20
Cu	159	12	51	35	184
Zn	95	10	64	50	140
Pb	5	4	7	4	0
La	9	3	1	2	6
Ce	14	0	5	4	18
Th	0	0	0	0	0
Nd	9	0	3	5	19
U	1	0	1	0	2
Sum	1350	1589	1248	1006	1507

Note: FeO*: all Fe calculated as FeO.

TABLE 5. CONTINUED WHOLE ROCK ANALYSIS

Sample	D213B	D214	D217A	D213A	D217C
Rock type	Intermediate granulite	Intermediate granulite	Grt-Ky paragneiss	Tonalite	Rt-bearing tonalite
Major element oxide (wt%)					
SiO_2	56.03	54.62	67.98	72.79	69.44
TiO_2	0.426	0.493	0.791	0.053	0.491
Al_2O_3	15.94	18.48	15.32	15.55	16.16
FeO*	8.50	8.90	5.35	0.49	1.32
MnO	0.185	0.194	0.083	0.010	0.014
MgO	5.77	3.75	1.47	0.32	1.12
CaO	9.27	9.21	1.78	2.42	2.52
Na_2O	2.37	3.14	1.53	6.18	6.00
K_2O	0.28	0.22	4.03	0.43	1.09
P_2O_5	0.127	0.159	0.142	0.010	0.171
Sum	98.88	99.17	98.47	98.25	98.32
LOI	0.80	0.66	0.58	1.04	1.12
Trace element (ppm)					
Ni	34	8	3	3	5
Cr	156	8	50	4	14
Sc	34	31	19	2	2
V	231	274	76	16	45
Ba	68	94	711	190	402
Rb	14	6	147	15	26
Sr	315	589	116	620	1004
Zr	8	7	230	55	118
Y	10	8	50	0	2
Nb	1.1	2.6	14.2	0.7	4.6
Ga	15	19	18	13	18
Cu	53	62	19	4	10
Zn	77	88	60	14	31
Pb	2	2	9	22	16
La	7	4	3	0	68
Ce	14	13	10	0	132
Th	1	1	13	0	31
Nd	9	0	3	5	19
U	1	0	1	0	2
Sum	1049	1222	1555	958	1977

Note: FeO*: all Fe calculated as FeO.

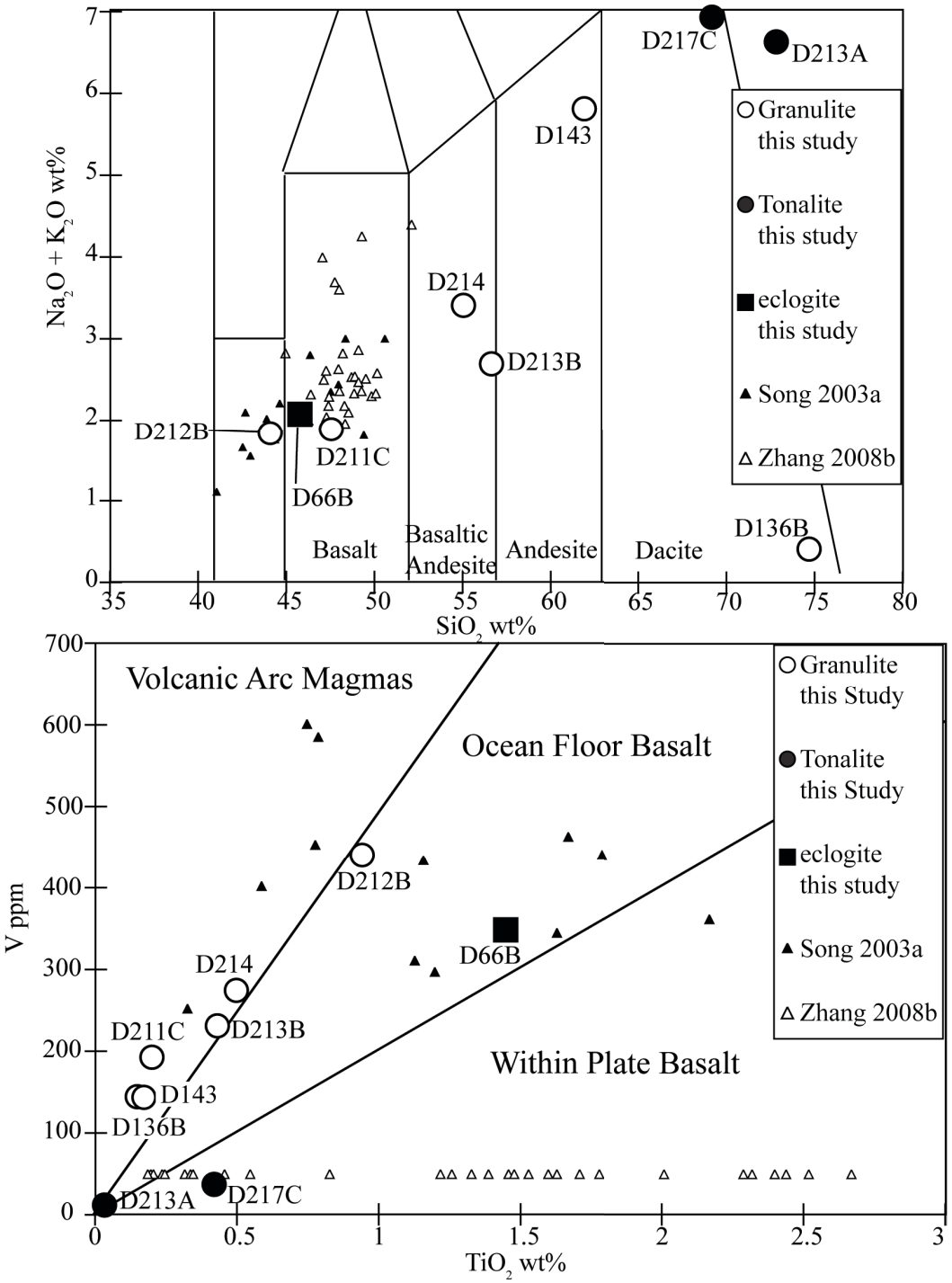

Figure 12. Whole rock results for nine metamorphic and igneous samples from this study. A) Total alkali-silica diagram including data from other studies from the Dulan eclogites. B) Discrimination diagram of V vs. TiO_2 (after Shervais, 1982) of samples from this study plotted against eclogite samples from Song et al., 2003. Data from Zhang et al., 2008b did not include V concentrations, and the TiO_2 data is plotted at V = 50 ppm for reference.

The two tonalite samples, D213A and D217C, have SiO_2 compositions of ~73 and ~69 wt%. Rt-bearing sample D217C contains elevated amounts of TiO_2, FeO, MgO, K_2O, and P_2O_5 compared to sample D213A (Table 5). The difference in TiO_2 is especially high. Sample D217C contains ~0.5 wt% TiO_2, similar to the granulite samples, whereas sample D213A contains <0.1 wt% TiO_2.

Mineral Chemistry Mafic Granulite D212B

Garnet from the mafic granulite is up to 5 mm across and garnets analyzed from the sample (Fig. 13 and 14) show a composition change from core ($Alm_{62-68}Grs_{17-23}Prp_{12-18}Sps_{1-3}$) to rim ($Alm_{46-64}Grs_{18-24}Prp_{16-32}Sps_{1}$). Almandine decreases towards the rim while Prp increases. The very edge of garnet grains (<200 μm) show the opposite trend where Alm increases and Prp decreases. Grossular varies by <10% mole fraction, and increases from core to rim, with a decrease at the very edge.

Clinopyroxene compositions are homogenous throughout the sample and vary by no more than ~5% ($Aug_{80-85}Jd_{09-15}Aeg_{04-08}$; Fig. 15A). End-member mole fractions were calculated after Harlow (1999). The CaTs component also varies by ~5% throughout the sample ($CaTs_{13-17}$), with higher CaTs associated with lower Jd component (Fig. 15B).

Plagioclase in the mafic granulite varies in composition from grain to grain (An_{23-29}), but individual grains vary by <3 % An content. Grains do not show evidence of zoning from the core to the rim.

Clinozoisite varies in compositions from core to rim in both matrix grains and inclusions. Matrix grains contain X_{Fe} = 0.114–0.187 (X_{Fe} = Fe/[Fe + Al], all Fe assumed

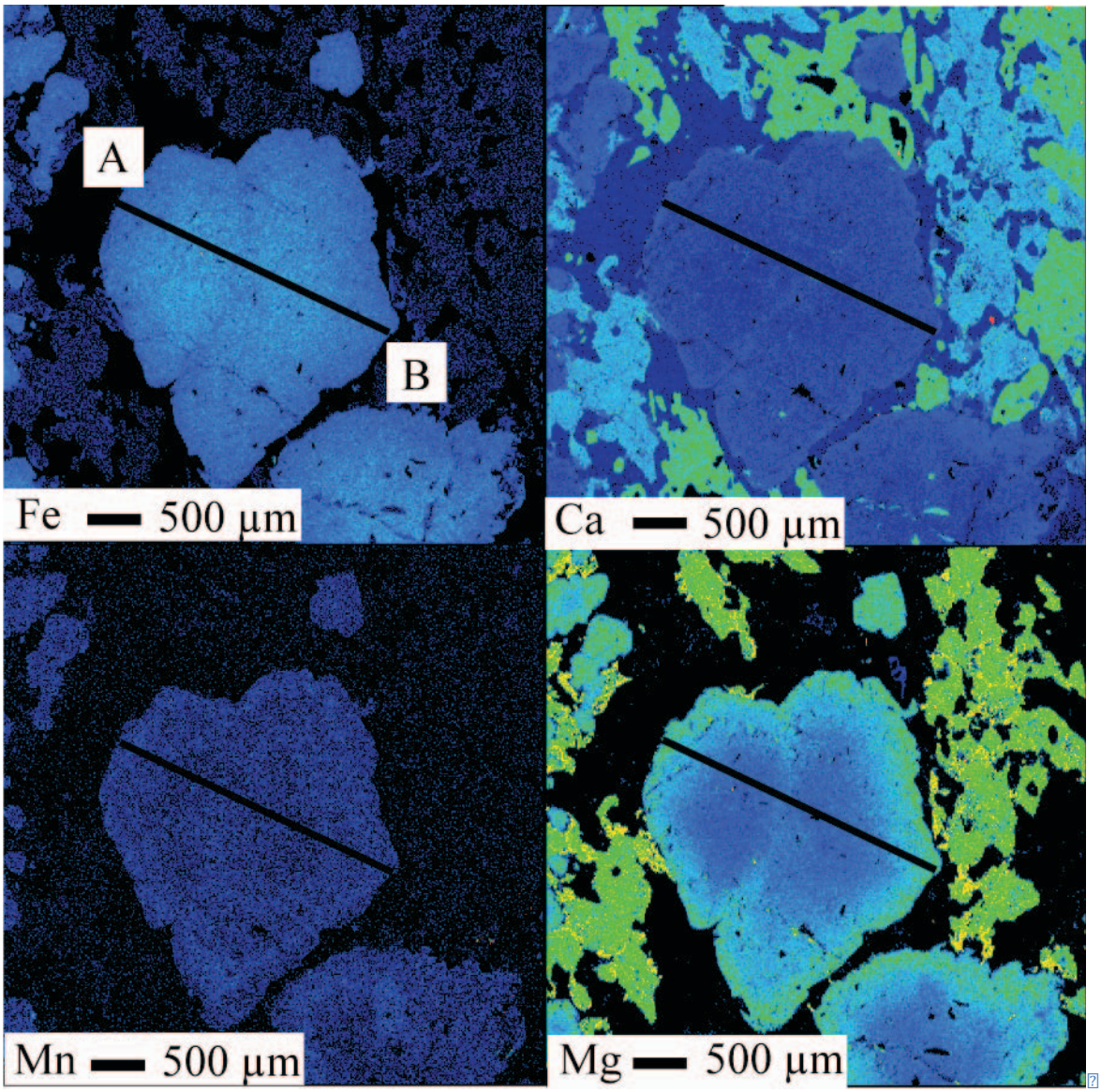

Figure 13. X-ray map showing the compositional change in garnet from mafic granulite sample D212B (transect Grt1, see Fig. 14). Dark lines indicate the EMP transect location used for P-T calculation (see text). Colors are relative with compositions increasing from black-blue-yellow-orange-red.

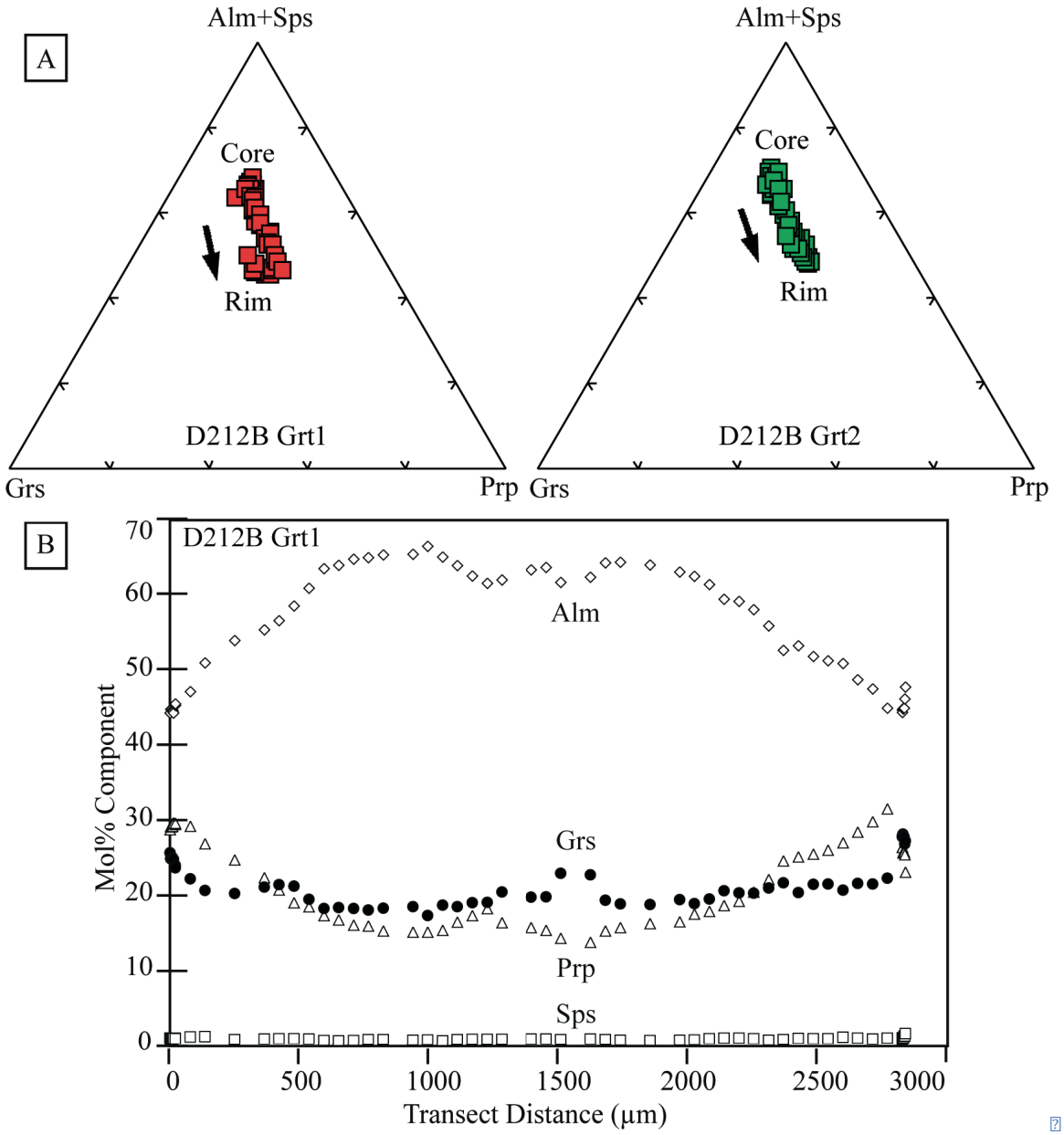

Figure 14. Representative plots for garnet from mafic granulite sample D212B. A) Ternary (Alm + Sps) + Prp + Grs diagrams of analyzed garnets with arrows showing core to rim trend. B) Compositional zoning profile of D212B Grt1 transect seen in Fig. 13.

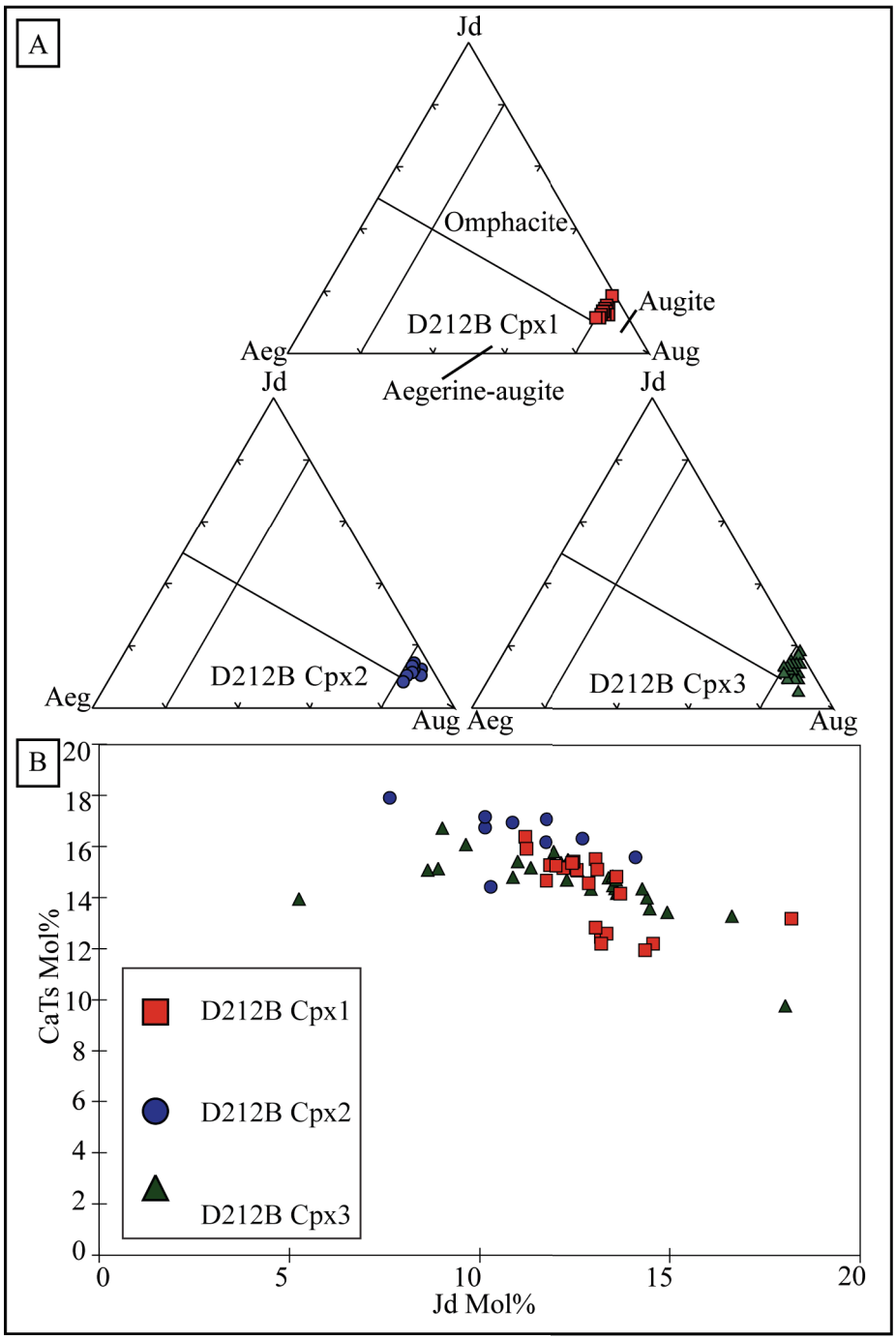

Figure 15. Plots for Cpx analysis from mafic granulite sample D212B. A) Ternary Jd-Aeg-Aug plots for three analyzed clinopyroxene grains; end-member compositions are calculated after Harlow (1999). B) Plot of CaTs vs. Jd for Cpx from the same sample.

to be Fe^{3+}; Fig. 16). The higher X_{Fe} values occur in the cores. All grains are somewhat deficient in calcium (Ca pfu < 1.974) with a trend to more Ca deficient cores with

increasing X_{Fe} values. Strontium or REE substitution for Ca may explain the Ca pfu values < 2.0; however, these elements were not measured in this study. One clinozoisite (Fig. 16, D212B Czo2) included within the rim of a garnet has a similar compositional trend as the matrix clinozoisite but contains higher X_{Fe} = 0.154-0.195. The included clinozoisite is also more deficient in calcium with Ca pfu <1.943.

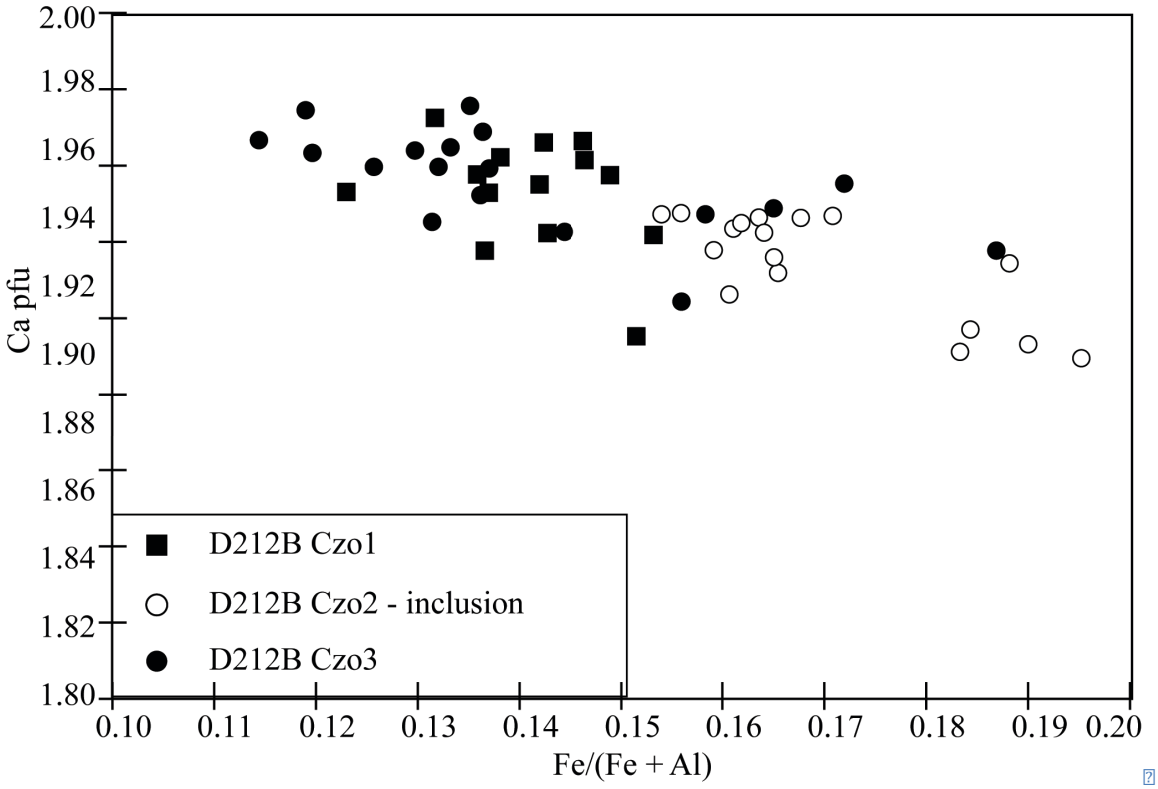

Figure 16. Plot of Ca vs. Fe/(Fe+Al) for mafic granulite sample D212B (all iron assumed Fe^{3+}). D212B Czo2 is an inclusion within D212B Grt2 (see Fig. 14 and appendix D).

Mineral Chemistry Intermediate Granulite D213B

Garnet from the intermediate granulite is up to 5 mm across and garnets analyzed from the sample (Fig. 17 and 18) show a composition change from core ($Alm_{51-59}Grs_{23-28}Prp_{11-20}Sps_{1-8}$) to rim ($Alm_{36-52}Grs_{18-24}Prp_{21-41}Sps_{1}$). Almandine and Grs decrease

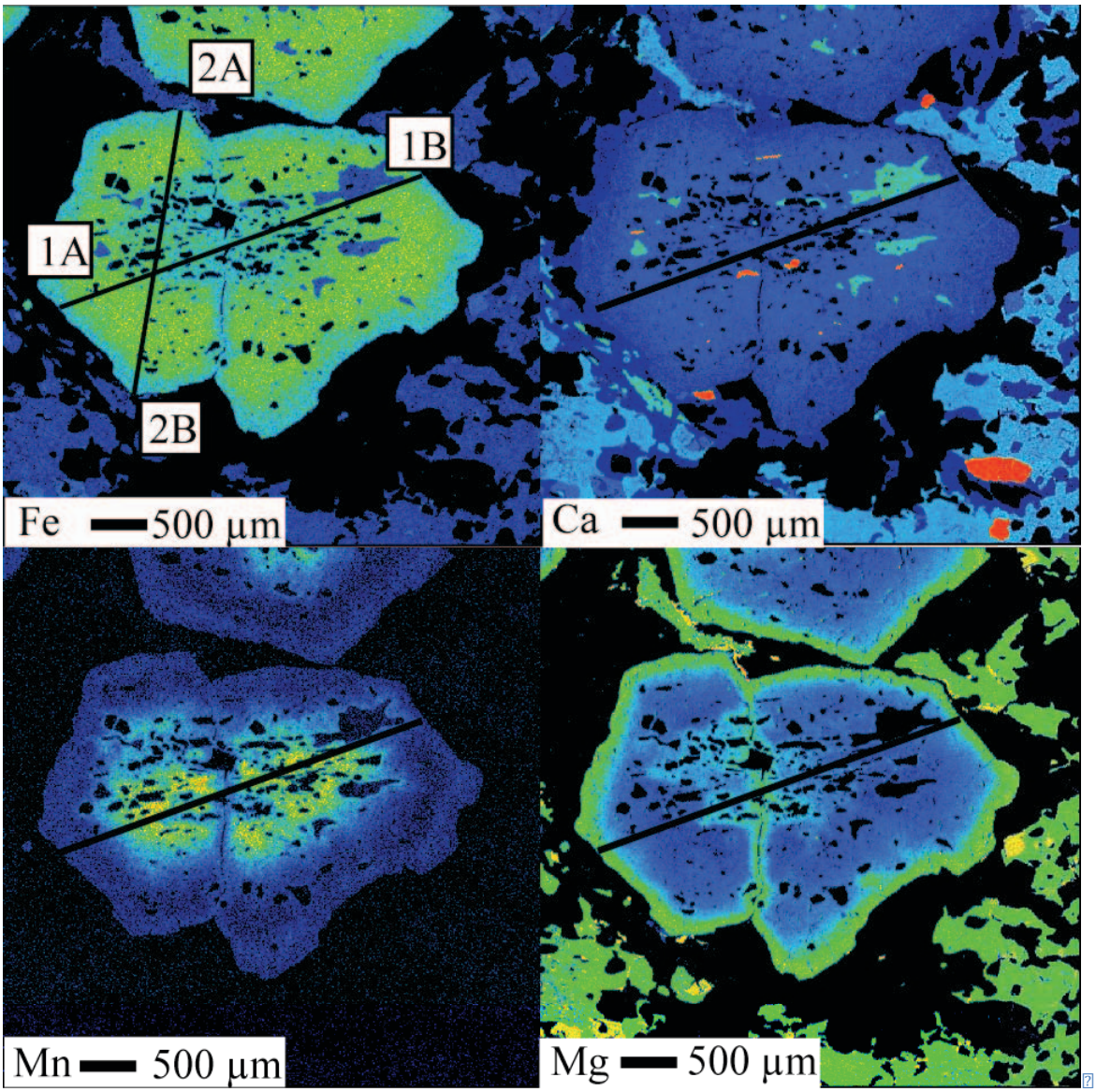

Figure 17. X-ray map showing the compositional change in garnet from intermediate granulite sample D213B (transect Grt1 and Grt2, see Fig. 18). Dark lines indicate the location of EMP transects (Grt1) used for P-T calculations (see text). Colors are relative with compositions increasing from black-blue-yellow-orange-red.

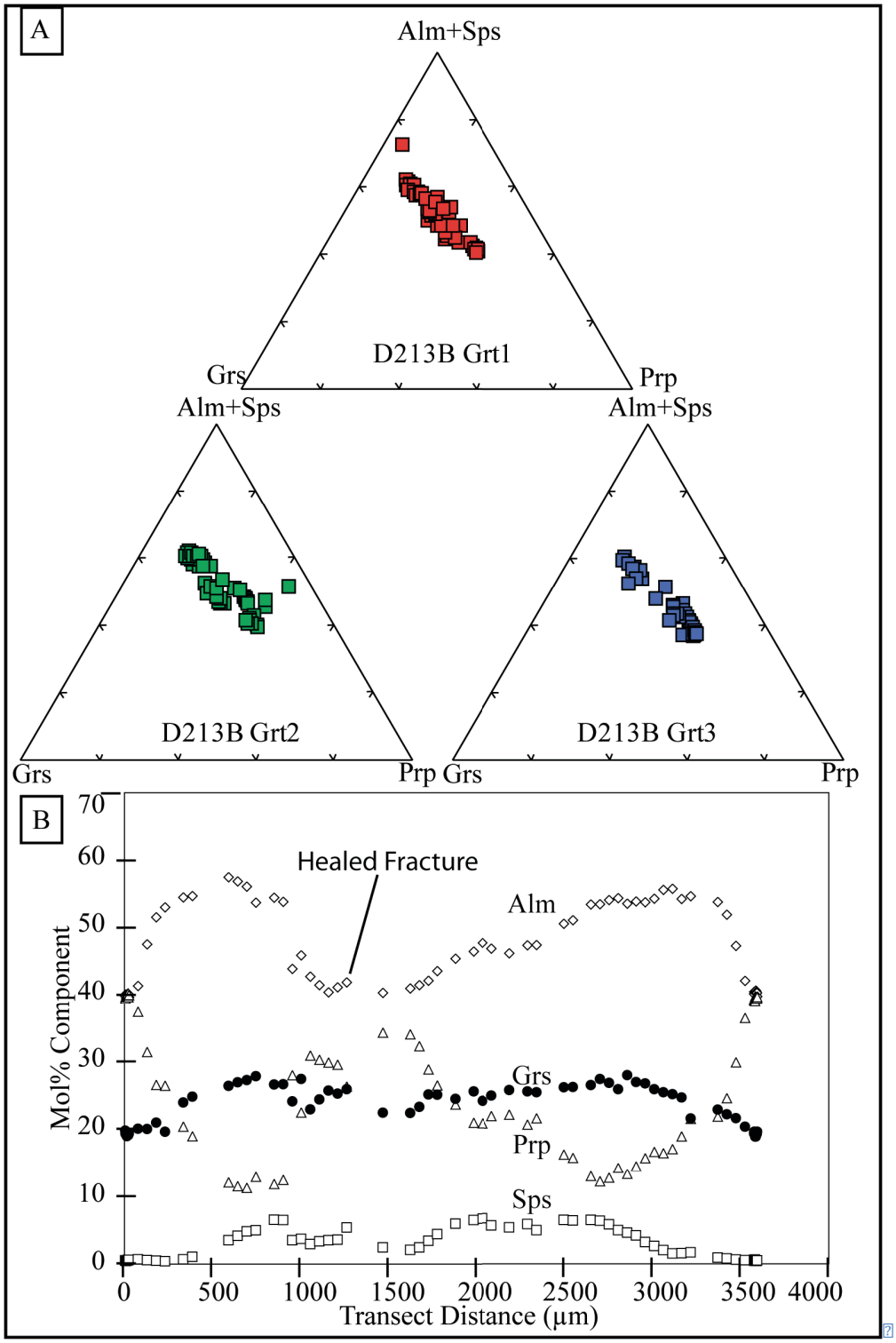

Figure 18. Representative plots for garnet from intermediate granulite sample D213B. A) Ternary (Alm + Sps) + Prp + Grs diagrams of analyzed garnets. Transect D213B Grt2 comes from the same grain as D213B Grt1 (see Fig. 17). B) Compositional zoning profile of D213B Grt1 transect seen in Fig. 17.

towards the rim while Prp increases.

Clinopyroxene grains are homogenous throughout the sample, with end-member mole fractions varying by <6 % ($Aug_{79-85}Jd_{10-16}Aeg_{04-08}$; Fig. 19A). The CaTs component varies by ~6% throughout the sample ($CaTs_{12-17}$), with higher CaTs associated with lower Jd component (Fig. 19B).

Plagioclase in the intermediate granulite varies in composition from grain to grain (An_{24-29}), with individual grains varying by <4% in An content. Grains show no compositional trends from core to rim.

Clinozoisite matrix grains contain X_{Fe} = 0.139–0.167 (Fig. 20). Values for X_{Fe} are higher in the Czo cores. All grains are somewhat deficient in calcium (Ca pfu <1.964) with cores containing less calcium than the rims. One clinozoisite (Fig. 20, D213B Czo4) included within the rim of a garnet (D213B Grt3) has a similar compositional trend as the matrix clinozoisite but contains higher X_{Fe} = 0.155–0.186. The other Czo inclusion, D213B Czo2 (in D213B Grt1/Grt2), shows the opposite trend in X_{Fe} and Ca content, with the lower X_{Fe} values and higher Ca content in the cores instead of the rims like the other analyzed grains.

Mineral Chemistry Grt-Ky Gneiss D217A

Garnets from the Grt-Ky gneiss are generally smaller than 0.5 mm, and are more homogeneous than the larger garnets in the granulite samples (Fig. 21 and 22). There is a slight variation in composition from core ($Alm_{58-62}Grs_{26-31}Prp_{8-11}Sps_{1-4}$) to rim ($Alm_{55-59}Grs_{18-26}Prp_{10-24}Sps_{1}$).

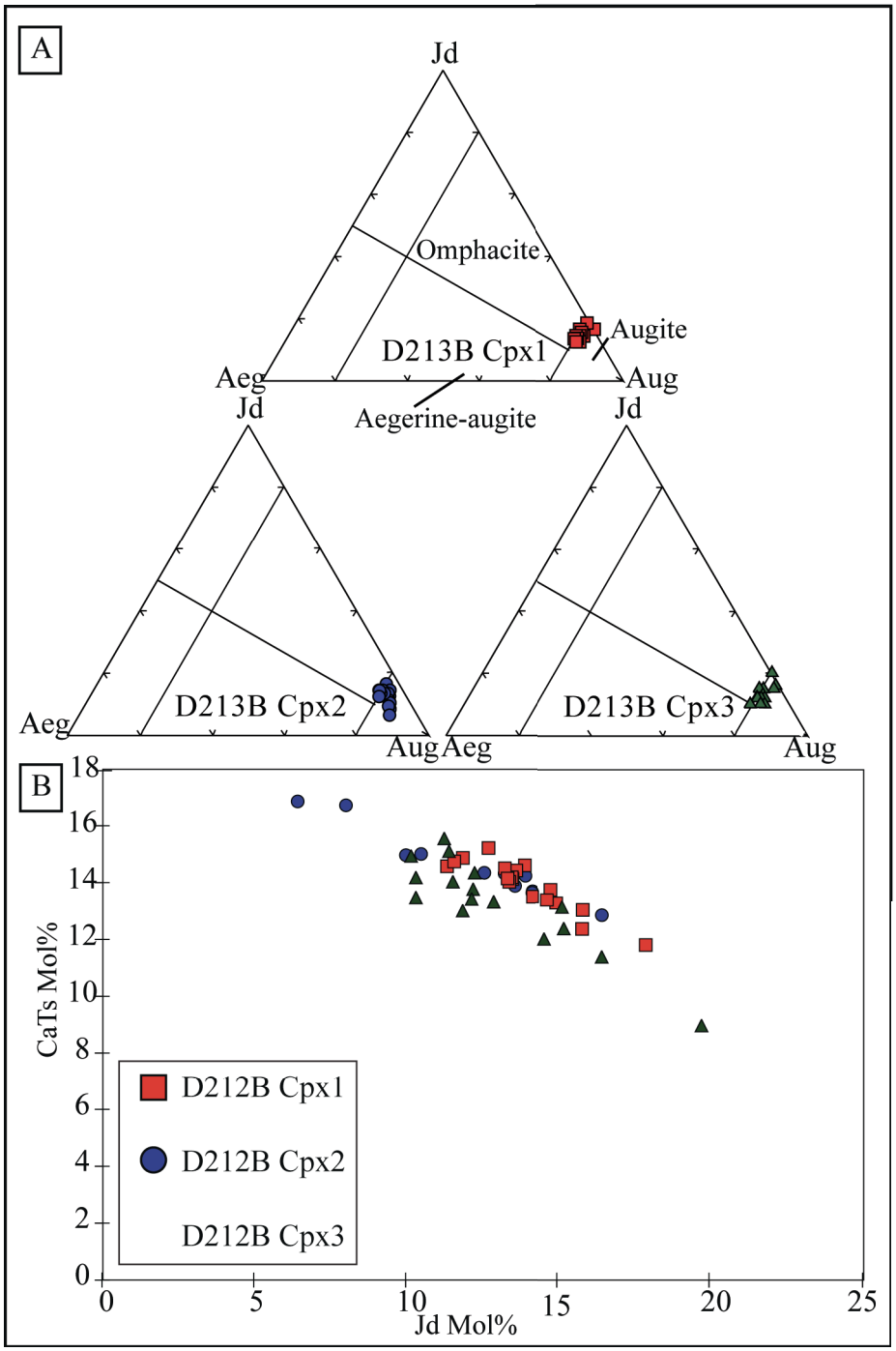

Figure 19. Plots for Cpx analysis from intermediate granulite sample D213B. A) Ternary Jd-Aeg-Aug plots for three analyzed clinopyroxene grains; end-member compositions are calculated after Harlow (1999). B) Plot of CaTs vs. Jd for Cpx from the same sample.

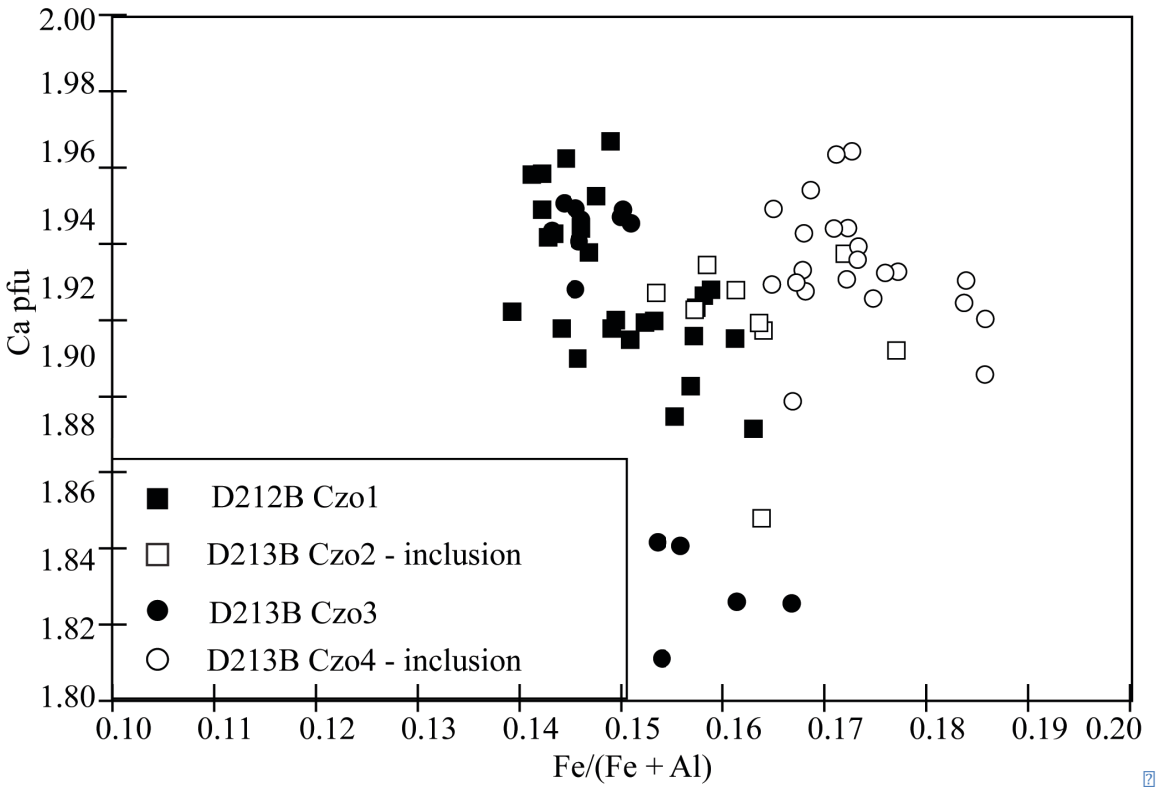

Figure 20. Plot of Ca vs. Fe/(Fe + Al) for intermediate granulite sample D213B (all iron assumed Fe^{3+}). Analysis D213B Czo2 was an inclusion within D213 Grt1 (and Grt2) and analysis D213B Czo4 was an inclusion within D213B Grt3 (see Fig. 17 and appendix D).

Pressure-Temperature-Time Analysis

Mafic Granulite D212B

Zircons from the mafic granulite sample (D212B) show sector and oscillatory zoned medium CL cores and unzoned dark CL rims up to ~25 µm wide (analyses 6 and 7, Fig. 23A). Some grains also have CL bright rims, which are <15 µm wide (analysis 10, Fig. 23A). Twenty-two analyses of cores and CL dark rims yield 54–1148 ppm U, 23–558 ppm Th, 0.44–0.84 Th/U, and ages from 429 to 459 Ma (Table 6). Based on 17 of the analyses, these zircons yield a mean age of 449 ± 3 Ma (Fig. 23B, MSWD = 1.83). Two analyses of the CL bright rims yield 1–11 ppm U, 0.4–1 ppm Th, 0.32–0.60 Th/U,

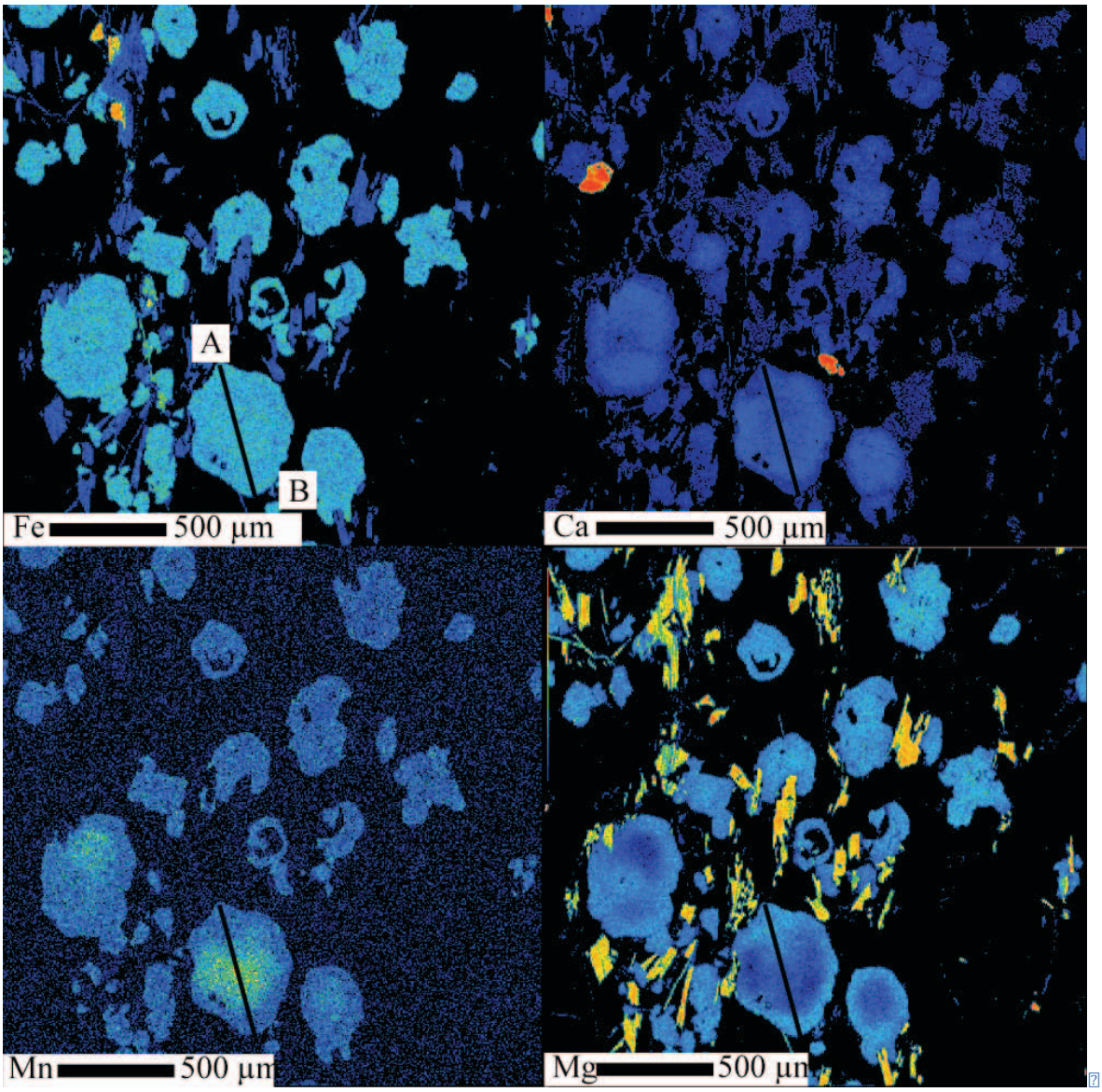

Figure 21. X-ray map showing the compositional change in garnet from Grt-Ky gneiss sample D217A (transect Grt1, see Fig. 22), dark lines indicate the location of EMP transect which started at A and ended at B. Colors are relative with compositions increasing from black-blue-yellow-orange-red.

and ages of 377 ± 15 and 421 ± 63 Ma. The larger uncertainty in these bright CL ages is due to the low U concentrations.

Of 37 trace element analyses, 6 contain elevated contaminants (Table 7, Fig. 24A). Cores and dark CL rims are characterized by a weak Eu anomaly (Eu/Eu* = 0.38–

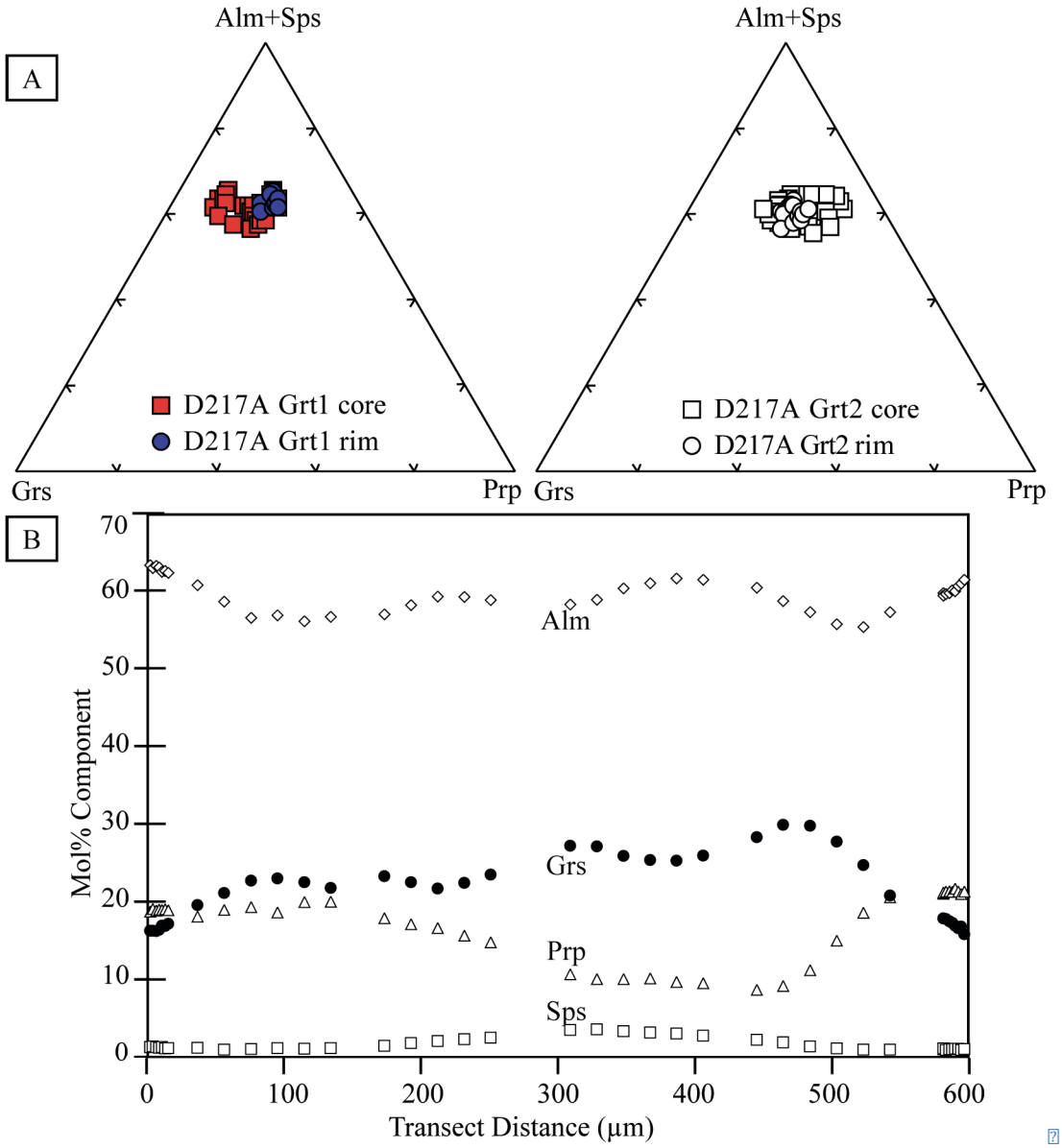

Figure 22. Representative plots for garnet from Grt-Ky gneiss sample D217A. A) Ternary (Alm + Sps) + Prp + Grs diagrams of analyzed garnets. B) Compositional zoning profile of D217A Grt1 transect seen in Fig. 21.

0.91) and steep HREE patterns (Yb/Gd = 28–47). Ti-in-zircon thermometry (Ferry and Watson, 2007) yields temperatures of 667–761 ˚C, with one outlier at 802 ˚C (Fig. 24B). Four analyses of bright CL rims contain low abundances of REEs (Fig. 24A, Eu/Eu* = 0.23–1.7, Yb/Gd = 83–1153) and Ti-in-zircon temperatures from 604–697 ˚C. Rare earth

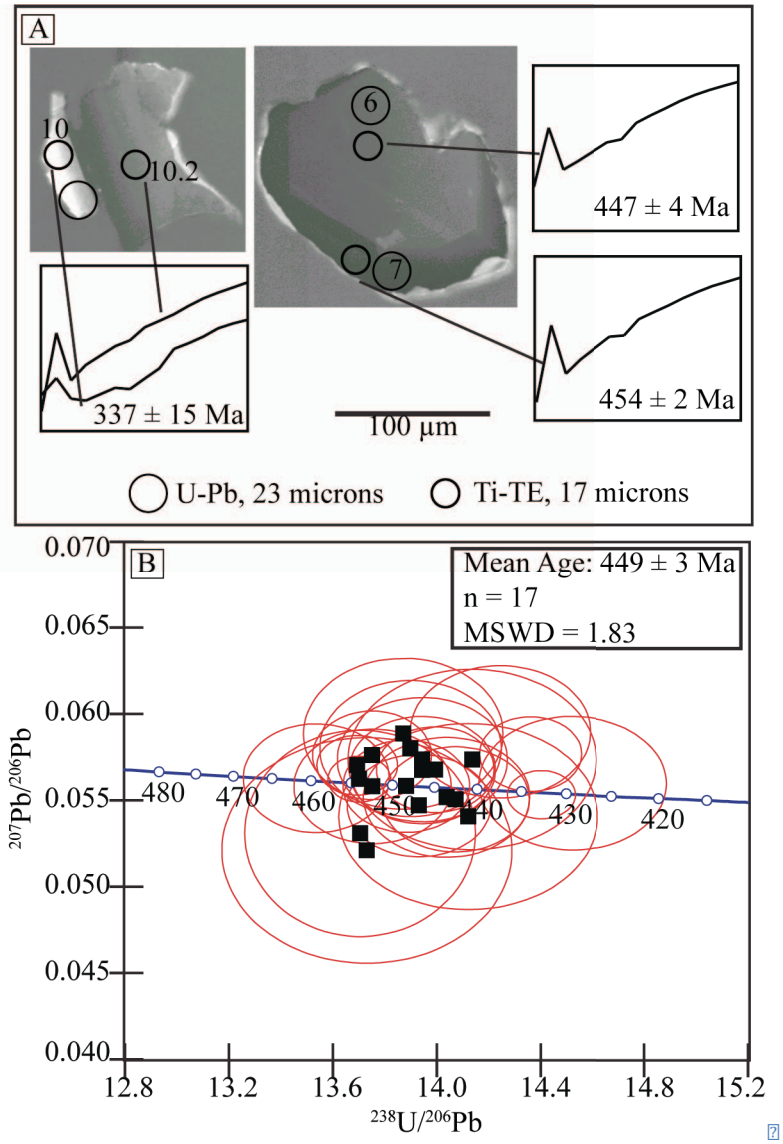

Figure 23. Results for SHRIMP-RG U-Pb zircon analysis for mafic granulite sample D212B. A) Example zircons taken from the sample showing zoned cores (spot 6 and 10.2), dark CL rims (spot 7), and bright CL rims (spot 10). U-Pb indicates spots for geochronology, Ti-TE indicates spots for trace element analysis. B) U-Pb Terra-Wasserburg (Terra and Wasserburg, 1972) plot for sample D212B, squares represent analyses used in mean age calculation (error ellipses are 2 sigma; mean age includes both cores and rims).

element abundances are low for these bright CL rims and approach the detection limit of the instrument, causing zero values for some trace elements. Only two albite inclusions, located in the zircon cores, were identified by EDS analyses.

TABLE 6. ZIRCON U-Pb ISOTOPIC DATA, MAFIC GRANULITE SAMPLE D212B, NORTH QAIDAM TERRANE, WESTERN CHINA

Analysis	CL	$^{206}Pb_c$ %	U (ppm)	Th (ppm)	$^{232}Th/^{238}U$	^{207}Pb-corr $^{206}Pb/^{238}U$ age (Ma, ±1σ err)	Total $^{238}U/^{206}Pb$ (± % err)	Total $^{207}Pb/^{206}Pb$ (± % err)
D212B-1*	C	0.13	320	169	0.55	444.3 ± 2.9	14.00 ± 0.7	0.0568 ± 1.8
D212B-2	R	0.43	145	70	0.49	435.6 ± 4.3	14.24 ± 1.0	0.0590 ± 2.6
D212B-3	R	-	920	390	0.44	432.8 ± 1.6	14.40 ± 0.4	0.0554 ± 1.0
D212B-4*	C	0.27	147	68	0.48	446.7 ± 4.6	13.90 ± 1.0	0.0581 ± 2.8
D212B-5*	C	0.00	285	135	0.49	448.4 ± 3.2	13.88 ± 0.7	0.0559 ± 2.0
D212B-6*	C	-	232	110	0.49	447.4 ± 3.6	13.93 ± 0.8	0.0549 ± 2.2
D212B-7*	R	0.03	1148	558	0.50	453.9 ± 1.6	13.70 ± 0.4	0.0563 ± 1.0
D212B-8*	R	0.13	672	286	0.44	453.7 ± 2.1	13.70 ± 0.5	0.0571 ± 1.2
D212B-9*	R	0.22	77	34	0.45	439.7 ± 6.0	14.14 ± 1.4	0.0574 ± 3.7
D212B-10	BR	0.75	11	3	0.52	376.9 ± 15	16.48 ± 4.0	0.0602 ± 12
D212B-11	C	0.28	449	364	0.84	432.8 ± 2.4	14.36 ± 0.6	0.0577 ± 1.5
D212B-12*	R	0.38	117	52	0.46	447.1 ± 5.0	13.87 ± 1.1	0.0589 ± 3.0
D212B-13	C	0.08	134	104	0.80	428.9 ± 4.3	14.52 ± 1.0	0.0561 ± 2.8
D212B-14*	C	0.21	326	219	0.69	451.6 ± 3.0	13.75 ± 0.7	0.0577 ± 1.8
D212B-15*	C	0.20	166	75	0.47	445.6 ± 4.2	13.95 ± 1.0	0.0574 ± 2.6
D212B-16*	R	-	54	23	0.44	455.2 ± 7.5	13.73 ± 1.7	0.0522 ± 5.1
D212B-17*	R	0.12	222	96	0.45	445.9 ± 3.6	13.94 ± 0.8	0.0568 ± 2.2
D212B-18*	C	-	221	182	0.85	442.9 ± 3.6	14.07 ± 0.8	0.0551 ± 2.3
D212B-19	BR	13	0.74	0.43	0.60	421.3 ± 63	12.82 ± 14	0.1638 ± 22
D212B-20	C	0.02	223	133	0.62	459.3 ± 3.9	13.54 ± 0.8	0.0564 ± 2.3
D212B-21*	C	-	174	90	0.53	443.9 ± 4.1	14.04 ± 0.9	0.0552 ± 2.6
D212B-22*	R	-	86	38	0.46	455.5 ± 6.0	13.71 ± 1.3	0.0532 ± 4.6
D212B-23*	C	-	189	115	0.63	452.5 ± 4.0	13.75 ± 0.9	0.0559 ± 2.4
D212B-24*	C	-	73	37	0.52	441.9 ± 6.3	14.12 ± 1.4	0.0541 ± 4.1

Note: Cathodoluminescence abbreviations as follows: C = Core, R = Rim, and BR = Bright CL rim.
*Analysis used in weighted mean age calculation.

TABLE 7. ZIRCON TRACE-ELEMENT RESULTS (PPM) FOR MAFIC GRANULITE SAMPLE D212B, NORTH QAIDAM, WESTERN CHINA

Analysis	CL	Li	Be	B	F	Na	Al	P	K	Ca	Sc	^{48}Ti	^{49}Ti	Fe	Y	Nb	^{94}ZrH	La	Ce	Nd
D212B-1	C	0.3	0.00	0.0	4	6	12	449	5	2	196	8.8	8.9	2	856	1	1.6	0.010	12	0.44
D212B-2	R	5.4	0.00	0.0	6	17	32	317	12	4	176	10	11	1	761	2	2.3	0.014	16	0.67
D212B-2.2	BR	5.1	0.01	0.1	6	4	35	287	1	17	124	7.4	7.0	2	364	1	1.7	0.000	8	0.33
D212B-3	R	1.0	0.00	0.2	8	5	19	399	4	4	316	4.5	4.6	4	953	7	1.9	0.021	32	0.72
D212B-4	C	8.5	0.00	0.2	6	13	13	297	11	2	162	8.0	7.2	1	582	2	1.8	0.024	14	0.55
D212B-5	C	0.3	0.00	0.1	5	4	12	271	2	2	189	7.8	7.0	1	601	3	1.7	0.019	17	0.39
D212B-6	C	0.3	0.00	0.2	7	6	16	330	4	3	167	5.0	4.8	1	417	1	1.8	0.002	11	0.28
D212B-7	R	1.3	0.00	0.0	5	7	14	505	6	2	260	4.5	4.0	3	719	2	1.7	0.024	20	0.57
D212B-8	R	1.0	0.00	0.1	6	5	13	344	4	3	280	5.7	5.3	2	856	5	1.8	0.015	27	0.64
D212B-9	R	4.5	0.01	1.3	6	53	84	208	22	15	113	8.3	7.6	14	377	1	1.7	0.018	8	0.34
D212B-9.2	R	5.5	0.00	0.2	4	6	85	153	9	14	82	10	10	15	192	1	1.6	0.020	5	0.13
D212B-10	BR	0.7	0.00	0.1	5	10	12	24	6	6	70	4.4	4.5	1	12	0	1.6	0.011	0	0.01
D212B-10.2	C	5.5	0.00	0.0	5	5	13	281	3	2	167	10	9.5	1	510	3	1.6	0.002	13	0.41
D212B-11	C	21	0.01	0.3	5	126	260	312	64	8	119	11	10	12	1201	2	1.8	0.029	17	1.8
D212B-12	R	0.7	0.01	0.1	5	9	20	189	4	2	83	5.3	6.0	5	199	1	1.6	0.009	7	0.11
D212B-13	C	5.1	0.00	0.9	7	8	20	323	5	10	177	9.6	9.7	18	752	2	1.7	0.013	16	0.59
D212B-13.2	C	1.6	0.02	0.5	8	9	21	341	8	7	255	6.0	6.0	7	766	5	2.2	0.031	25	0.55
D212B-14	C	3.8	0.01	0.1	6	4	11	175	1	2	112	6.4	6.0	1	1084	1	1.8	0.058	12	2.0
D212B-14.2	C	8.2	0.01	0.4	7	9	18	234	5	7	117	5.9	6.1	3	404	1	1.7	0.011	6	0.29
D212B-15	C	6.7	0.00	0.1	5	10	14	304	11	2	200	9.6	9.6	1	678	3	1.6	0.009	17	0.61
D212B-16	R	6.9	0.00	0.3	8	7	376	193	10	5	85	10	10	44	202	0	1.5	0.020	4	0.15
D212B-16.2	R	6.4	0.00	0.0	3	4	19	180	2	4	87	18	18	2	195	1	1.6	0.018	5	0.12
D212B-16.3	BR	3.2	0.00	0.1	4	82	31	42	74	37	28	4.6	3.8	1	16	0	1.9	0.059	0	0.01
D212B-17	R	6.3	0.01	0.1	4	5	11	318	5	2	212	9.7	9.4	1	770	3	1.7	0.016	18	0.76
D212B-18	C	8.2	0.00	0.2	7	136	14	245	143	20	149	5.6	5.6	1	861	1	2.5	0.358	19	2.4
D212B-18.2	C	17	0.02	0.0	8	7	225	301	15	4	178	7.0	6.8	110	1125	2	1.8	0.027	25	3.4
D212B-19	BR	0.0	0.00	0.0	7	15	22	16	11	5	21	6.3	5.8	1	5	0	2.8	0.011	0	0.01
D212B-19.2	C	6.4	0.00	0.1	6	4	18	196	3	2	111	11	12	1	324	1	1.7	0.020	7	0.24
D212B-19.3	BR	3.4	0.00	0.1	7	136	244	388	58	12	194	16	16	3	1380	3	1.7	0.014	32	1.1
D212B-20	C	0.2	0.00	0.1	5	8	19	369	18	5	185	8.4	8.4	3	531	1	1.8	0.007	12	0.52
D212B-21	C	5.7	0.02	0.2	7	6	25	273	4	2	179	9.7	10	1	654	2	2.5	0.009	16	0.51
D212B-21.2	R	0.1	0.00	0.2	6	6	17	21	6	3	40	2.1	1.7	0	9	0	1.5	0.019	0	0.01
D212B-21.3	BR	13	0.01	0.2	6	5	15	358	3	6	290	9.6	9.9	4	767	4	1.7	0.012	21	0.46
D212B-22	R	5.1	0.01	0.3	6	751	875	201	96	20	109	8.1	7.9	2	307	1	1.8	0.027	7	0.35
D212B-23	C	4.4	0.00	0.1	8	11	12	338	11	4	177	11	11	1	1075	3	2.0	0.030	23	0.78
D212B-23.2	C	4.7	0.00	0.1	5	4	12	279	3	3	140	5.4	5.1	1	392	1	1.5	0.009	8	0.34
D212B-24	C	3.6	0.00	0.0	4	3	17	294	2	3	140	7.9	7.6	1	435	1	1.7	0.047	9	0.41

Note: Cathodoluminescence abbreviations as follows: C = Core, R = Rim, and BR = Bright CL rim

TABLE 7. CONTINUED.

Analysis	Sm†	Eu	Gd	Ho	Tb	Dy	Er	Tm	Yb	Lu	Hf	Th	U	Th/U	Ce/Ce*	Eu/Eu*	Yb/Gd	T ˚C ^{48}Ti	T ˚C ^{49}Ti
D212B-1	1.42	0.765	11	30	4.69	61	167	43	439	98	8728	193	333	0.58	166	0.59	40.2	725	735
D212B-2	1.29	0.790	10	26	3.67	51	143	37	378	88	8242	65	136	0.47	149	0.66	37.0	741	752
D212B-2.2	0.69	0.464	5	12	2.02	26	69	18	198	47	8252	29	59	0.50	–	0.73	36.4	712	714
D212B-3	1.53	0.712	13	33	5.00	65	186	49	516	121	16874	521	1165	0.45	227	0.48	39.1	672	679
D212B-4	1.01	0.641	7	20	2.90	37	113	31	329	78	9241	74	162	0.46	100	0.72	45.6	718	716
D212B-5	1.02	0.576	9	21	3.09	43	116	30	312	72	11242	124	243	0.51	153	0.59	35.9	715	713
D212B-6	0.86	0.373	6	14	2.36	30	77	21	213	50	13543	107	219	0.49	472	0.48	33.0	680	681
D212B-7	1.18	0.607	11	26	4.22	56	137	34	351	77	16012	415	708	0.59	142	0.52	32.5	672	667
D212B-8	1.55	0.664	12	30	4.38	59	170	46	465	108	13263	237	540	0.44	240	0.46	37.9	690	689
D212B-9	0.81	0.488	6	13	2.19	26	71	19	207	51	8969	34	74	0.46	84	0.67	33.9	721	721
D212B-9.2	0.44	0.179	2	7	1.10	14	38	10	112	27	10655	26	63	0.41	61	0.53	46.6	739	748
D212B-10	0.01	0.005	0	0	0.02	1	2	1	9	2	24358	2	5	0.42	6	0.56	187	671	677
D212B-10.2	0.84	0.567	7	17	2.49	32	100	27	298	74	10386	79	198	0.40	486	0.70	41.6	737	741
D212B-11	2.90	1.69	25	46	8.50	99	228	54	524	114	9404	399	479	0.83	71	0.60	21.0	743	746
D212B-12	0.46	0.210	4	7	1.06	15	38	10	102	23	12152	58	113	0.51	168	0.50	28.5	684	700
D212B-13	1.44	0.811	12	26	4.32	53	142	37	377	87	8566	75	140	0.54	166	0.60	32.2	734	743
D212B-13.2	1.47	0.517	11	28	4.15	55	147	38	388	90	16639	490	976	0.50	148	0.38	34.2	694	700
D212B-14	2.80	1.92	19	42	7.32	89	216	52	515	113	8910	212	322	0.66	31	0.81	27.7	699	701
D212B-14.2	0.53	0.518	6	15	2.31	30	85	22	243	56	8571	64	145	0.45	90	0.91	43.7	693	701
D212B-15	1.34	0.673	8	23	3.41	45	134	34	367	87	9329	83	176	0.47	223	0.61	44.4	734	742
D212B-16	0.29	0.278	3	6	1.08	14	38	10	112	28	9344	18	44	0.42	49	0.94	40.3	737	748
D212B-16.2	0.37	0.227	3	7	1.05	14	36	10	109	26	10678	28	61	0.45	68	0.70	41.7	789	802
D212B-16.3	0.03	0.014	0	1	0.01	1	5	2	27	10	9285	0	17	0.02	3	1.7	1153	674	663
D212B-17	1.18	0.793	10	27	3.80	52	151	40	425	98	9414	102	215	0.48	151	0.71	43.9	735	740
D212B-18	3.48	1.77	20	32	6.32	70	151	36	344	77	10060	197	222	0.89	14	0.64	16.9	689	695
D212B-18.2	4.12	2.27	25	40	7.37	87	208	52	534	120	10003	278	366	0.76	92	0.68	21.4	707	711
D212B-19	0.08	0.000	0	0	0.02	1	1	0	3	1	17724	0	1	0.63	3	0.00	113	699	697
D212B-19.2	0.59	0.461	5	11	1.60	20	63	17	197	48	8872	31	80	0.39	74	0.85	42.8	749	761
D212B-19.3	2.18	1.55	20	50	8.18	105	261	64	634	137	8115	175	232	0.75	258	0.71	31.4	783	794
D212B-20	1.10	0.620	8	19	3.21	40	105	28	290	69	10755	118	199	0.60	191	0.62	34.5	722	730
D212B-21	1.40	0.690	9	22	3.14	41	121	32	330	78	8684	75	151	0.50	222	0.61	38.7	735	751
D212B-21.2	0.02	0.003	0	0	0.01	1	3	1	6	2	12539	0	1	0.13	2	0.23	82.6	616	604
D212B-21.3	1.17	0.687	11	27	3.81	49	152	41	427	99	11640	161	375	0.43	254	0.58	38.1	733	745
D212B-22	0.61	0.382	5	11	1.64	21	59	16	173	44	9479	38	85	0.45	57	0.64	32.5	719	725
D212B-23	1.71	1.19	17	38	6.26	80	201	51	510	114	8074	115	178	0.65	127	0.68	30.4	747	755
D212B-23.2	0.69	0.576	7	14	2.23	30	72	20	209	50	8549	31	63	0.50	134	0.81	31.3	686	687
D212B-24	0.83	0.547	7	14	2.34	32	80	22	232	55	8255	35	68	0.51	48	0.68	32.1	717	720

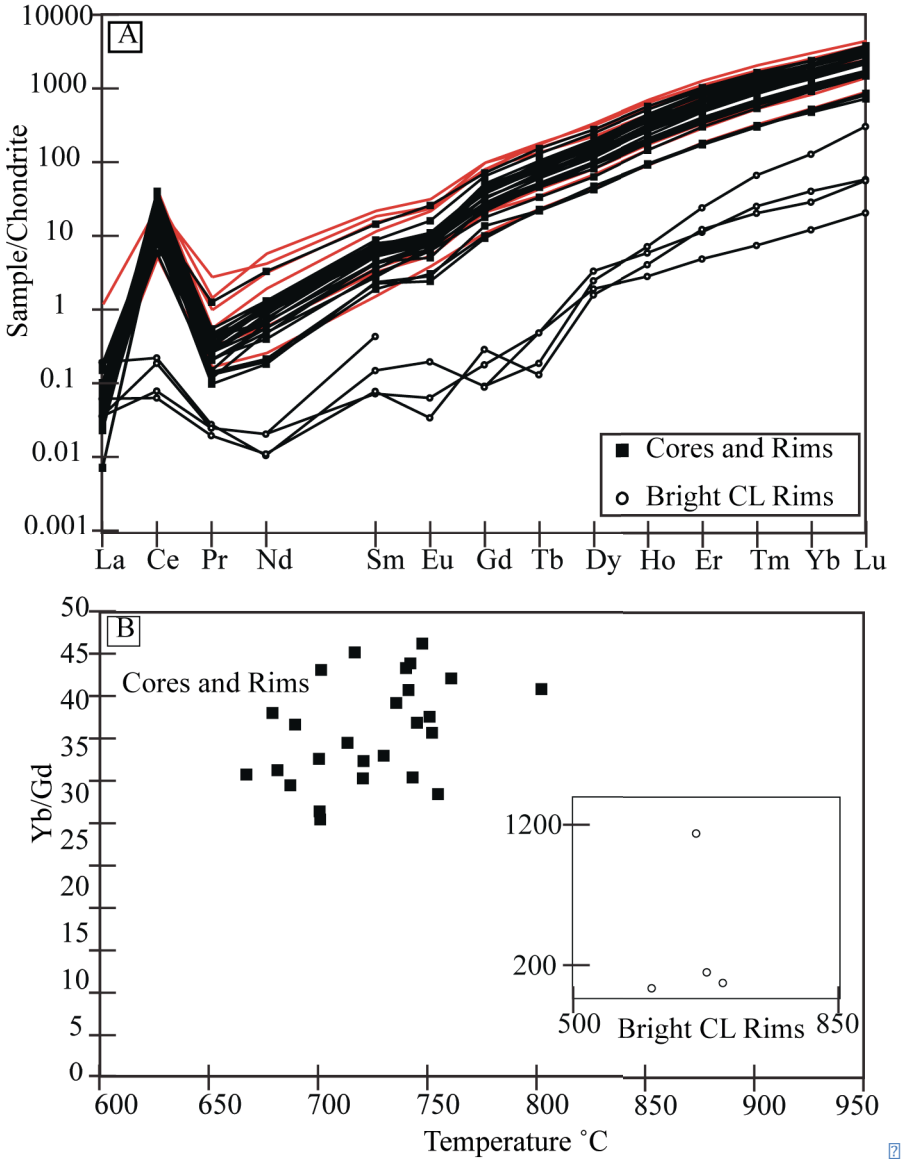

Figure 24. Zircon trace-element results for mafic granulite sample D212B. A) REE patterns for zircons, red lines indicate analyses with high contaminant levels (see text and table 7). B) Plot of Yb/Gd vs. Ti-in-zircon temperatures (Ferry and Watson, 2007; insert is for bright CL rims, see Fig. 23).

Garnet-clinopyroxene Fe-Mg exchange and GASP, GADS and Ab-Jd-Qtz barometry for the mafic granulite yield 790–880 ˚C and 14–16.5 kbar (Fig. 25). Results using the average mineral compositions are presented in Table 8.

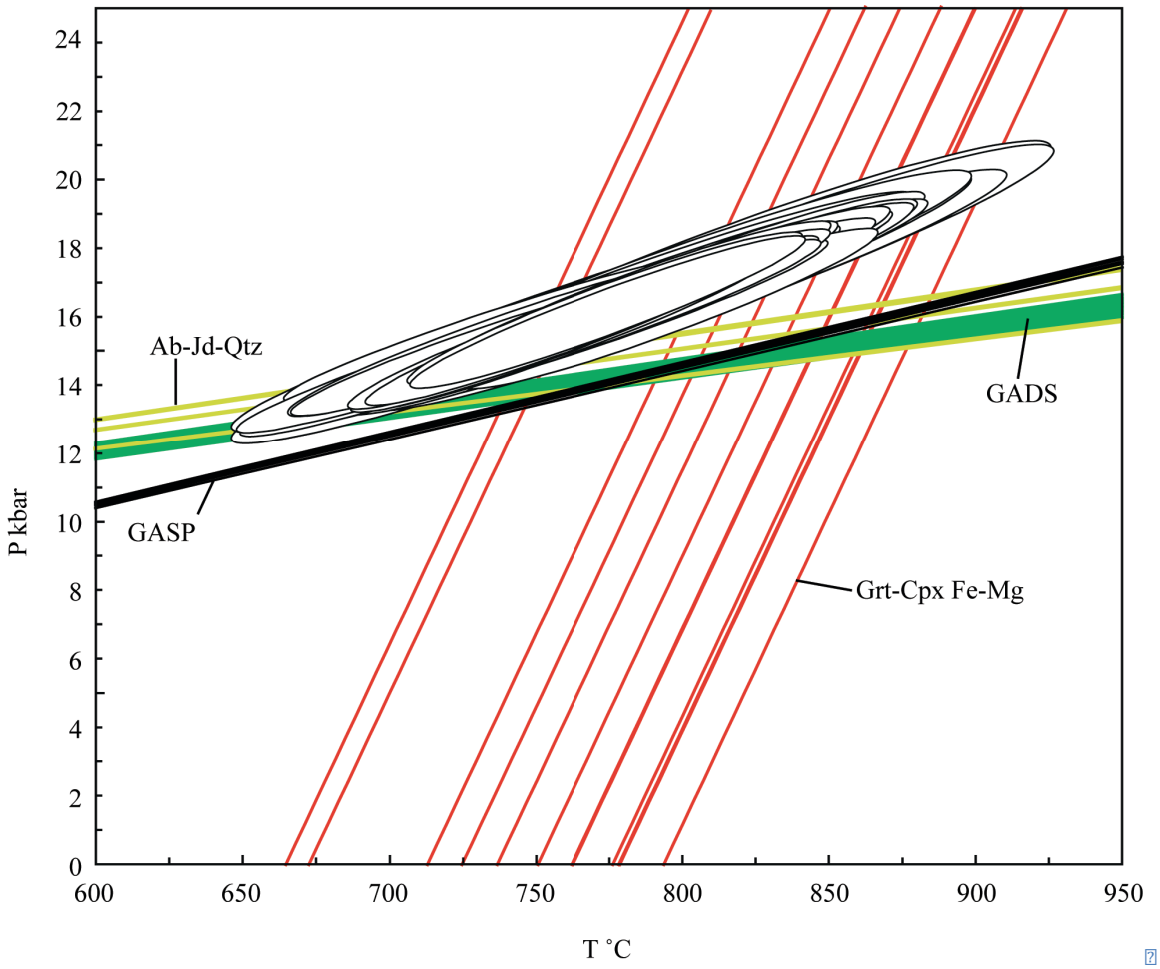

Figure 25. Pressure-temperature results for mafic granulite sample D212B. Iron-Magnesium exchange thermometer is after Pattison and Newton (1985), GASP barometer is after Hodges and Spear (1982), GADS barometer is after Newton and Perkins (1982) and Ab-Jd-Qtz barometer is after Holland (1982; see text for equations). White ellipses are average P-T results for program THERMOCALC v.3.33 (Holland and Powell, 1998), errors are 1 sigma.

Mineral compositions input into the program THERMOCALC v.3.33 yield a mean of 770 ˚C, 16 kbar (Fig. 25). Calculated errors range from 56–92 ˚C and 1.8–2.9 kbar. The program a-X did not calculated an activity for the Jd end-member for Cpx, which may explain the high activities of the CaTs component (~0.3). Such high CaTs activities drive the average P-T calculation beyond 1000 ˚C. This is well beyond peak conditions based on other data from this study, so the CaTs component was not used

TABLE 8. PRESSURE-TEMPERATURE CONDITIONS USING AVERAGE MINERAL COMPOSITIONS PLUGGED INTO PROGRAM GTB v.2.1

Mafic Granulite – D212B		Grt1A+Cpx1avg	Grt1A+Cpx2avg	Grt1B+Cpx1avg	Grt1B+Cpx2avg
Thermometer	P(kbar)	T (˚C)			
Grt-Cpx	14	802	855	790	839
	15	807	861	795	844
	16	813	866	801	850
		Grt1A+Cpx1avg+Pl1avg	Grt1A+Cpx2avg+Pl1avg	Grt1B+Cpx1avg+Pl1avg	Grt1B+Cpx2avg+Pl1avg
Barometer	T (˚C)	P (kbar)			
GADS*	750	14	14	14	14
	800	15	15	15	15
	850	15	15	15	15
GASP†		Grt1A+Pl1avg	Grt1B+Pl1avg		
	750	14	14		
	800	15	15		
	850	16	16		
Ab-Jd-Qtz§		Cpx1avg+Pl1avg	Cpx2avg+Pl1avg		
	750	15	15		
	800	16	15		
	850	16	16		

Note: Grt-Cpx thermometer is after Pattison and Newton, 1989.

*GASP barometer is after Hodges and Spear, 1982.

†GADS barometer is after Newton and Perkins, 1982.

§Ab-Jd-Qtz barometer is after Holland, 1982.

TABLE 8. CONTINUED

Intermediate Granulite–D213B		Grt1A+Cpx1avg	Grt1A+Cpx2avg	Grt1B+Cpx1avg	Grt1B+Cpx2avg
Thermometer	P(kbar)	T (˚C)			
Grt-Cpx	14	831	835	819	823
	15	836	841	824	829
	16	842	846	830	834
		Grt1A+Cpx1avg+Pl1avg	Grt1A+Cpx1avg+Pl2avg	Grt1A+Cpx2avg+Pl1avg	Grt1A+Cpx2avg+Pl2avg
Barometer	T (˚C)	P (kbar)			
GADS*	750	14	14	14	14
	800	14	14	14	14
	850	15	15	15	15
		Grt1B+Cpx1avg+Pl1avg	Grt1B+Cpx1avg+Pl2avg	Grt1B+Cpx2avg+Pl1avg	Grt1B+Cpx2avg+Pl2avg
	750	14	14	14	14
	800	14	14	14	14
	850	15	15	15	15
		Grt1A+Pl1avg	Grt1A+Pl2avg	Grt1B+Pl1avg	Grt1B+Pl2avg
GASP†	750	13	13	13	13
	800	14	14	14	14
	850	15	15	15	15
		Cpx1+Pl1avg	Cpx2avg+Pl1avg	Cpx1avg+Pl2avg	Cpx2avg+Pl2avg
Ab-Jd-Qtz§	750	15	15	15	15
	800	16	15	16	15
	850	16	16	16	16

Note: Grt-Cpx thermometer is after Pattison and Newton, 1989.

*GASP barometer is after Hodges and Spear, 1982.

†GADS barometer is after Newton and Perkins, 1982.

§Ab-Jd-Qtz barometer is after Holland, 1982.

TABLE 8. CONTINUED

Grt-Ky gneiss–D217A		Grt1+Bt1avg	Grt1+Bt2avg	Grt2+Bt3avg
Thermometer	P(kbar)	T (˚C)		
Grt-Bt	14	746	750	784
	15	750	754	788
	16	754	758	792
		Grt1+Pl1avg	Grt1+Pl2avg	
Barometer	T (˚C)	P (kbar)		
GASP	750	13.4	13.4	
	800	14.4	14.4	
	850	15.4	15.4	

Note: Grt-Bt thermometer and GSAP barometer after Hodges and Spear (1982).

in the average P-T calculations. Lowering the H_2O activity to 0.7 reduces the calculated temperature by ~20 ˚C and reduces the calculated pressure by ~0.4 kbar, with results being indistinguishable within error from calculations using higher activities. Lowering the activity of H_2O lowers the significance of fit from 0.94 to 0.87; however, there is no indication that one activity is better than the other. Based on the overlap in the calculated errors, an activity of 1.0 was chosen to represent metamorphic conditions. Results calculated using average mineral compositions are presented in Table 9.

Only one (D212B Grt1) of two Grt transects was used for P-T calculation for the mafic granulite sample. Garnet transect D212B Grt2 (analyzed with nearby Cpx3, Pl2 and Czo3, see appendix D) yielded low temperatures through Fe-Mg thermometry and high-errors for THERMOCALC average P-T calculations, therefore it was interpreted to not represent peak compositions.

Pressure-temperature conditions for this sample indicate peak conditions in the HP-granulite facies, which agrees with Ti-in-zircon temperatures. Based on albite inclusions in zircon, and Eu anomalies in zircon REE patterns, the mean age of 449 Ma is interpreted to represent HP-granulite metamorphism.

TABLE 9. AVERAGE PRESSURE-TEMPERATURE CONDITIONS CALCULATED USING THE PROGRAM THERMOCALC v3.33 AND AVERAGE MINERAL COMPOSITIONS

Sample	Mineral Combination	Temp (°C)	Error (°C)	Pressure (kbar)	Error (kbar)	Error Correlation	Significance of Fit	Reactions
D212B	Grt1A+Cpx1avg+Pl1max+Czo1avg	760	56	15.6	1.8	0.954	0.94	1,2,3,4
	Grt1A+Cpx2avg+Pl1max+Czo1avg	763	58	15.8	1.9	0.953	1.05	1,3,4,8
	Grt1B+Cpx1avg+Pl1max+Czo1avg	773	55	16.2	1.8	0.949	0.98	1,3,8,10
	Grt1B+Cpx2avg+Pl1max+Czo1avg	780	59	16.4	1.9	0.948	1.09	1,3,8,10
D213B	Grt1A+Cpx1avg+Pl1avg+Czo1avg	744	69	14.9	2.1	0.960	1.16	1,8,10,12
	Grt1A+Cpx1avg+Pl2avg+Czo1avg	743	69	14.9	2.1	0.958	1.16	1,8,10,12
	Grt1A+Cpx2avg+Pl1avg+Czo1avg	743	67	14.8	2.1	0.960	1.14	1,8,10,12
	Grt1A+Cpx2avg+Pl2avg+Czo1avg	743	68	14.9	2.1	0.958	1.14	1,8,10,12
	Grt1B+Cpx1avg+Pl1avg+Czo1avg	747	74	14.9	2.3	0.960	1.24	1,8,10,12
	Grt1B+Cpx1avg+Pl2avg+Czo1avg	746	74	15.0	2.3	0.958	1.25	1,8,10,12
	Grt1B+Cpx2avg+Pl1avg+Czo1avg	747	70	14.9	2.2	0.960	1.18	1,8,10,12
	Grt1B+Cpx2avg+Pl2avg+Czo1avg	746	71	15.0	2.2	0.958	1.19	1,8,10,12
D217A	Grt1+Ksp1avg+Pl1avg+Bt1avg	799	47	15.5	1.4	0.663	0.13	1,16,20,25
	Grt1+Ksp1avg+Pl1avg+Bt12avg	798	46	15.5	1.4	0.661	0.13	1,16,17,18

Intermediate Granulite D213B

Zircons from intermediate granulite sample, D213B, have medium CL cores with sector and oscillatory zones. Dark CL rims are monotonous or oscillatory zoned and up to ~30 μm wide (analysis 9, Fig. 26A). There are also CL medium to bright rims on some grains (analysis 19, Fig. 26A). Fourteen analyses of the zircon cores yield 85–268 ppm U, 7–49 ppm Th, 0.07–0.19 Th/U, and ages from 405 to 429 Ma (Table 10). Twelve analyses of the dark CL rims yield 360–673 ppm U, 56–207 ppm Th, 0.16 – 0.32 Th/U, and ages from 412 to 422 Ma (Table 10). Two spots on CL bright rims yield 57 and 76 ppm U, 5–6 ppm Th, 0.08 Th/U, and ages of 406 ± 6 and 416 ± 16 Ma. Ages were indistinguishable between the cores and rims and yield a mean age of 418 ± 2 Ma (Fig. 26B, n = 25, MSWD = 1.31).

Of 34 trace element analyses, 3 contain elevated contaminants (Table 11, Fig. 27A). Cores are characterized by the lack of an Eu anomaly (Eu/Eu* = 1.02–1.23, outlier at 1.40) and flat HREE patterns (Yb/Gd = 3.4–5.6). Rims generally have a slightly more negative Eu anomaly (Eu/Eu* = 0.98–1.10, outlier at 0.88) and flatter HREE patterns (Yb/Gd = 1.4–3.4) than cores. Bright CL rims are similar to the zircon cores: Eu/Eu* = 1.07–1.45 and Yb/Gd = 1.7–5.4. Along with the different Th/U values between the cores and rims (see above) there is also a large difference in Y between the cores and rims. Cores contain 129–262 (outlier 57) ppm Y while rims contain 306–693 ppm Y (outliers at 173, 189 and 981 ppm). Ti-in-zircon temperatures also differ from core to rim (Fig. 27B). Cores yield temperatures from 758–823 ˚C; rims yield temperatures from 866–941 ˚C (outlier at 813 ˚C). Bright CL rims yield temperatures from 724–760 ˚C. Inclusions

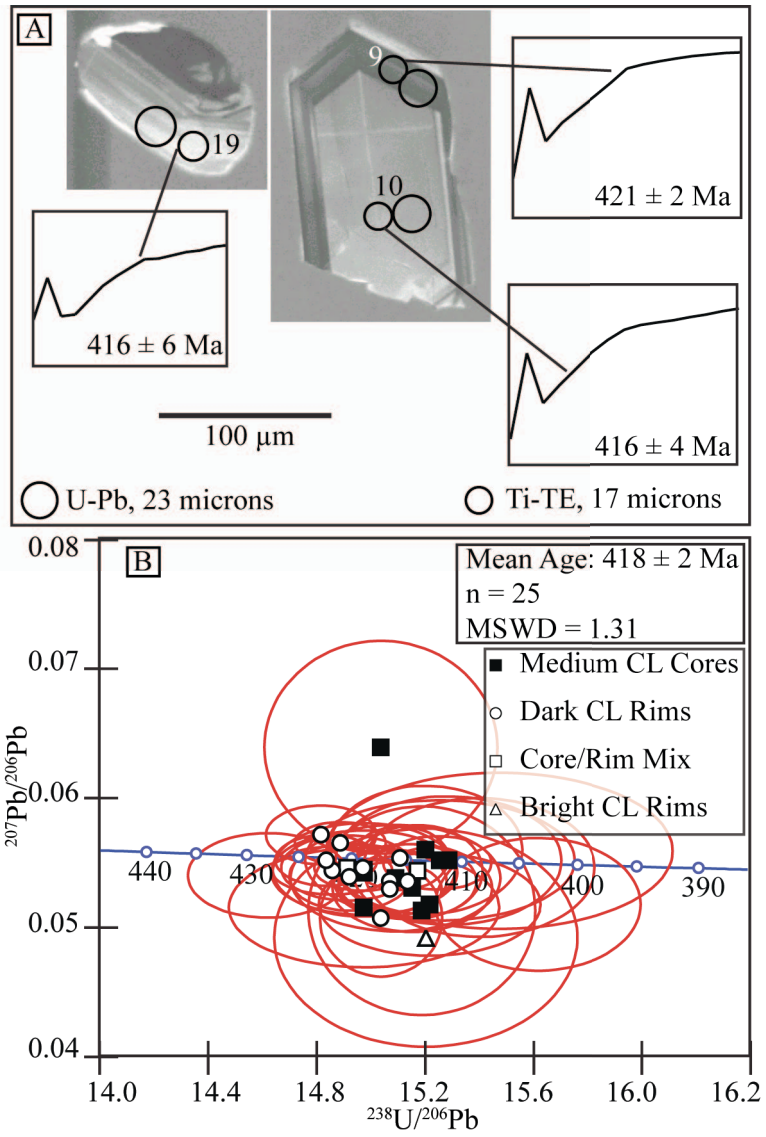

Figure 26. Results for SHRIMP-RG U-Pb zircon analysis for intermediate granulite sample D213B. A) Example zircons taken from the sample showing zoned cores (spot 10), dark CL rims (spot 9), and bright CL rims (spot 19). U-Pb indicates spots for geochronology, Ti-TE indicates spots for trace element analysis. B) U-Pb Terra-Wasserburg plot (Terra and Wasserburg, 1972) for sample D213B, points represent analyses used in mean age calculation (error ellipses are 2 sigma; mean age includes both cores and rims).

analyzed with EDS were identified as garnet + apatite, biotite, albite, rutile, quartz, and clinozoisite. Possible inclusions of alkali feldspar, muscovite, or re-crystallized melt

TABLE 10. ZIRCON U-Pb ISOTOPIC DATA, INTERMEDIATE GRANULITE SAMPLE D213B, NORTH QAIDAM, WESTERN CHINA

Analysis	CL	$^{206}Pb_c$ %	U (ppm)	Th (ppm)	$^{232}Th/^{238}U$	^{207}Pb-corr $^{206}Pb/^{239}U$ age (Ma ± 1σ err)	Total $^{238}U/^{206}Pb$ (± % err)	Total $^{207}Pb/^{206}Pb$ (± % err)
D213B-1*	R	0.15	807	123	0.16	420.5 ± 0.9	14.81 ± 0.4	0.0564 ± 1.2
D213B-2	C	0.03	174	20	0.12	404.9 ± 0.9	15.42 ± 0.9	0.0551 ± 2.5
D213B-3*	C	0.45	188	17	0.09	412.8 ± 0.6	15.05 ± 0.9	0.0587 ± 2.4
D213B-4*	R	-	585	137	0.24	422.3 ± 0.6	14.79 ± 0.6	0.0543 ± 1.4
D213B-5*	C/R	0.00	363	46	0.13	420.8 ± 0.5	14.83 ± 0.6	0.0552 ± 1.7
D213B-6*	R	-	576	136	0.24	417.6 ± 0.9	14.97 ± 0.5	0.0538 ± 1.3
D213B-7*	C	-	184	18	0.10	419.4 ± 0.8	14.90 ± 0.9	0.0541 ± 2.4
D213B-8	C	-	225	40	0.18	428.7 ± 0.6	14.55 ± 0.8	0.0551 ± 2.1
D213B-9*	R	0.01	444	92	0.21	420.9 ± 1.0	14.82 ± 0.6	0.0553 ± 1.6
D213B-10*	C	0.19	139	16	0.12	415.5 ± 1.0	14.99 ± 1.0	0.0566 ± 2.7
D213B-11*	C	-	150	12	0.09	416.7 ± 0.5	14.98 ± 1.0	0.0548 ± 2.7
D213B-12*	R	0.29	557	141	0.26	422.0 ± 0.5	14.74 ± 0.5	0.0576 ± 1.5
D213B-13*	R	0.05	668	189	0.31	422.5 ± 1.0	14.76 ± 0.5	0.0557 ± 1.3
D213B-14	C	0.29	133	12	0.10	408.7 ± 0.5	15.24 ± 1.0	0.0572 ± 2.9
D213B-15*	R	-	528	133	0.26	417.3 ± 0.5	14.97 ± 0.5	0.0544 ± 1.5
D213B-16*	R	-	657	169	0.27	419.3 ± 1.0	14.89 ± 0.5	0.0549 ± 1.3
D213B-17*	C	0.21	129	12	0.09	413.0 ± 0.4	15.08 ± 1.0	0.0567 ± 2.8
D213B-18*	R	0.05	673	207	0.32	415.5 ± 1.4	15.01 ± 0.4	0.0555 ± 1.7
D213B-19*	BR	-	76	6	0.08	416.2 ± 0.5	15.01 ± 1.4	0.0545 ± 3.8
D213B-20*	R	0.23	477	100	0.22	419.6 ± 0.7	14.84 ± 0.5	0.0570 ± 1.5
D213B-21*	C	-	268	49	0.19	415.5 ± 1.3	15.03 ± 0.7	0.0545 ± 2.0
D213B-22*	C	-	85	10	0.13	420.8 ± 0.5	14.90 ± 1.3	0.0515 ± 3.6
D213B-23	R	0.06	590	176	0.31	412.3 ± 1.0	15.13 ± 0.5	0.0555 ± 1.4
D213B-24*	C	0.01	96	7	0.07	411.9 ± 1.6	15.15 ± 1.0	0.0551 ± 3.4
D213B-25	BR	0.11	57	5	0.08	406.2 ± 0.6	15.36 ± 1.6	0.0558 ± 4.4
D213B-26*	R	-	360	56	0.16	415.7 ± 1.0	15.02 ± 0.6	0.0549 ± 1.8
D213B-27*	C	0.21	127	10	0.09	411.2 ± 0.8	15.15 ± 1.0	0.0567 ± 2.8
D213B-28*	C	0.05	187	19	0.11	419.3 ± 0.6	14.87 ± 0.8	0.0556 ± 2.4
D213B-29*	C/R	-	381	53	0.14	414.4 ± 1.0	15.08 ± 0.6	0.0542 ± 2.7
D213B-30*	C	-	177	19	0.11	414.5 ± 4.2	15.09 ± 1.0	0.0535 ± 2.5

Note: Cathodoluminescence abbreviations are as follows: C = Core, R = Rim, C/R = Core-rim mixture, BR = Bright CL rim.
*Analysis used in weighted mean age calculation.

TABLE 11. ZIRCON TRACE-ELEMENT RESULTS (ppm) FOR INTERMEDIATE GRANULITE SAMPLE D213B, NORTH QAIDAM, WESTERN CHINA

Analysis	CL	Li†	Be	B	F	Na	Al	P	K	Ca	Sc	^{48}Ti	^{49}Ti	Fe	Y	Nb	^{94}ZrH	La	Ce	Nd
1	R	16	0.05	0.1	8	3	46	244	1	2	291	49.9	49.7	6	599	2	2.0	0.009	29	1.06
2	C	11	0.01	0.2	6	3	17	204	2	2	245	16.2	16.3	8	178	1	1.9	0.002	4	0.25
3	C	1.8	0.02	0.1	5	3	36	123	1	2	121	15.8	15.5	3	129	1	2.0	0.007	4	0.12
4	R	5.0	0.04	0.1	4	3	38	181	1	2	174	42.6	40.8	9	315	3	2.1	0.007	26	1.27
5	C/R	2.1	0.03	0.5	11	9	60	161	6	9	135	27.7	27.1	19	158	3	1.9	0.052	8	0.30
5.2	C	0.5	0.00	0.3	4	6	35	98	3	3	75	11.6	11.4	2	57	1	1.8	0.002	3	0.10
6	R	0.2	0.18	0.3	6	12	39	376	1	5	476	40.5	39.7	7	981	2	1.8	0.047	31	2.20
6.2	R	0.2	0.02	0.1	6	7	15	141	2	3	169	21.1	19.5	4	306	1	1.8	0.043	21	2.83
7	C	0.1	0.04	0.2	5	5	16	223	1	2	275	17.7	17.0	7	216	1	1.9	0.012	5	0.36
8	C	2.3	0.04	0.1	4	4	36	216	8	3	237	51.7	51.5	12	510	2	2.0	0.021	31	1.46
9	R	26	0.07	0.3	7	3	46	218	1	3	231	33.7	33.4	4	443	2	2.0	0.007	19	0.98
10	C	0.3	0.03	0.2	6	8	32	200	2	4	235	14.9	14.9	5	132	1	1.8	0.002	4	0.29
11	C	0.3	0.04	0.2	6	2	29	213	1	2	254	15.8	16.1	5	202	1	1.8	0.002	3	0.25
12	R	1.9	0.05	0.3	9	3	50	244	1	5	289	57.4	57.1	9	693	3	1.9	0.154	41	1.94
13	R	0.5	0.28	0.4	4	4	51	248	2	3	238	39.9	41.2	6	478	2	1.8	0.012	24	1.09
14	C	0.2	0.01	0.1	5	3	34	202	2	1	227	15.1	15.8	3	162	1	2.0	0.021	5	0.26
15	R	3.4	0.02	0.3	6	2	37	172	1	1	132	30.6	31.3	6	189	2	2.0	0.032	23	0.80
16	R	1.7	0.16	1.5	24	13	489	384	19	133	369	38.9	39.0	193	676	1	2.1	90.6	454	116
17	C	0.1	0.03	0.3	6	3	41	211	1	14	267	15.8	15.6	5	169	1	1.6	19.2	46	14.0
17.2	R	3.5	0.03	0.2	6	2	42	173	1	1	107	33.0	34.3	8	173	2	1.7	0.007	24	0.74
18	R	0.4	0.09	0.1	7	2	36	298	1	3	326	57.4	56.5	16	764	2	1.8	0.041	42	2.04
19	BR	5.4	0.00	0.2	4	2	37	62	1	1	59	8.5	8.7	1	38	0	1.7	0.017	2	0.05
20	R	6.9	0.05	0.2	6	3	26	211	1	2	201	34.2	34.5	8	355	2	1.6	0.032	21	1.09
21	C	0.2	0.05	0.1	5	2	15	246	1	3	240	20.5	21.4	10	262	1	1.6	0.013	13	0.59
22	C	0.4	0.04	0.3	6	5	108	104	71	3	135	13.0	12.5	6	97	0	1.7	0.265	8	0.55
23	R	1.6	0.29	0.1	7	6	22	239	1	4	258	54.0	54.3	18	690	2	1.6	0.019	40	2.24
24	C	0.0	0.02	0.1	4	3	18	143	1	2	208	13.1	13.6	3	122	1	1.7	0.009	2	0.08
25	BR	0.2	0.01	0.1	5	10	40	66	1	2	56	11.0	11.6	1	53	1	1.9	0.017	3	0.10
26	R	0.8	0.07	0.1	4	3	32	204	1	2	247	41.7	43.1	8	575	3	1.7	0.018	29	1.34
27	C	1.1	0.10	0.1	4	3	14	246	1	2	272	18.9	18.5	9	235	1	1.6	0.013	5	0.28
28	C	0.3	0.03	0.1	6	5	16	229	3	3	275	17.4	17.4	9	229	1	2.3	0.010	6	0.26
28.2	BR	0.5	0.00	0.1	3	2	41	63	1	2	57	7.6	7.8	2	17	0	1.6	0.013	0	0.01
29	C/R	1.1	0.03	0.3	7	30	48	208	8	5	216	29.4	29.9	8	315	2	1.3	0.010	11	0.45
30	C	0.5	0.04	0.1	6	3	13	226	1	2	252	19.4	18.9	8	201	1	1.6	0.011	6	0.38

Note: Abbreviations for cathodoluminescence are as follows: C = Core, R = Rim, C/R = Core/rim, and BR = Bright CL rim.

TABLE 11. CONTINUED

Analysis	Sm	Eu	Gd	Ho	Tb	Dy	Er	Tm	Yb	Lu	Hf	Th	U	Th/U	Ce/Ce*	Eu/Eu*	Yb/Gd	T˚C ^{48}Ti	T˚C ^{49}Ti
1	3.96	4.382	40	24	10.7	83	81	15	114	18	9076	122	513	0.24	316	1.06	2.9	900	923
2	0.93	0.946	8	7	2.38	21	28	5	44	9	9428	15	149	0.10	175	1.02	5.2	781	794
3	0.56	0.724	6	5	1.79	15	19	3	29	5	10152	18	217	0.08	98	1.21	4.8	778	789
4	3.30	3.309	27	11	5.96	43	36	6	51	8	9583	144	531	0.27	314	1.07	1.9	881	898
5	1.00	1.142	9	6	2.59	22	23	4	29	5	9827	62	437	0.14	43	1.13	3.1	834	849
5.2	0.30	0.362	3	2	0.89	7	8	1	12	2	10359	9	103	0.08	208	1.12	3.6	750	758
6	6.97	6.845	61	39	16.2	131	144	27	206	38	8297	195	744	0.26	90	1.01	3.4	876	894
6.2	6.63	5.480	36	12	7.81	50	40	7	49	8	9708	93	364	0.26	57	1.08	1.4	807	813
7	0.95	1.356	10	8	2.97	25	32	6	52	10	9297	19	184	0.10	67	1.34	5.3	789	798
8	4.63	4.764	41	20	9.93	73	68	12	89	15	9048	119	496	0.24	174	1.04	2.2	904	927
9	2.38	2.563	27	17	7.03	60	58	10	76	12	9214	73	430	0.17	252	0.96	2.8	855	873
10	1.11	1.118	9	5	2.28	18	18	3	30	5	9393	14	121	0.12	185	1.10	3.4	773	784
11	1.01	1.177	8	8	2.54	26	31	6	46	8	9344	15	166	0.09	142	1.23	5.4	778	793
12	5.25	5.604	54	28	14.6	104	93	17	116	19	9412	179	667	0.27	55	1.01	2.1	916	941
13	3.54	3.531	35	17	8.22	63	60	11	88	14	9031	92	481	0.19	219	0.97	2.5	874	899
14	0.99	1.090	8	6	2.35	22	27	5	44	8	9375	17	160	0.10	49	1.19	5.6	774	791
15	2.92	2.125	18	7	3.80	28	25	5	37	6	9426	104	640	0.16	120	0.88	2.0	845	866
16	28.4	12.09	61	27	13.1	96	95	16	127	21	8319	156	619	0.25	2	0.88	2.1	871	892
17	3.52	1.766	12	7	2.62	21	23	4	36	7	9682	15	136	0.11	1	0.83	3.0	779	790
17.2	2.71	2.218	18	6	3.82	26	22	4	29	5	9497	148	568	0.26	367	0.98	1.7	853	877
18	6.60	6.829	61	31	15.4	109	102	17	135	23	8995	200	718	0.28	134	1.03	2.2	916	939
19	0.23	0.214	2	1	0.63	4	5	1	9	2	10600	4	57	0.07	38	1.07	5.4	723	733
20	3.20	2.995	25	13	6.15	47	46	8	63	11	8979	68	362	0.19	96	1.02	2.5	857	877
21	2.27	2.071	16	10	4.21	34	38	8	63	12	8791	40	227	0.17	135	1.04	3.9	804	823
22	1.10	0.904	7	4	1.67	13	13	2	19	3	9873	13	98	0.13	11	0.98	2.6	761	767
23	9.03	8.090	62	27	15.0	101	86	15	108	18	8884	183	598	0.31	206	1.04	1.7	909	934
24	0.43	0.664	5	4	1.55	15	16	3	23	4	10125	9	110	0.08	61	1.40	4.8	761	776
25	0.49	0.475	3	2	0.99	8	7	1	11	2	10155	13	86	0.15	53	1.17	3.5	745	760
26	4.07	4.529	39	23	11.4	84	81	14	103	16	9346	122	585	0.21	188	1.10	2.7	879	904
27	1.48	1.404	12	9	3.30	30	34	7	53	10	9061	23	193	0.12	67	1.02	4.4	796	807
28	1.13	1.335	11	9	2.97	26	32	7	52	9	8745	21	190	0.11	91	1.14	4.7	788	801
28.2	0.15	0.157	1	1	0.33	3	2	0	1	0	10341	0	8	0.01	20	1.45	1.7	714	724
29	1.68	1.846	17	12	5.12	43	48	8	70	12	10552	80	519	0.16	145	1.06	4.2	841	860
30	1.64	1.659	12	7	3.16	25	25	5	37	7	9351	21	163	0.13	82	1.15	3.2	798	809

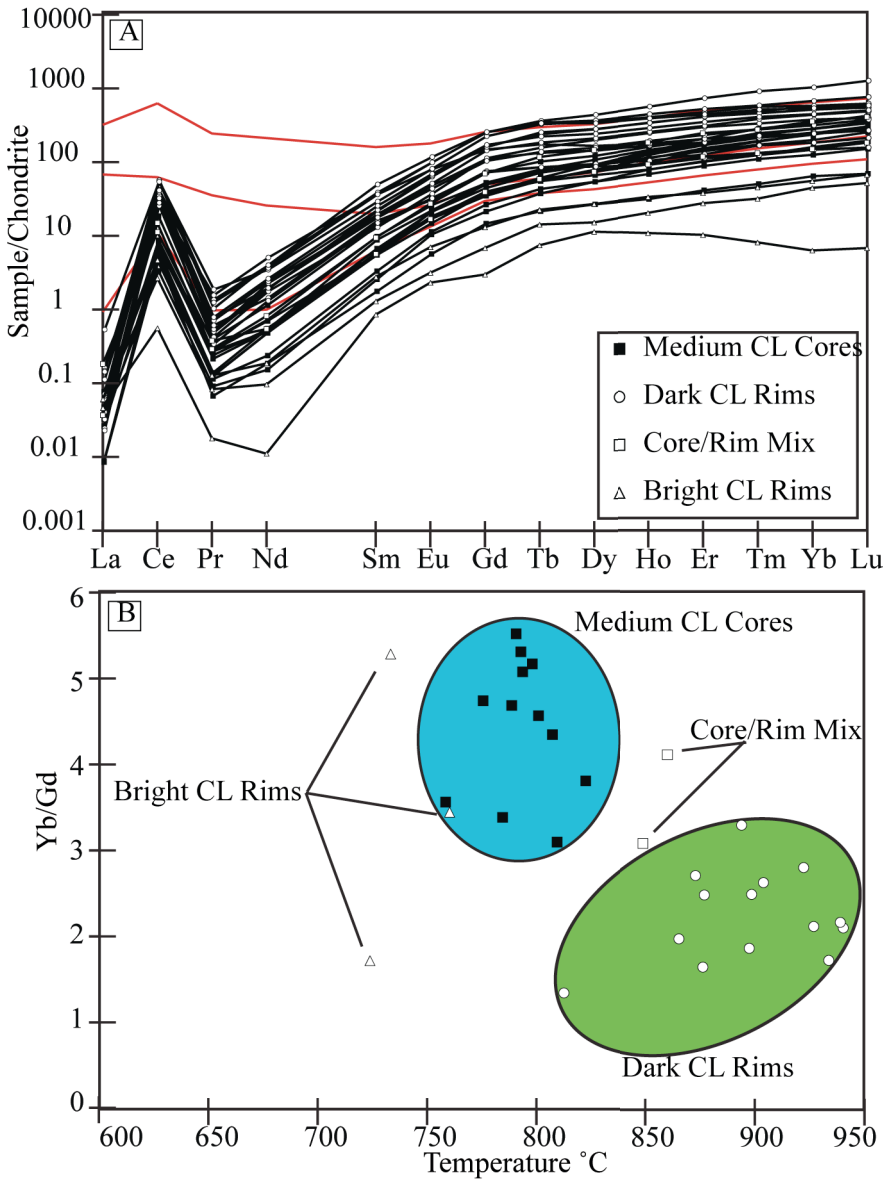

Figure 27. Zircon trace-element results for intermediate granulite sample D213B. A) REE patterns for zircons, red lines indicate analyses with high contaminant levels (see text and Table 11). B) Plot of Yb/Gd vs. Ti-in-zircon temperatures (Ferry and Watson, 2007).

were recognized; however, identification is uncertain due to interference from multiple inclusions and the surrounding zircon. All inclusions were found in the zircon cores and the rims were inclusion free.

Two analyses, D213B spots 5 and 29 (Tables 10 and 11), are a mix between the core and rim populations. Ti-in-zircon temperatures are 849 and 860, respectively, similar to the temperatures from the zircon rims. Both have lower Th/U values that fall between the core and rim trends. Spot 5 yields 158 ppm Y, while spot 29 yields 315 ppm Y. Based on these compositions these analyses appear to represent an overlap between the core and rims of the zircon grains.

Garnet-clinopyroxene Fe-Mg exchange and GASP, GADS and Ab-Jd-Qtz barometers for the intermediate granulite yield 775–875 ˚C and 14–17 kbar (Figure 28).

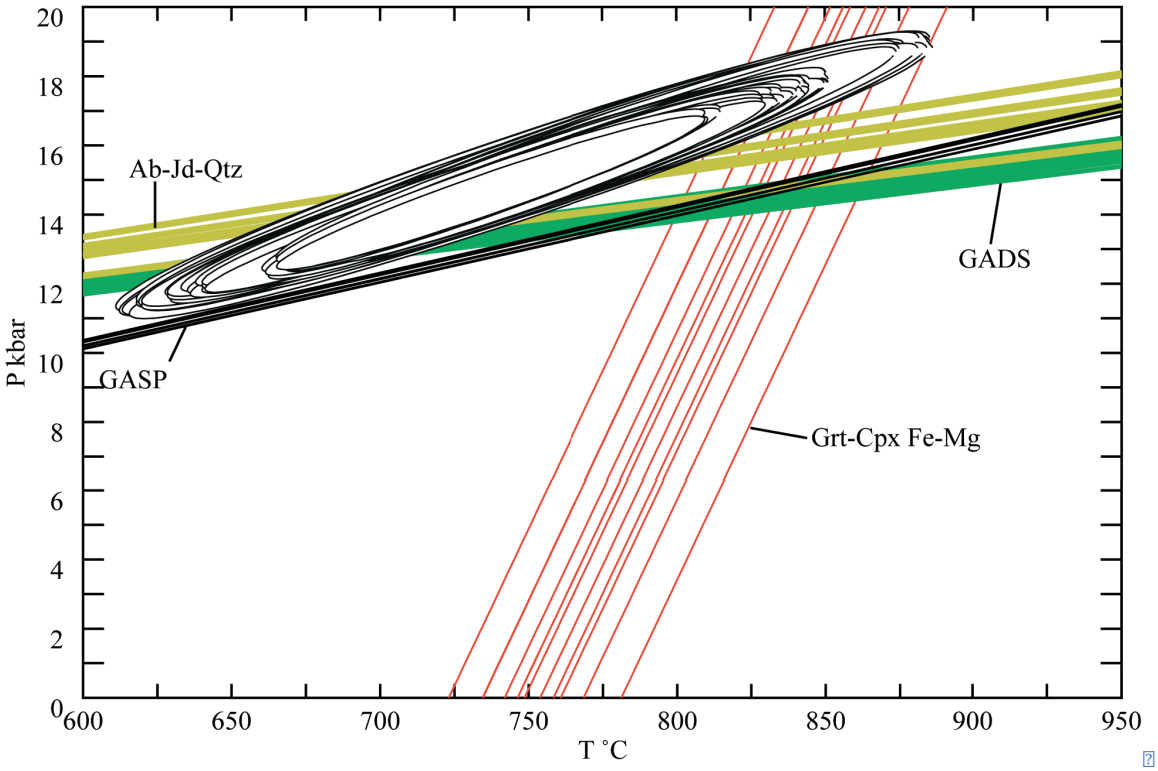

Figure 28. Pressure-temperature results for intermediate granulite sample D213B. Iron-Magnesium exchange thermometer is after Pattison and Newton (1989), GASP barometer is after Hodges and Spear (1982), GADS barometer is after Newton and Perkins (1982) and Ab-Jd-Qtz barometer is after Holland (1982; see text for equations). White ellipses are average P-T results for program THERMOCALC v.3.33 (Holland and Powell, 1998), errors are 1 sigma.

Results from mineral combinations using the average mineral compositions are presented in Table 8.

Mineral compositions input into the program THERMOCALC v.3.33 yield a mean of 749 ˚C, 15 kbar (Figure 28). Calculated errors range from 59–111 ˚C and 1.8–3.3 kbar. Lowering the H_2O activity to 0.7 lowers the calculated temperature by ~20 ˚C and lowers the calculated pressure by ~0.5 kbar, with results being indistinguishable within error from calculations with higher activities. The significance of fit increased from 1.16 to 1.29 with decreasing H_2O activity. Though this increase in the significance of fit does still fall within acceptable parameters, the increase may suggest that lower H_2O activities are not realistic, and that an activity of 1.0 best represents metamorphic conditions. Results based on the average mineral compositions are presented in Table 9.

Only one (D213B Grt1, Fig. 17 and 18) of three garnet transects (from two different grains) was used for P-T calculations of intermediate granulite D213B. Garnet transect D213B Grt2 touches a Cpx grain on one end, and a Czo grain on the other (Fig. 17). This close proximity to other mafic minerals clearly affects the Grt composition. Transect Grt2 shows an increase in Alm and a decrease in Prp and Grs not seen in transect Grt1, and is interpreted to represent retrograde exchange with adjacent mafic minerals. Garnet transect Grt2 was therefore not used in P-T calculation (see appendix D). Garnet transect D213B Grt3 shows no indication of an obvious core-rim trend, and may represent a cluster of smaller garnets that have combined to form one large grain. Because of this complexity, reliable compositions representing peak conditions could not be determined and so this transect was also not used for P-T calculations (see appendix D).

Pressure-temperature conditions for this sample indicate peak conditions in the HP-granulite facies, which agree with Ti-in-zircon temperatures. Based on the inclusions in zircon and depleted HREE patterns in zircon the mean age of 418 Ma is interpreted to represent HP-granulite metamorphism.

Intermediate Granulite D214

Only 7 zircon grains were separated from intermediate granulite D214, from which 8 spots were analyzed. Two grains contain medium to dark CL cores with sector and oscillatory zoning. These same grains show dark CL monotonous rims ~15 μm wide. Other grains are composed entirely of this monotonous dark CL region. All grains have very thin CL bright rims < 5 μm wide. Eight analyses yield 411–4696 ppm U, 43–4097 ppm Th, 0.10–0.90 U/Th, and ages from 400 to 496 Ma, with discordia intercept age of 211 ± 350 Ma and 472 ± 54 Ma, (Fig. 29A, n = 6, MSWD = 0.56). During analysis, the SHRIMP-RG had a malfunction in the chilling water system and the instrument had to be reset. Because of this, the first two analyses were not included in the intercept-age (D214-1 and D214-2, 474 ± 0.9 Ma and 496 ± 9.0 Ma). Results are listed in appendix C.

Separate trace element analyses were not done for this sample, but trace elements measured as part of the U/Pb analysis show two groups of REE patterns (Fig. 29B). All grains have negative Eu anomalies (Eu/Eu* = 0.25–0.41) and differ in their Ce values and HREE patterns. Three spots yield 169–226 ppm Ce and steep HREE patterns (Yb/Gd = 13–14). Four spots contain 11–28 ppm Ce and have flat HREE patterns (Yb/Gd = 1.8–

7.5). One spot lacks values for LREE, which was most likely due to the instrument shut down occurring during analysis.

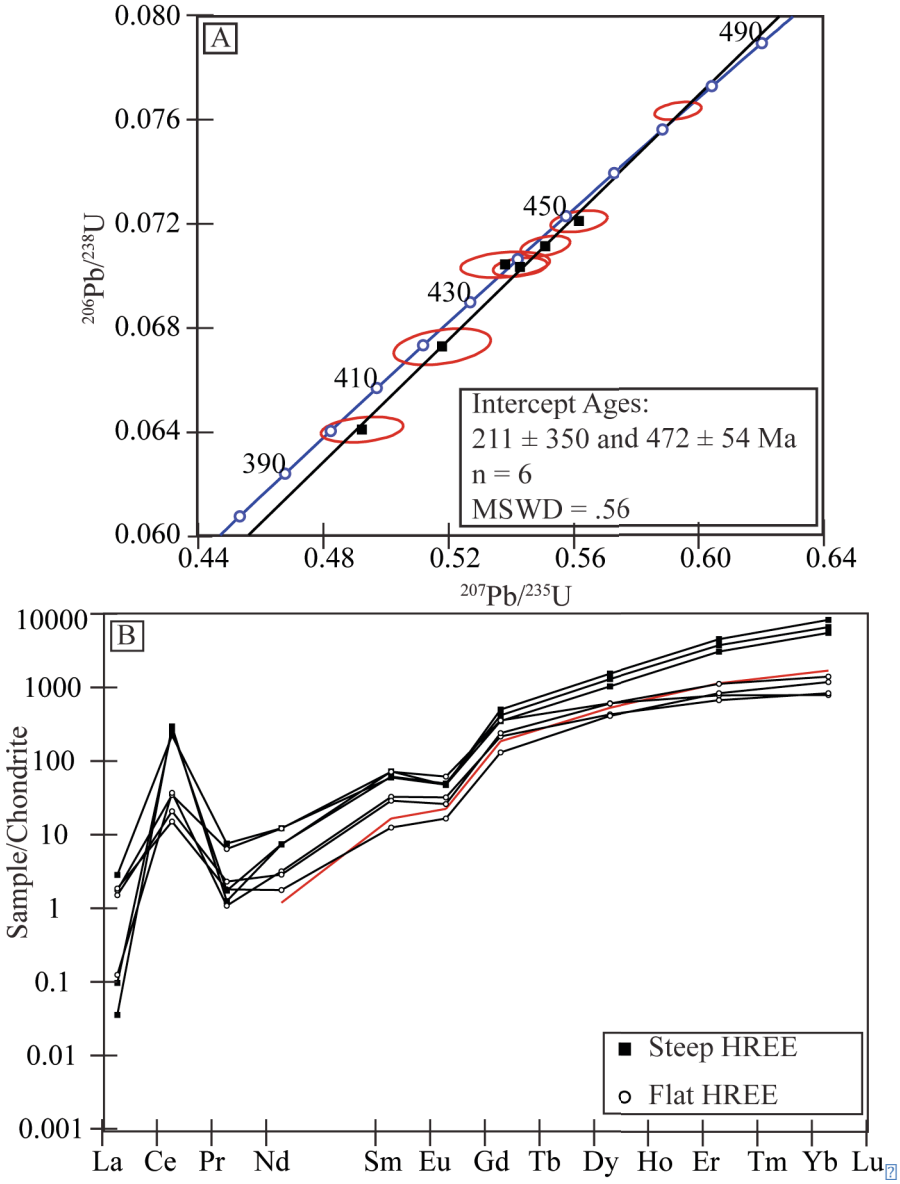

Figure 29. Results for SHRIMP-RG U-Pb and trace-element zircon analysis for intermediate granulite sample D214. A) U-Pb concordia plot (isotopic ratios corrected for ^{204}Pb), points represent analyses used in intercept ages (error ellipses are 2 sigma). B) REE patterns for zircons, red lines indicate incomplete analysis caused by instrument failure (see text).

Based on zircon REE patterns the upper intercept age of 472 ± 54 Ma is interpreted as the age for HP-granulite metamorphism in this sample. The lower intercept age for this sample (211 ± 350 Ma) is interpreted to represent a later lead loss event; however, due to the high errors, ages for this sample are not considered as reliable indicators for HP-granulite metamorphism.

Grt-Ky Gneiss D217A

The Grt-Ky gneiss zircons show three distinct zones: rounded cores with oscillatory zoning (CL dark–bright), subhedral to euhedral CL dark to medium rims with oscillatory zoning and sector zoning, and thin, unzoned, CL dark rims generally ~5 µm wide but up to ~25 µm wide (Fig. 30A). Three analyses of the zircon cores yield 159–583 ppm U, 133–197 ppm Th, 0.55–0.87 Th/U, and ages of 1351 to 1476 Ma, and are interpreted as inherited detrital grains (Table 12, Fig. 30B). Fourteen analyses of the subhedral rims yield 172–1021 ppm U, 32–138 ppm Th, 0.04–0.72 Th/U, and ages of 836–950 Ma. One analysis was obtained for the thin CL dark rim and contains 726 ppm U, 16 ppm Th, 0.02 U/Th, and yields an age of 429 ± 2 Ma. Discordia intercept ages for the subhedral and dark CL rims are 413 ± 36 and 938 ± 20 Ma, with the upper intercept interpreted as the best estimate for the age of the subhedral rims (n = 15, MSWD = 1.6; Fig. 30B).

Of 31 trace element analyses, 6 contain elevated contaminants (Table 13, Fig. 31A). Three zircon cores show strong negative Eu anomalies (Eu/Eu* = 0.07–0.26) and steep HREE patterns (Yb/Gd = 14.0–18.8). Eighteen analyses of the subhedral rims show strong negative Eu anomalies (Eu/Eu* = 0.1–0.08, outlier at 0.19) and steep HREE

patterns (Yb/Gd = 12–62). Four analyses of the thin CL dark rims are characterized by low concentrations of LREE, moderate negative Eu anomalies (Eu/Eu* = 0.35–0.51), and

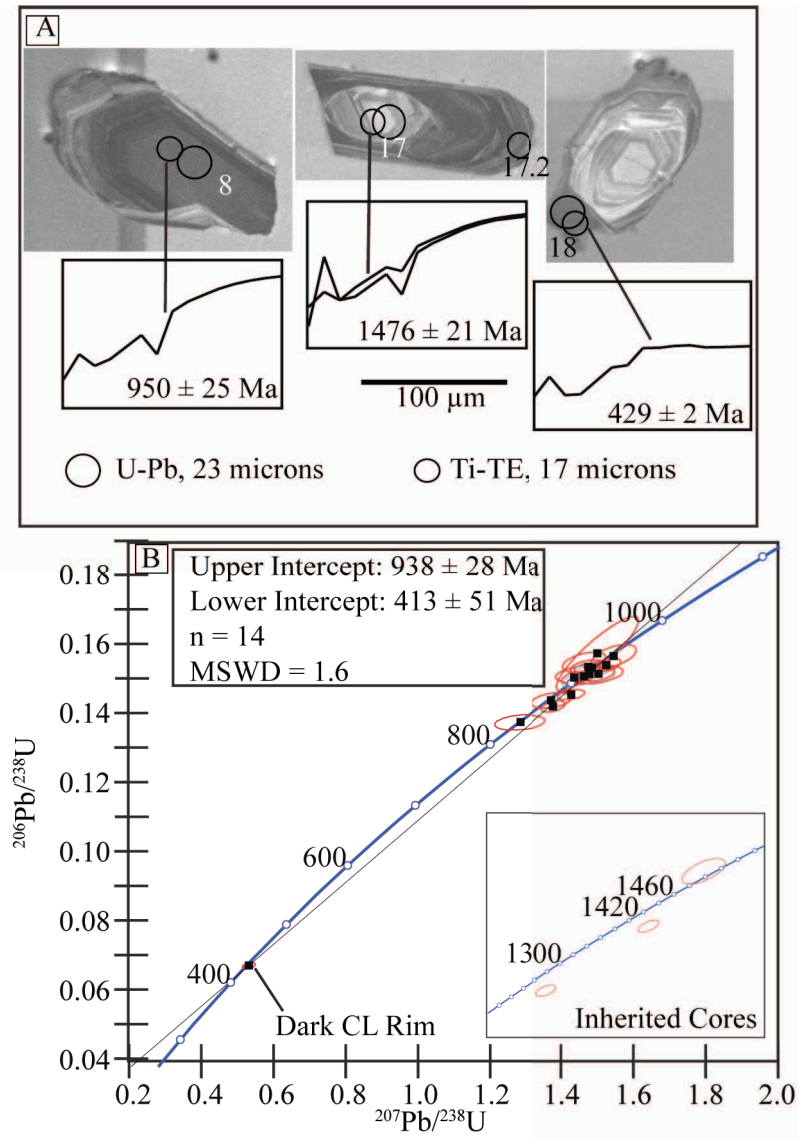

Figure 30. Results for SHRIMP-RG U-Pb zircon analysis for Grt-Ky gneiss sample D217A. A) Example zircons taken from the sample showing inherited cores (spot 17), medium CL rims (spot 8 and 17.2), and dark CL rims (spot 18). U-Pb indicates spots for geochronology, Ti-TE indicates spots for trace element analysis. B) U-Pb concordia plot (isotopic ratios corrected for ^{204}Pb) for sample D217A, points represent analyses used in intercept ages (error ellipses are 2 sigma; insert is concordia plot with inherited cores).

TABLE 12. ZIRCON U-Pb ISOTOPIC DATA, GRT-KY SAMPLE D217A, NORTH QAIDAM, WESTERN CHINA

Analysis	CL	$^{206}Pb_c$ %	U (ppm)	Th (ppm)	$^{232}Th/^{238}U$	^{207}Pb-corr $^{206}Pb/^{239}U$ age (Ma ± 1σ err)			Total $^{238}U/^{206}Pb$ (± % err)			Total $^{207}Pb/^{206}Pb$ (± % err)		
D217A-1*	R	0.24	485	59	0.13	861.0	±	3.8	6.98	±	0.5	0.0697	±	0.9
D217A-2*	R	0.27	172	32	0.19	914.1	±	6.7	6.55	±	0.7	0.0718	±	2.3
D217A-3*	R	0.27	235	30	0.13	872.1	±	5.2	6.88	±	0.6	0.0704	±	1.2
D217A-4*	R	0.05	300	58	0.20	926.5	±	5.1	6.47	±	0.6	0.0704	±	1.1
D217A-5*	R	0.29	308	34	0.12	913.3	±	4.9	6.55	±	0.5	0.0719	±	1.0
D217A-6*	R	-	548	51	0.10	909.6	±	4.1	6.60	±	0.5	0.0538	±	1.3
D217A-7	C	0.59	369	197	0.55	†1351	±	14	4.74	±	0.5	0.0863	±	0.7
D217A-8*	R	-	532	52	0.10	949.9	±	25.2	6.31	±	2.7	0.0690	±	1.4
D217A-9*	R	0.53	259	33	0.13	836.3	±	5.2	7.18	±	0.6	0.0713	±	1.2
D217A-10*	R	0.15	373	38	0.10	927.9	±	4.6	6.45	±	0.5	0.0713	±	1.0
D217A-11*	R	0.09	488	56	0.12	924.7	±	4.0	6.48	±	0.4	0.0707	±	1.2
D217A-12	R	-	172	92	0.55	936.1	±	6.8	6.41	±	0.7	0.0696	±	1.4
D217A-13*	R	0.08	1021	44	0.04	910.3	±	3.5	6.59	±	0.4	0.0557	±	1.3
D217A-14	C	0.62	583	310	0.55	†1485	±	11	4.16	±	0.5	0.0932	±	0.5
D217A-15*	R	0.56	848	40	0.05	879.7	±	3.5	6.80	±	0.4	0.0731	±	0.7
D217A-16*	R	0.12	197	138	0.72	942.8	±	7.9	6.34	±	0.9	0.0715	±	1.3
D217A-17	C	-	159	133	0.87	†1474	±	21	3.78	±	0.9	0.0932	±	1.0
D217A-18*	DR	0.03	726	16	0.02	429.2	±	2.3	14.5	±	0.6	0.0557	±	1.1

Note: Cathodoluminescence abbreviations are as follows: C = Core, R = Rim, C/R = Core-rim mixture, BR = Bright CL rim.

* Analysis used in discordia intercept age calculation.

† Ages > 1 Ga are ^{204}Pb corrected $^{207}Pb/^{206}Pb$.

TABLE 13. ZIRCON TRACE-ELEMENT RESULTS (PPM) FOR GRT-KY GNEISS SAMPLE D217A, NORTH QAIDAM, WESTERN CHINA

Analysis	CL	Li	Be	B	F	Na	Al	P	K	Ca	Sc	^{48}Ti	^{49}Ti	Fe	Y	Nb	^{94}ZrH	La	Ce	Nd
1	R	2.6	0.02	0.3	8	17	79	1122	16	5	178	9.7	10	4	1765	1	1.4	0.007	1	0.64
2	R	1.2	0.55	0.2	3	18	156	1356	21	6	157	11	9.6	3	2219	1	1.4	0.040	1	0.87
2.2	DR	2.6	0.04	0.2	5	11	19	25	11	3	26	1.8	1.8	5	76	1	1.6	0.015	0	0.01
3	R	2.6	0.05	0.4	6	13	93	887	12	4	132	10	10	3	1215	1	1.5	0.049	1	0.40
4	R	3.5	0.01	0.3	7	14	99	1783	11	3	186	11	10	4	2585	1	1.5	0.005	1	0.61
5	R	2.7	0.02	0.1	8	14	83	1145	14	4	143	9.2	8.6	3	1796	1	1.3	0.010	1	0.46
6	R	2.2	0.03	0.2	6	15	43	1150	11	4	206	6.1	6.6	5	1747	1	1.4	0.023	1	0.24
7	C	0.1	0.04	0.1	11	13	23	488	13	3	16	14	15	4	1487	12	1.4	0.016	21	1.35
8	R	3.8	0.06	0.5	8	14	107	1097	12	4	260	3.5	3.7	7	1517	1	1.5	0.047	1	0.60
9	R	7.4	0.06	3.3	83	110	464	1078	504	49	129	31	30	176	1528	2	2.1	3.094	31	15
9.2	DR	52	1.28	41.0	2023	321	1421	495	109	174	147	118	119	416	716	2	5.2	32	312	121
10	R	2.8	0.03	0.2	8	27	97	754	31	7	148	7.7	8.7	1	923	1	1.4	0.003	1	0.33
11	R	2.6	0.01	0.0	3	11	59	1233	9	4	166	9.0	8.5	3	1785	2	1.5	0.008	1	0.47
12	R	0.2	0.05	0.2	13	8	17	515	7	3	82	20	20	1	938	2	1.5	0.008	2	0.45
12.2	R	6.4	0.09	0.2	33	12	31	767	16	5	104	21	22	3	1978	1	1.5	0.016	4	1.84
13	R	6.9	0.06	0.4	11	17	39	1417	24	5	360	6.2	5.3	14	1811	1	1.7	0.075	1	0.40
14	C	0.1	0.03	0.2	9	18	39	322	18	4	29	8.8	8.5	3	672	6	1.4	0.005	20	0.29
15	R	8.2	0.05	0.3	9	29	237	1286	42	14	280	22	24	17	1976	1	1.7	0.151	1	0.57
16	R	0.6	0.09	0.2	27	9	21	1533	13	4	85	24	24	2	3470	2	1.5	0.035	4	3.88
16.2	DR	4.3	0.00	0.3	6	13	63	46	18	5	33	6.0	5.9	10	27	1	1.7	0.079	1	0.38
17	C	0.3	0.01	0.0	9	6	17	835	4	3	183	13	12	2	1887	6	1.6	0.029	50	2.09
17.2	R	2.9	0.02	0.1	16	13	75	916	13	27	121	10	11	13	1530	2	1.8	0.174	2	0.89
18	DR	6.4	0.04	0.3	6	72	47	64	41	16	33	5.2	5.4	8	50	1	3.5	0.070	1	0.17
19	DR	650	4.84	162	23404	7693	18562	15291	2087	3437	602	1882	1865	16742	10142	7	46	506	6122	2955
20	DR	4.0	0.02	0.2	13	17	111	1249	23	20	172	9.9	10	17	2027	2	2.2	0.607	6	3.37
21	DR	18	0.19	0.3	20	125	1362	89	459	27	25	136	135	1040	59	4	9.5	5.784	21	5.94
21.2	R	2.5	0.02	0.0	7	15	77	1325	27	4	181	9.1	8.8	4	1826	2	1.5	0.019	1	0.47
22	DR	18	0.38	22.5	1302	280	1752	631	188	123	183	87	86	3902	1148	2	8.6	24	351	168
23	DR	7.8	0.03	0.2	6	10	130	109	17	4	30	11.6	10	12	88	1	6.6	1.419	7	1.27
24	DR	12	0.05	3.9	135	69	406	71	107	30	43	72.2	62	135	249	3	15	9.872	66	36
25	DR	2.1	0.04	0.1	4	8	28	87	8	3	38	3.7	4.1	4	140	2	1.3	0.014	1	0.21

Note: Cathodoluminescence abbreviations are as follows: C = Inherited core, R = Medium CL im, and DR = Dark CL rim.

TABLE 13. CONTINUED

Spot	Sm	Eu	Gd	Ho	Tb	Dy	Er	Tm	Yb	Lu	Hf	Th	U	Th/U	Ce/Ce*	Eu/Eu*	Yb/Gd	T°C ^{48}Ti	T°C ^{49}Ti
1	2.39	0.089	32	69	13.6	172	295	61	457	79	13403	52	383	0.14	12	0.03	14.5	735	748
2	2.31	0.092	34	91	15.4	209	430	91	744	133	13255	37	202	0.18	4	0.03	22.1	745	742
2.2	0.18	0.121	3	3	1.10	10	7	1	9	1	14880	2	579	0.00	20	0.51	3.2	605	608
3	1.54	0.082	21	46	8.92	112	224	47	403	73	12857	37	253	0.15	4	0.04	19.0	739	747
4	2.59	0.048	37	100	17.0	228	478	102	839	147	12397	60	337	0.18	17	0.01	22.7	742	751
5	1.96	0.071	24	73	11.4	157	355	79	675	119	13146	43	379	0.11	19	0.03	28.3	730	732
6	1.65	0.067	23	70	10.4	153	350	80	724	135	12880	38	471	0.08	8	0.03	31.3	696	708
7	3.29	0.240	31	61	12.0	146	274	57	471	82	10747	232	340	0.68	151	0.07	15.3	767	785
8	1.86	0.118	23	55	10.8	134	247	52	440	77	13125	46	477	0.10	6	0.05	18.9	652	660
9	13.8	1.468	37	62	12.1	139	291	63	539	98	12707	179	297	0.60	3	0.20	14.5	847	861
9.2	88.6	8.802	114	24	18.1	95	96	23	231	47	15799	203	879	0.23	3	0.27	2.0	1010	1038
10	1.51	0.062	17	34	7.64	90	154	32	270	46	12967	29	260	0.11	26	0.04	15.5	715	732
11	1.98	0.105	27	71	12.5	159	327	72	589	108	12604	52	358	0.15	14	0.04	21.6	728	731
12	1.33	0.069	20	37	6.94	86	169	35	277	50	11783	59	152	0.39	34	0.04	13.8	799	815
12.2	5.19	0.264	51	82	17.9	203	340	67	511	85	11078	141	261	0.54	22	0.05	10.0	805	823
13	1.31	0.088	15	71	10.4	156	376	97	949	178	17471	38	1120	0.03	4	0.06	61.7	696	690
14	1.09	0.056	12	26	4.51	57	120	27	226	43	12243	144	268	0.54	473	0.05	18.8	726	731
15	1.66	0.145	23	71	12.7	180	280	52	371	53	15422	48	842	0.06	3	0.07	16.2	812	833
16	8.30	0.522	88	144	30.7	355	592	115	879	148	9938	148	202	0.73	12	0.06	10.0	818	834
16.2	0.82	0.212	4	1	0.70	5	3	0	2	0	13279	9	439	0.02	5	0.35	0.5	694	698
17	4.56	1.216	45	79	15.9	192	356	75	622	111	10934	277	262	1.06	203	0.26	14.0	762	766
17.2	2.37	0.135	25	63	11.0	141	287	63	504	91	13177	63	552	0.11	3	0.05	20.2	741	753
18	0.70	0.327	6	2	1.09	9	5	1	5	1	11850	14	686	0.02	6	0.49	0.9	683	691
19	2763	315	4554	400	649	2507	1182	226	1722	318	20362	3930	2587	1.52	3	0.27	0.4	1571	1694
20	3.70	0.275	28	79	12.8	176	378	82	681	120	13595	60	471	0.13	3	0.08	24.3	736	746
21	3.91	0.409	10	3	0.94	6	4	0	2	1	9155	31	442	0.07	2	0.20	0.3	1031	1067
21.2	1.75	0.084	25	72	11.6	158	336	75	638	119	12577	48	331	0.15	10	0.04	25.1	729	734
22	155	16	225	49	39.9	212	197	50	475	95	15337	754	1015	0.74	4	0.26	2.1	969	998
23	2.38	0.296	9	4	1.96	12	10	2	13	2	12291	27	465	0.06	2	0.19	1.4	750	747
24	34.6	3.670	58	10	6.33	32	24	4	25	5	12313	133	654	0.20	2	0.25	0.4	945	952
25	0.45	0.179	4	5	1.69	16	21	4	33	6	14680	6	540	0.01	9	0.42	8.8	657	669

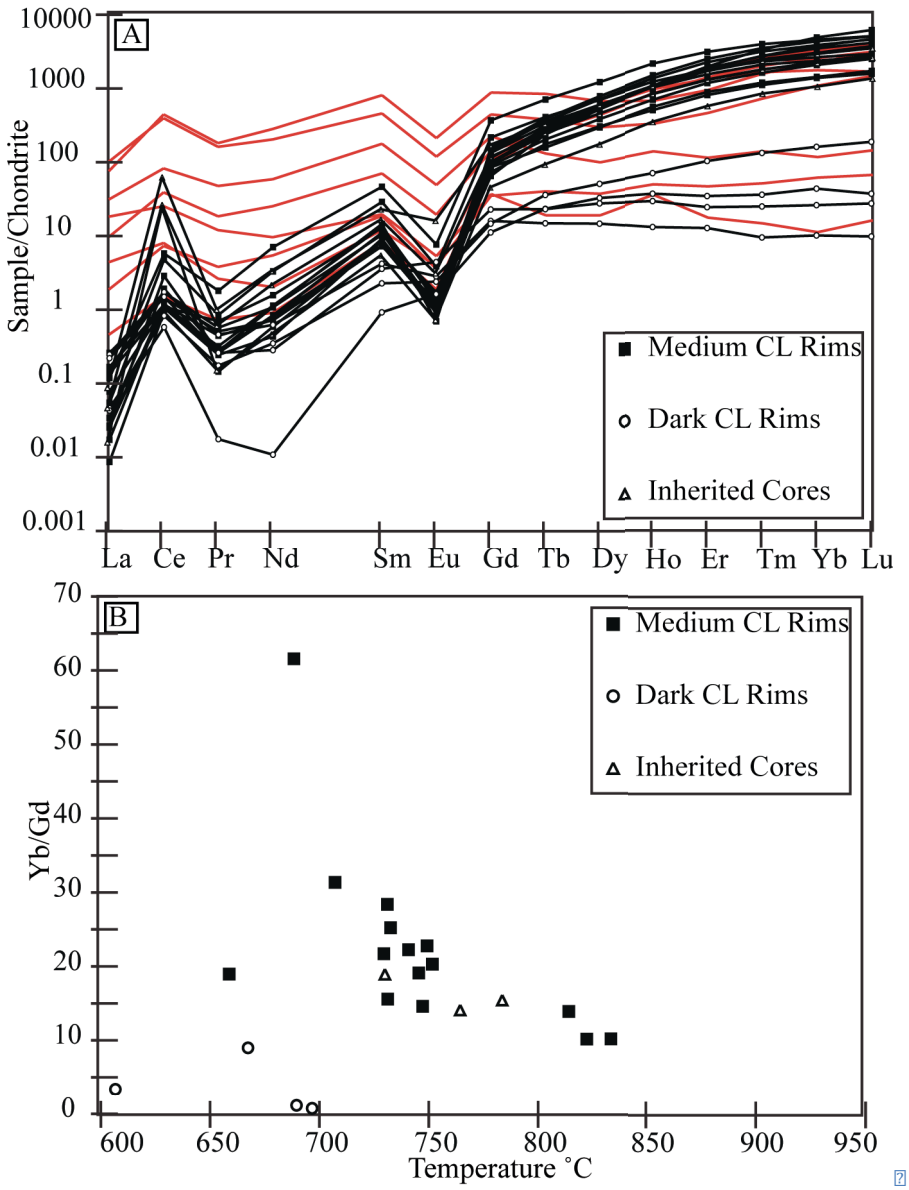

Figure 31. Zircon trace-element results for Grt-Ky gneiss sample D217A. A) REE patterns for zircons, red lines indicate analyses with high contaminant levels (see text and Table 13). B) Plot of Yb/Gd vs. Ti-in-zircon temperatures (Ferry and Watson, 2007).

flat HREE patterns (Yb/Gd = 0.5–3.2, outlier at 8.8). Ti-in-zircon thermometry (Ferry and Watson, 2007) yields temperatures from 731–785 ˚C for zircon cores, 600–834 ˚C for subhedral rims, and 660–691 ˚ for the CL dark rims (Fig. 31B). Inclusions of Qtz,

Ms, Bt, Kfs and Grt were identified by EDS analysis. All inclusions were located in the ~938 Ma zircon rims.

Garnet-biotite Fe-Mg exchange and GASP barometry for the Grt-Ky gneiss yield 740–775 ˚C and 13–15 kbar (Fig. 32). Results from mineral combinations using the average mineral compositions are presented in Table 8.

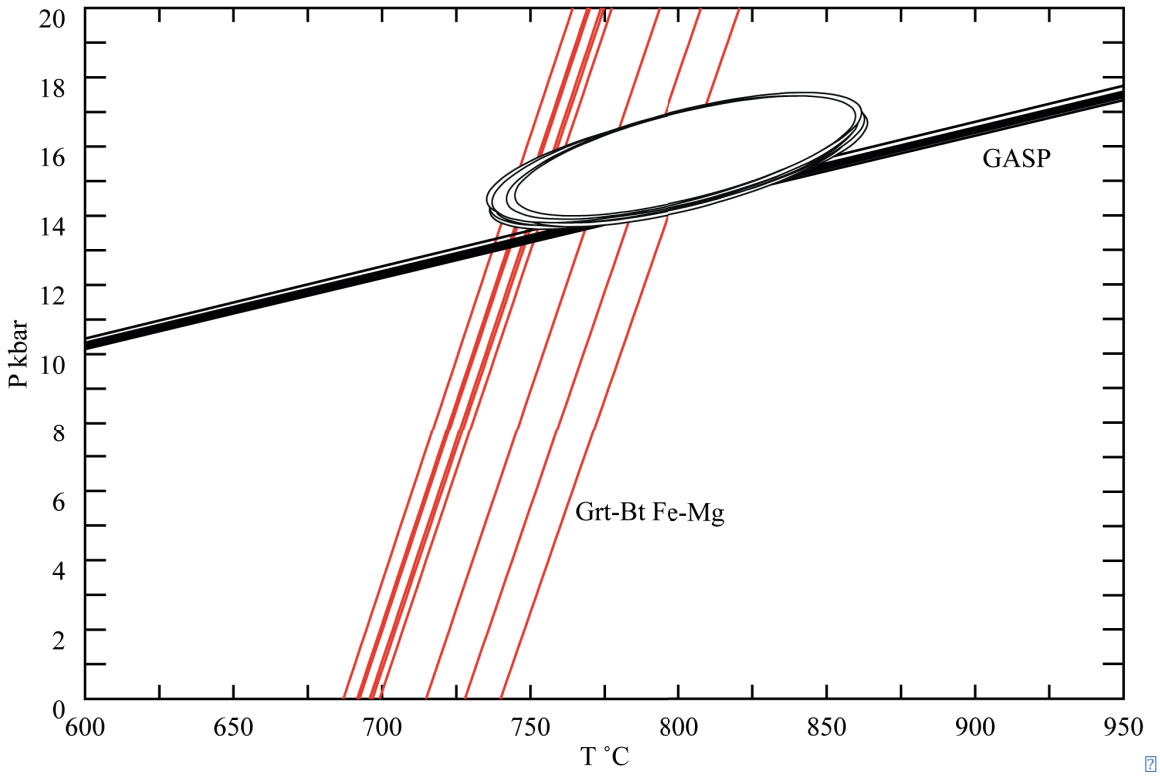

Figure 32. Pressure-temperature results for Grt-Ky gneiss sample D217A. Iron-Magnesium exchange thermometer and GASP barometer are after Hodges and Spear (1982; see text for equations). White ellipses are average P-T results for program THERMOCALC v.3.33 (Holland and Powell, 1998), errors are 1 sigma.

Mineral compositions input into the program THERMOCALC v.3.33 yield a mean of 800 ˚C, 15.5 kbar (Fig. 32). Calculated errors range from 45-48 ˚C and 1.3-1.4 kbar. Lowering the H_2O activity to 0.7 reduces the calculated temperature by ~25 ˚C and reduces the calculated pressure by ~0.7 kbar. The significance of fit increases from 0.13 to 0.24 with decreasing H_2O activity; however, since all runs for sample D217A have

very low significance of fits, it is difficult to determine if one result water activity is better than the other. Because all results are indistinguishable within error, an activity of 1.0 was selected to represent metamorphic conditions. Results based on the average mineral compositions are presented in Table 9.

Pressure-temperature conditions for this sample indicate peak conditions in the HP-granulite facies. Based on REE patterns for zircon dark CL rims the lower intercept age of 413 ± 36 Ma (anchored by one point at 429 ± 2 Ma) is interpreted to represent HP-granulite metamorphism in this sample. The upper intercept age of 938 ± 28 Ma is interpreted to represent a previous metamorphic event based on inclusions of Bt + Ms + Qtz + Kfs + Pl and zircon REE patterns.

Tonalite D213A

The tonalite sample D213A contains subhedral zircon with both sector and oscillatory zones (Fig. 33A). Twelve U/Pb analyses yield 58–354 ppm U, 0.1–10 ppm Th, 0.004–0.03 Th/U and ages from 398–426 Ma, with a mean age of 419 ± 3 Ma (n = 10, MSWD = 1.46, Table 14, Fig. 33B).

Of 24 trace element analyses on zircons from sample D213A, 4 contain elevated contaminants and 5 contain incomplete REE patterns due to LREE abundances below the instrument detection limit (Table 15, Fig. 34A). The remaining REE patterns have weak positive and negative Eu anomalies (Eu/Eu* = 0.3–1.37, outlier at 1.61). Analyses with positive Eu anomalies are generally characterized by steep HREE patterns, while analyses with negative Eu anomalies are characterized by flatter HREE trends; however, there is significant overlap and a definite pattern cannot be resolved. Ti-in-zircon

thermometry (Ferry and Watson, 2007) yields temperatures from 618–814 ˚C (Fig. 34B).

There is no rutile in this sample, indicating the sample is Ti-under-saturated, therefore

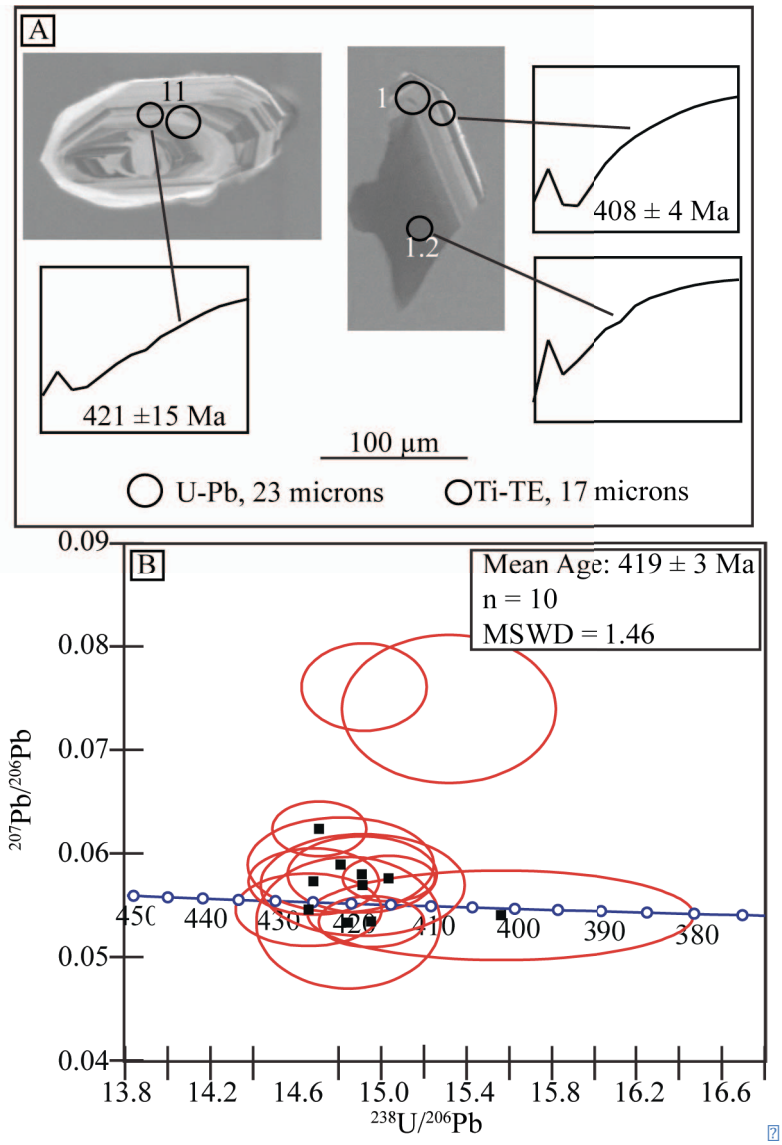

Figure 33. Results for SHRIMP-RG U-Pb zircon analysis for tonalite D213A. A) Example zircons taken from the sample showing negative Eu anomaly analyses (spot 1.2 and spot 11) and positive Eu anomaly analysis (spot 1). U-Pb indicates spots for geochronology, Ti-TE indicates spots for trace element analysis. B) U-Pb Terra-Wasserburg plot (Terra and Wasserburg, 1972) for sample D213A, points represent analyses used in mean age calculation (error ellipses are 2 sigma).

assuming a Ti activity of 1.0 (as used for the other samples which are Ti-saturated) may

be inaccurate. Temperatures calculated using an activity of 1.0 most likely provide a

TABLE 14. ZIRCON U-Pb ISOTOPIC DATA, TONALITE SAMPLE D213A, NORTH QAIDAM, WESTERN CHINA

Analysis	$^{206}Pb_c$ %	U (ppm)	Th (ppm)	$^{232}Th/^{238}U$	^{207}Pb-corr $^{206}Pb/^{239}U$ age (Ma ± 1σ err)	Total $^{238}U/^{206}Pb$ (± % err)	Total $^{207}Pb/^{206}Pb$ (± % err)
D213A-1	2.61	176	3.00	0.020	407.8 ± 3.3	6.98 ± 0.5	0.0760 ± 2.3
D213A-2*	0.89	316	2.00	0.010	420.5 ± 2.6	6.55 ± 0.7	0.0624 ± 1.7
D213A-3*	-	140	1.00	0.004	426.0 ± 4.1	6.88 ± 0.6	0.0546 ± 2.6
D213A-4*	-	287	3.00	0.010	418.3 ± 2.8	6.47 ± 0.6	0.0535 ± 1.9
D213A-5*	0.25	179	5.00	0.030	423.9 ± 3.6	6.55 ± 0.5	0.0573 ± 2.3
D213A-6	2.38	58	0.34	0.010	398.4 ± 5.4	6.60 ± 0.5	0.0739 ± 3.9
D213A-7*	0.23	72	0.18	0.002	417.6 ± 5.5	4.74 ± 0.5	0.0570 ± 3.5
D213A-8*	-	106	2.00	0.020	401.9 ± 9.4	6.31 ± 2.7	0.0541 ± 3.3
D213A-9*	0.46	85	.14.00	0.002	419.5 ± 5.1	7.18 ± 0.6	0.0589 ± 3.2
D213A-10*	0.32	354	10.00	0.030	414.0 ± 2.4	6.45 ± 0.5	0.0576 ± 1.6
D213A-11*	-	86	1.00	0.010	421.3 ± 5.1	6.48 ± 0.4	0.0534 ± 4.8
D213A-12*	0.36	140	3.00	0.020	417.2 ± 4.0	6.41 ± 0.7	0.0580 ± 2.6

*Analysis used in weighted mean age calculation.

TABLE 15. ZIRCON TRACE-ELEMENT (PPM) RESULTS FOR TONALITE SAMPLE D213A, NORTH QAIDAM, WESTERN CHINA

Analysis	Li	Be	B	F	Na	Al	P	K	Ca	Sc	^{48}Ti	^{49}Ti	Fe	Y	Nb	^{94}ZrH	La	Ce	Nd
D213A-1	12.8	0.09	0.3	8	11	17	91	14	2	363	5.0	5.0	2	194	1	1.4	0.005	0	0.01
D213A-1.2	2.4	0.18	0.3	10	13	18	238	15	4	697	17.9	17.4	6	882	4	1.5	0.002	3	0.26
D213A-2	0.8	0.08	0.4	10	15	22	85	18	9	446	3.5	3.3	2	146	2	1.6	0.017	0	0.05
D213A-2.2	0.0	0.01	0.2	6	12	17	27	11	3	93	3.2	3.0	1	32	1	1.5	0.000	0	0.00
D213A-3	9.2	0.08	0.4	9	13	29	50	13	12	308	5.1	5.4	3	128	1	1.6	0.107	1	0.43
D213A-3.2	63.3	0.21	0.4	8	36	24	245	12	6	748	20.7	19.8	7	1047	5	1.6	0.000	3	0.35
D213A-4	21.7	0.07	1.0	8	62	51	61	43	51	170	5.1	4.8	3	158	2	1.7	1.162	3	2.85
D213A-4.2	1.6	0.03	0.2	8	8	24	44	6	3	160	10.5	11.9	2	44	2	1.3	0.081	0	0.07
D213A-5	0.5	0.01	0.3	5	6	19	106	5	3	273	10.7	9.8	1	213	20	1.4	0.007	0	0.01
D213A-5.2	0.1	0.02	0.0	4	11	13	51	9	5	269	3.8	3.7	2	121	4	1.6	0.010	0	0.01
D213A-5.3	2.6	0.09	0.3	7	6	14	68	5	3	244	6.2	6.1	2	117	8	1.5	0.012	0	0.00
D213A-6	2.4	0.01	0.3	8	10	20	25	9	12	182	3.0	2.8	1	54	1	1.6	0.017	0	0.02
D213A-7	10.1	0.06	0.2	10	10	259	58	9	8	83	2.7	2.8	23	30	2	1.5	0.118	1	0.60
D213A-8	1.1	0.01	0.2	7	9	15	50	7	3	247	3.0	2.9	1	71	2	1.4	0.010	0	0.01
D213A-9	0.5	0.01	0.2	8	26	27	59	19	8	70	2.2	2.1	1	21	2	1.6	0.013	0	0.02
D213A-10	2.8	0.06	0.1	5	7	21	174	8	4	374	10.1	10.2	3	263	3	1.4	0.008	1	0.07
D213A-11	1.5	0.01	0.2	7	8	19	82	6	4	351	3.6	3.7	2	125	2	1.5	0.013	0	0.06
D213A-12	1.6	0.01	0.3	5	9	17	63	6	4	214	7.0	7.2	2	88	9	1.5	0.016	0	0.00
D213A-12.2	1.7	0.01	0.4	5	11	26	113	6	6	294	17.9	18.1	5	210	22	1.5	0.008	0	0.01
D213A-12.3	12.0	0.10	0.5	10	20	192	130	49	14	362	19.8	20.6	75	275	24	1.6	0.127	2	0.87
D213A-13	1.9	0.15	0.8	10	28	1446	45	94	22	51	2.0	2.0	218	17	2	1.5	0.065	1	0.41
D213A-13.2	0.6	0.02	0.2	5	7	17	36	4	3	174	2.5	2.2	1	45	1	1.4	0.005	0	0.01
D213A-13.3	0.6	0.00	0.2	6	8	24	61	5	3	62	2.7	2.8	1	19	2	1.4	0.005	0	0.00
D213A-13.4	3.2	0.10	0.4	6	9	33	82	7	5	65	3.9	4.2	56	49	2	1.4	0.052	1	0.12

TABLE 15. CONTINUED

Analysis	Sm†	Eu	Gd	Ho	Tb	Dy	Er	Tm	Yb	Lu	Hf	Th	U	Th/U	Ce/Ce*	Eu/Eu*	Yb/Gd	T °C ^{48}Ti	T °C ^{49}Ti
D213A-1	0.13	0.214	2	7	1.01	15	34	8	74	14	13504	2	231	0.01	29	1.21	32.4	680	685
D213A-1.2	1.73	1.354	22	34	8.77	93	136	26	212	36	12109	46	1309	0.04	110	0.66	9.4	790	801
D213A-2	0.08	0.087	1	5	0.45	9	34	9	101	22	16128	0	86	0.00	3	1.12	137.9	652	651
D213A-2.2	0.01	0.044	0	1	0.17	3	5	1	10	2	14876	0	74	0.00	–	2.54	29.1	647	643
D213A-3	0.34	0.239	2	5	0.89	12	21	5	43	8	13798	1	156	0.00	3	0.84	19.3	681	691
D213A-3.2	1.66	1.528	25	38	9.95	107	157	31	234	38	12331	57	1539	0.04	–	0.73	9.5	805	814
D213A-4	1.37	0.731	5	6	1.29	14	25	5	45	9	13205	3	231	0.01	1	0.90	9.9	681	681
D213A-4.2	0.05	0.021	0	1	0.12	2	9	3	34	8	16396	0	41	0.00	2	0.69	182.3	741	763
D213A-5	0.06	0.033	1	8	0.79	13	45	12	122	24	22518	6	201	0.03	5	0.35	87.8	743	744
D213A-5.2	0.01	0.010	0	4	0.29	6	33	12	141	33	20924	0	30	0.00	1	0.62	430.3	659	660
D213A-5.3	0.02	0.010	0	4	0.32	7	28	9	108	24	22222	1	91	0.01	–	0.30	228.2	697	702
D213A-6	0.03	0.046	0	2	0.21	4	11	3	26	6	14628	1	65	0.01	6	1.30	70.3	641	639
D213A-7	0.37	0.183	1	1	0.21	3	5	2	17	4	15956	0	87	0.00	3	0.88	15.6	634	639
D213A-8	0.02	0.020	0	2	0.15	3	15	5	57	13	16277	0	54	0.00	5	0.84	163.0	643	641
D213A-9	0.01	0.013	0	1	0.08	2	5	1	12	3	15764	0	58	0.00	1	1.61	151.6	620	618
D213A-10	0.47	0.461	6	9	2.21	25	39	8	71	13	12787	12	424	0.03	28	0.82	11.2	738	748
D213A-11	0.17	0.156	1	4	0.59	9	27	8	76	16	14887	1	102	0.01	8	1.21	84.8	654	660
D213A-12	0.01	0.022	0	3	0.23	5	22	8	87	21	20674	1	81	0.01	–	1.35	294.5	707	716
D213A-12.2	0.15	0.120	2	7	0.88	13	47	13	146	30	17701	6	237	0.02	8	0.69	81.3	791	805
D213A-12.3	0.92	0.444	4	10	1.56	20	53	13	122	22	17569	8	999	0.01	5	0.71	30.8	800	818
D213A-13	0.32	0.185	2	1	0.24	2	4	1	11	2	17643	0	13	0.02	2	0.80	7.2	614	614
D213A-13.2	0.02	0.015	0	2	0.10	3	10	3	35	8	16320	0	34	0.00	2	1.37	688.5	629	620
D213A-13.3	0.02	0.013	0	1	0.04	2	4	1	9	2	14085	0	85	0.00	–	0.88	74.3	635	639
D213A-13.4	0.10	0.103	1	2	0.34	4	7	2	15	2	13038	2	209	0.01	4	1.00	14.9	662	670

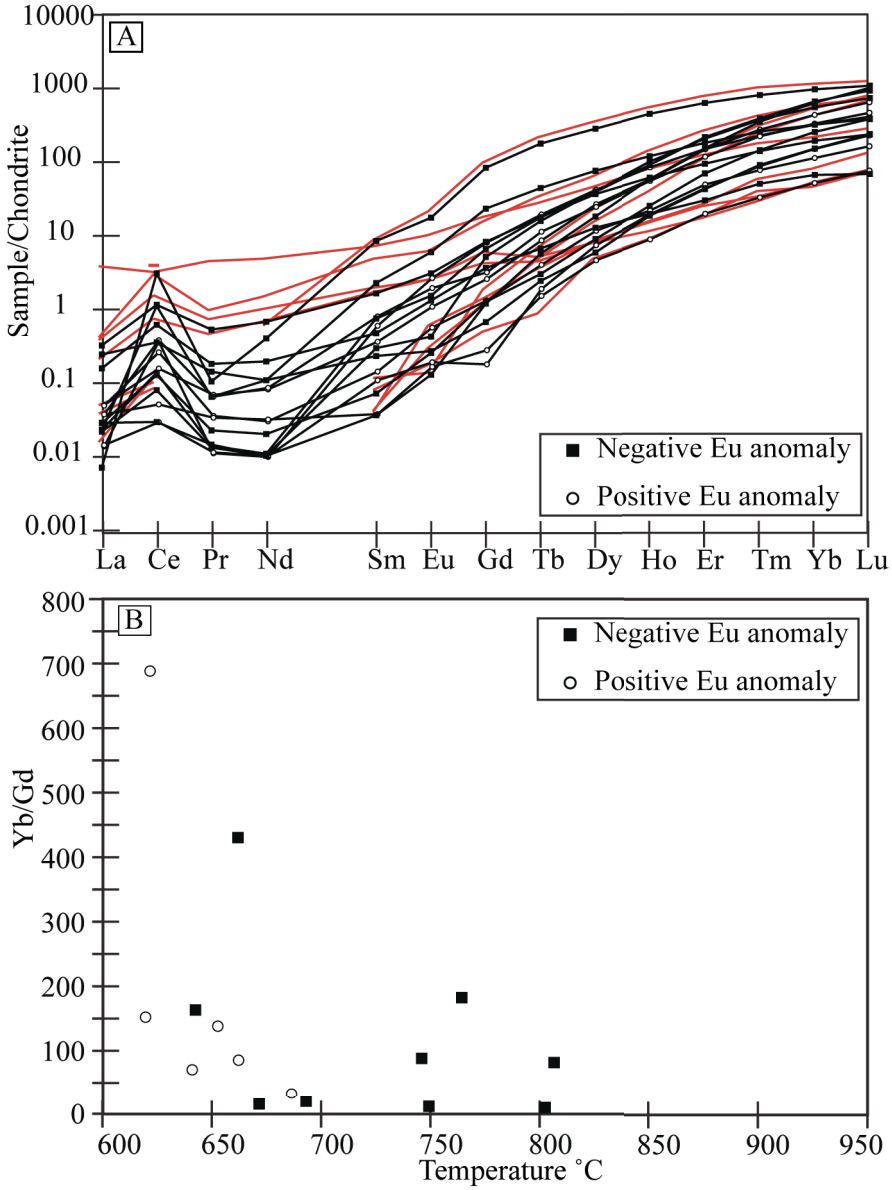

Figure 34. Zircon trace-element results for tonalite sample D213A. A) REE patterns for zircons, red lines indicate analyses with high contaminant levels (see text and table 14). B) Plot of Yb/Gd vs. Ti-in-zircon temperatures (Ferry and Watson, 2007). Temperatures are uncorrected for the lack of Rt in the sample and are calculated with a Ti activity of 1.0 (see text).

minimum temperature estimate. Calculated temperatures for a Ti activity of 0.7 are 642–846 ˚C, which overlaps the temperatures using an activity of 1.0. Based on zircon CL

zoning, Ti-in-zircon temperatures, and zircon REE patterns the mean age of 419 ± 3 Ma is interpreted to represent the crystallization age for the tonalite.

Rt-bearing Tonalite D217C

The rutile-bearing tonalite sample D217C contains zircons with both sector and oscillatory zones that span a range from CL dark to CL bright. Fourteen analyses yield 145–282 ppm U, 1–742 ppm Th, 0.004–0.69 Th/U, and ages from 396–452 Ma (Fig. 35A). One analysis from a dark CL oscillatory-zoned grain contains 1366 ppm U, 105 ppm Th, 0.08 Th/U, and yields an age of 826 ± 2 Ma. Discordia intercept ages for this sample are 403 ± 12 Ma and 910 ± 52 Ma (n = 11, MSWD = 1.4).

Separate trace element analyses were not done for this sample, but trace elements measured as part of the U/Pb analysis show potential contamination in four spots based on extremely high LREE values (Fig. 35B). Four zircons are characterized by strongly negative Eu anomalies (Eu/Eu* = 0.07–0.41) and steep HREE patterns (Yb/Gd = 18–48). These four samples include the 826 Ma zircon (D217C spot 5). Remaining zircons have weak Eu anomalies (Eu/Eu* = 0.54–1.02) and flat HREE patterns (Yb/Gd = 0.6–2.8).

Based on zircon REE pattern the lower intercept age of 403 ± 12 Ma is interpreted to represent the crystallization age for the tonalite. The upper intercept age of 910 ± 52 Ma is interpreted to represent an inherited age from the tonalite source rock.

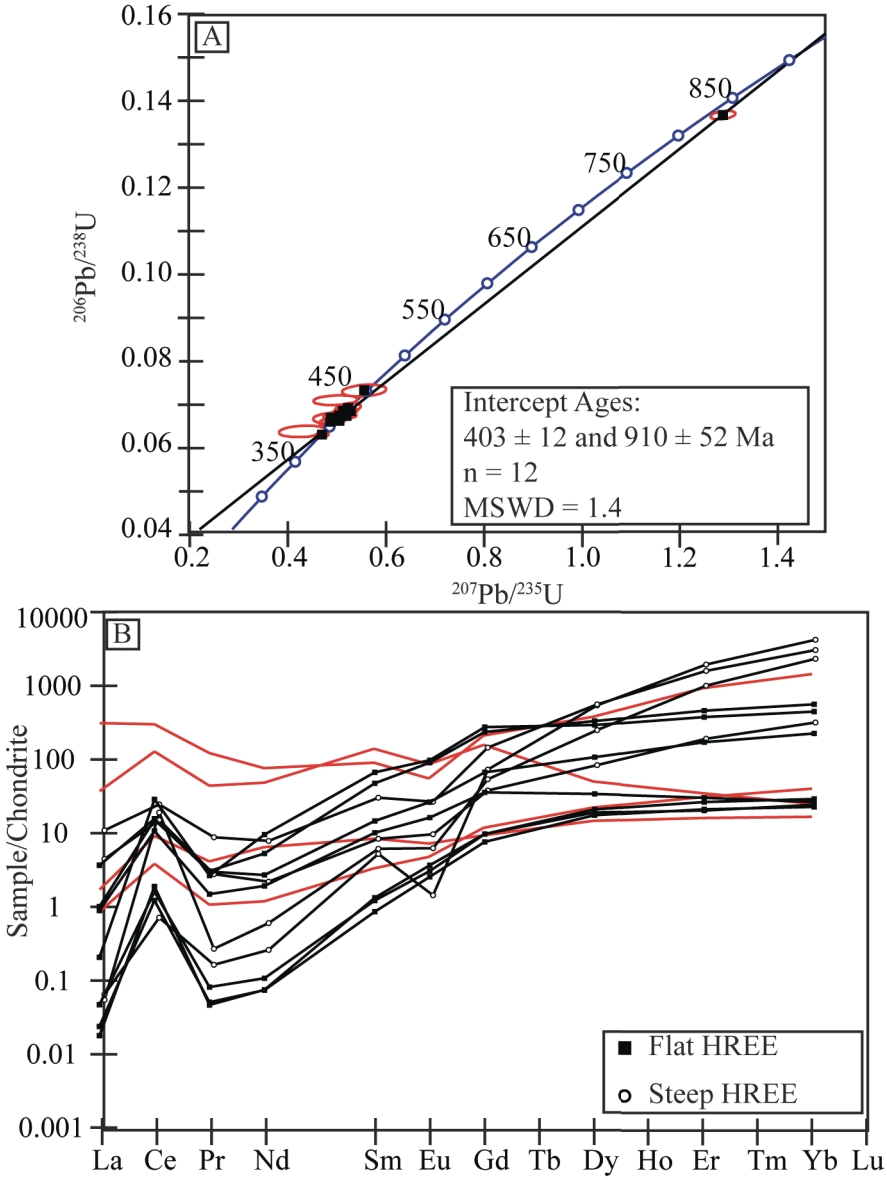

FIGURE 35. Results for SHRIMP-RG U-Pb and trace-element analysis for Rt-bearing tonalite sample D217C. A) U-Pb concordia plot (isotopic ratios corrected for ^{204}Pb), points represent analyses used in intercept ages (error ellipses are 2 sigma). B) REE patterns for zircons, red lines indicate presumed contamination based on high LREE values (see text)

CHAPTER VI

DISCUSSION

Whole Rock Chemistry

The broad SiO_2 range in the Dulan granulites differs from the typical Dulan eclogites, which tend to show a comparatively narrow SiO_2 composition and show no field and petrographic evidence of partial melting (Fig. 11A). Titanium oxide compositions of the granulites are similar to the Ky-eclogites from the SDB (<1.0 wt%; Fig. 11B; Song et al., 2003a; Zhang et al., 2008b). Ep-Eclogites and Phe-eclogite from both the NDB and SDB tend to have higher amounts of TiO_2, up to ~2.0 wt%. Previous studies have used the geochemical discrimination (including V vs. TiO_2) in eclogites to distinguish the NDB and SDB based on protolith type. This geochemical discrimination led to the NDB and SDB being classified as two separate tectonic units; however, as more data has been collected there is no indication of distinct chemical separation between the two belts, suggesting they are actually one unit (Song et al., 2003a, Zhang et al., 2008b). Discrimination diagrams have been shown to be unable to classify between mid-ocean ridge, ocean island, and island arc basalts with greater than ~60% accuracy (Snow, 2006), further suggesting that whole-rock chemistry alone is not enough to distinguish between metamorphic rocks from the Dulan area. If the NDB and SDB are one unit, this supports the conclusion that the Dulan granulites are a separate HP-HT unit since fresh eclogites from the NDB and SDB do not contain evidence of a HP-granulite facies.

Pressure-Temperature Conditions

The Dulan HP-granulites represent a separate HP-HT unit adjacent to the Dulan UHP rocks. Pressure-temperature calculations on two HP-granulite samples indicates peak conditions reached 750–880 ˚C, 13–17 kbar based on results from the programs GTB v2.1 and THEMOCALC v3.3 (Fig. 36). Inclusions in Grt cores of Qtz + Pl + Czo are not indicative of a previous UHP history but instead suggest a prograde path at lower pressures and temperatures. Yu et al. (2010) reported a prograde path for the HP-granulites that passes through the epidote-amphibolite facies, supporting this conclusion (Fig. 36).

Clinopyroxene from this study does not support previous eclogite facies conditions. The clinopyroxene of the two analyzed granulites (D212B, D213B) has a small Jd component (<17 %), indicating it is not omphacite but instead lies in the augite region, which is not characteristic of the eclogite facies. This low Jd composition conflicts with reports from Song et al. (2003a, 2003b) and Yu et al. (2010), which reported clinopyroxene from the granulites as being omphacite (Jd < 27%). The lower Jd component for this study is due to the calculation of a calcium tschermak (CaTs) component using the methods of Harlow (1999). Both Jadeite ($NaAlSi_2O_6$) and CaTs ($CaAlAlSiO_6$) are aluminum-rich clinopyroxene end-members. Aluminum is therefore allotted to two compositions, and calculating a CaTs component will lower the calculated Jd end-member. Previously reported omphacite in the Dulan granulites did not include a CaTs calculation. Clinopyroxene compositions from Song et al. (2003a) and Yu et al. (2010) do have low Si pfu (1.86–1.92, outliers at 1.96 and 1.99) and high Al pfu

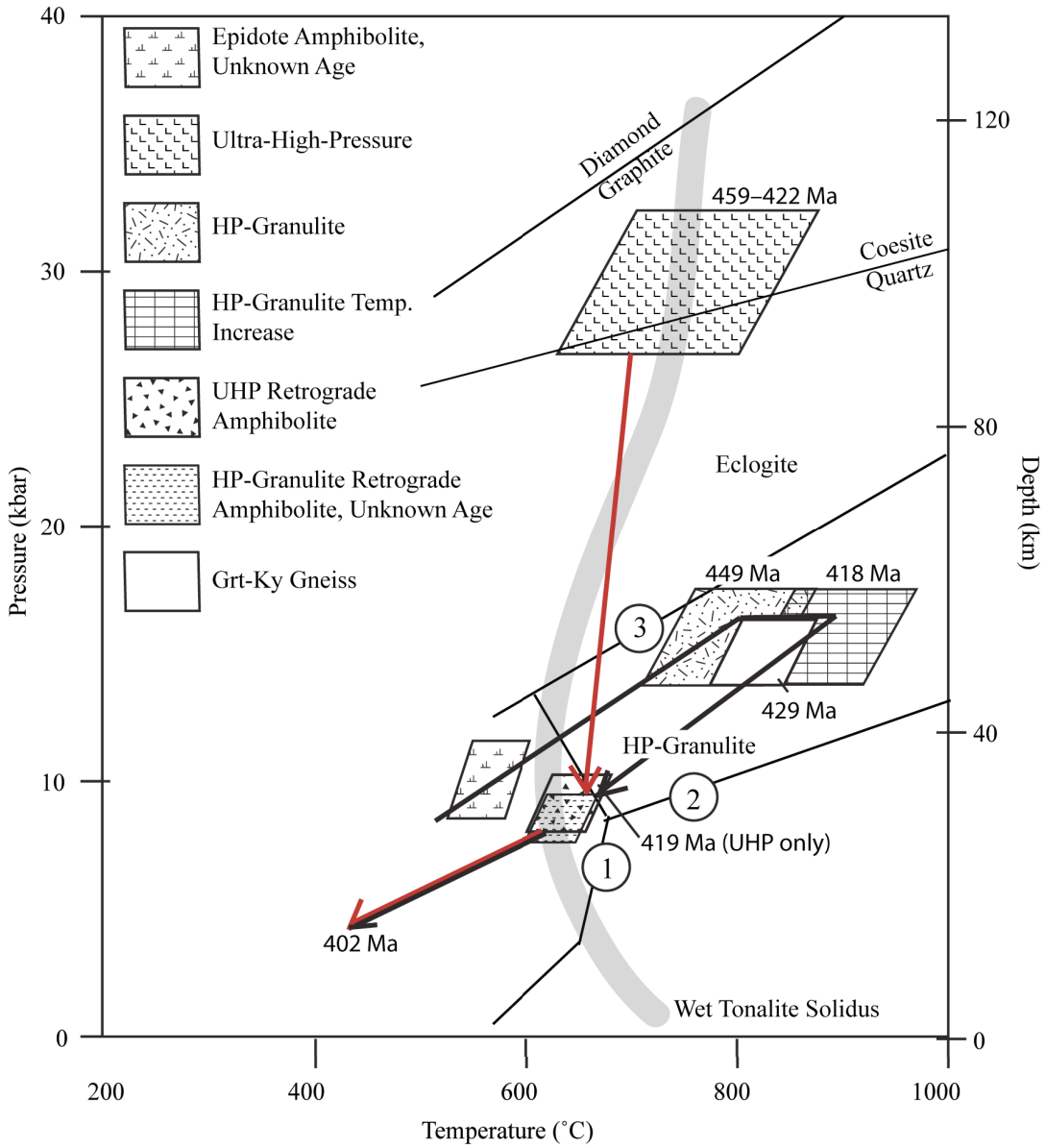

Figure 36. Summary of P-T-t paths for the Dulan HP-granulites and UHP rocks. Boundaries are amphibolite-granulite (1), MP-granulite-HP-granulite (2), and HP-granulite-eclogite. Prograde epidote-amphibolite stage for the HP-granulites is from Yu et al. (2010). Peak UHP conditions and ages are from Mattinson et al. (2007) and Zhang et al. (2010). Pressure-temperature data for the retrograde amphibolite facies is from Song et al. (2003b) and Yu et al. (2010). Amphibolite age is from Mattinson (personal communication). Facies boundaries are from Liou et al. (1998), and the wet tonalite solidus is from Lambert and Wyllie (1974).

(0.33–0.39) values. This combination of low Si and high Al indicates the possibility of a

significant CaTs component in the samples analyzed by those studies. The lack of a

significant Jd component (<20%) indicates the Cpx formed at pressures below the eclogite facies (O'Brien and Rötzler, 2003). The CaTs component is typical of high-temperature conditions, which when combined with pressures below the eclogite facies suggests growth under granulite conditions (Harlow, 1999).

Song et al. (2003a) also reports omphacite inclusions in kyanite (~$Jd_{47}Aug_{50}Aeg_{0-4}$). This analysis contains low Si pfu (1.9) and high Al pfu (0.51). This omphacite inclusion is one reason the Dulan granulites were reported as overprinted eclogites. This analysis is very different from any other Cpx analyzed in the Dulan granulites and with no other indication of previous eclogite conditions, it may represent a bad analysis caused by interference of surrounding minerals.

Pressure-temperature results for the Grt-Ky host gneiss match those recorded in the two analyzed granulite samples (D212B and D213B). Temperatures from the Grt-Bt thermometer are lower than those recorded by the Grt-Cpx thermometer used for the granulites, and this may be due to a higher diffusion rate between Grt and Bt during cooling.

Timing of HP-Granulite Conditions

Zircon U-Pb ages span a range from 449–418 Ma based on the U-Pb ages of the two granulite samples, D212B and D213B. Intermediate granulite sample D214 records an older age of 472 ± 54 Ma; however, the high error of this age makes it indistinguishable from the 449–418 Ma range. One zircon age spot from Grt-Ky gneiss sample D217A also falls within this age range. These ages are interpreted to represent

HP granulite facies conditions and reflect peak conditions recorded by matrix minerals despite zircon REE patterns being atypical for HP-granulite conditions (see below).

Temperatures calculated by Ti-in-zircon thermometry (Ferry and Watson, 2007) overlap the P-T conditions calculated from the matrix assemblage (670–940 ˚C compared to 750–880 ˚C). This suggests that the zircon results and P-T analysis record the same peak conditions, and that the U-Pb and trace element results represent HP-granulite metamorphism. The lowest Ti-in-zircon results are from the mafic granulite sample (D212B). The lower temperatures (667–761 ˚C) do not match the P-T conditions calculated from the matrix assemblage. This difference could be related to the lack of a pressure correction for the Ti-in-zircon thermometry, which would indicate this is a minimum temperature estimate for the HP granulites. Sample D217A also records low Ti-in-zircon temperatures (608–691 ˚C) for the thin CL dark rims associated with HP-granulite formation. Improper spot placement on these thin rims probably caused incomplete measurements of Ti compositions.

Zircon REE patterns seen in Dulan HP granulites do not resemble the typical zircon REE patterns for HP granulites, which are characterized by a negative Eu anomaly associated with the presence of plagioclase and the depletion of HREE due to the presence of garnet (Rubatto, 2002). Mafic granulite sample D212B records a negative Eu anomaly, but does not record the depleted HREE pattern. The lack of a Grt signature in this sample may be due to HREE enrichment in the whole rock. Though whole rock REE compositions were not collected in this study, the Y compositions can be used as a proxy for HREE patterns due to similar behavior. Sample D212B does have slightly higher

levels of Y compared to the other granulites: 24 ppm as opposed to 10 ppm in sample D213B and 8 ppm in sample D214. This does support the idea that HREE are enriched in the mafic granulite sample (at least compared to the other samples in this study), however, more research is needed.

Intermediate granulite sample D213B shows depleted zircon HREE patterns indicative of the presence of garnet, but lacks a Eu anomaly. The lack of Eu anomaly and depleted HREE is typical of zircon growth under eclogite conditions (Rubatto, 2002); however, inclusions of Qtz + Pl + Grt in the zircon cores supports granulite-facies conditions instead. The lack of a Eu anomaly may be caused by oxidized conditions in the granulites, causing Eu to switch from its 2+ state to its 3+ state. This switch lowers the affinity of Eu for plagioclase and would cause the element to be evenly incorporated into other minerals, leading to the lack on a Eu anomaly in zircon (Ballard et al., 2002).

Intermediate granulite sample D214 records two zircon populations, one with depleted zircon HREE patterns, the other with enriched HREEs. It is possible that one group records HP-granulite (depleted HREE) conditions while the other records pre-granulite growth (enriched HREE). There is no apparent age difference between the zircons, so differentiating between the two zircon groups is not possible.

Relationship Between the Granulite and UHP Gneiss

The Grt-Ky paragneiss from this study records a previous metamorphic event at 938 ± 20 Ma in dark CL zircon rims. Zircon REE patterns for this event indicate the presence of plagioclase but not Grt at this time. Mineral inclusions in zircons recording this zircon growth include Qtz and Kfs. Inclusion of Ms + Bt in other zircons from this

sample most likely apply to this period of zircon growth however zircons containing those inclusions were not analyzed for U-Pb. The REE patterns are all very similar and suggest metamorphic growth. A similar metamorphic event is recorded in a paragneiss sample from the UHP gneiss with a zircon U-Pb age of 914 ± 30 Ma (Fig. 37A; Mattinson, personal communication). Zircon REE patterns are also similar to those seen in the Grt-Ky gneiss, with enriched HREE and a strong negative Eu anomaly (Fig. 37B). This sample has ages as young as 425 Ma, which record flat HREE patterns and a much weaker Eu anomaly, which reflect eclogite facies conditions. This similar history in the HP-granulite and UHP host gneiss may reflect a shared origin between the UHP and HP-HT rocks prior to continental collision.

Origin of High-Pressure Granulites

There are essentially two varieties of high-pressure granulite: high or ultra-high temperature granulites that have formed under conditions >900 ˚C and 15 kbar and overprinted eclogites, which form under similar pressures but lower temperatures (700 – 850; O'Brien and Rötzler, 2003). Recorded conditions for the samples analyzed here span a temperature range from about 770–880 ˚C as calculated by the thermobarometers in this study. Though this is lower than temperatures associated with HP-HT granulites, Ti-in-zircon thermometry for the intermediate granulite sample D213B indicates a period of growth at 866-942 ˚C, and the presence of partial melts in the Dulan granulite area indicates temperatures beyond the wet solidus (~630 ˚C at 15 kbar for tonalite; Lambert and Wyllie, 1974). Combined with the lack of textural evidence indicating previous UHP conditions (no polycrystalline quartz replacement after coesite, lack of significant Cpx +

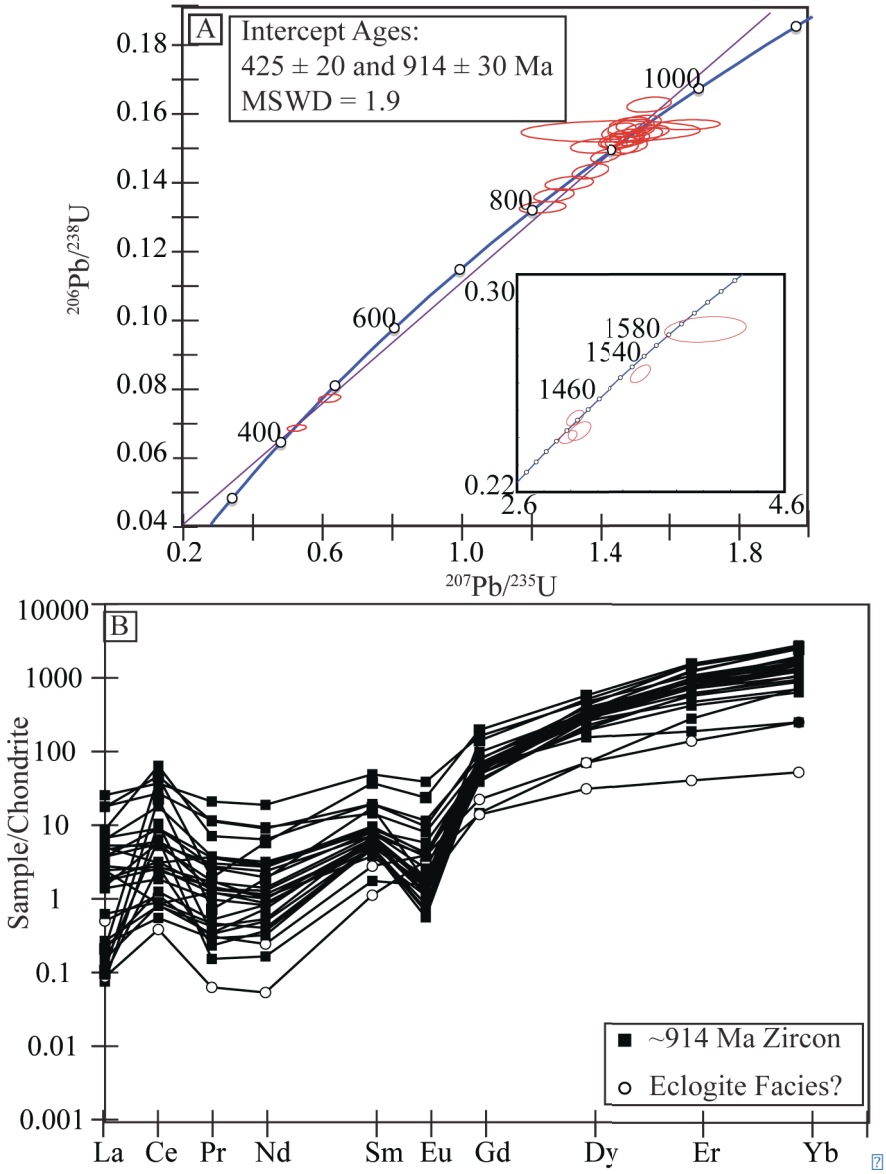

Figure 37. Previous results for SHRIMP-RG U-Pb and trace-element zircon analysis for UHP paragneiss sample D4A (Mattinson, personal communication). A) U-Pb concordia plot (isotopic ratios corrected for ^{204}Pb; error ellipses are 2 sigma) Results are similar to Grt-Ky gneiss sample D217A (see Fig. 25 and 26). B) REE patterns for D4A zircons, black squares are ~914 Ma zircon and inherited cores and open circles are younger zircons

Pl symplectite after Omp), P-T calculations from this study indicate that the Dulan granulites are HP-HT granulites and not overprinted eclogites. This agrees with the conclusions of Yu et al. (2010), who found peak conditions of 800–950 ˚C, 14.5–18.5

kbar (Fig. 36). Yu et al.'s (2010) P-T results are based on the same thermobarometers used in this study. The lower temperatures recorded in this study may be due to the differences between the Grt-Cpx exchange thermometers used. The calibration of Pattison and Newton (1989; this study) is known to consistently plot below other calibrations (e.g. 50 ˚C lower at 15 kbar), including Powell (1985; Spear, 1995; Yu et al., 2010). Since results for this study plot 50-75 ˚C below results from Yu et al. (2010), this may explain the discrepancy. Other possible explanations for the difference in temperature estimates include differences in rock compositions between studies or different degrees of diffusion during cooling between samples.

Yu et al. (2010) and Zhang et al. (2009c) both suggest the Dulan HP-granulite originated in the base of thickened overriding crust in a subduction zone with the Dulan eclogite forming in the subducting plate. The samples from this study suggest prolonged HP-granulite conditions from 449-418 Ma, which overlaps the Dulan HP/UHP age range of 459-422 Ma (Mattinson et al., 2006, 2007; Song et al., 2003a, 2003b; Zhang et al., 2008b, 2009a, 2009b, 2009d, 2010). The suggested relationship would explain these nearly identical metamorphic ages. The different P-T-t paths for the granulites and eclogites is also consistent with the interpretation by Yu et al. (2010) and Zhang et al. (2009c) that the granulites represent a separate unit from the UHP rocks.

Importance of the Partial Melts

The felsic granulites and tonalites from the Dulan HP-granulite unit represent partial melts derived from the mafic-intermediate granulites, and indicate conditions passed the wet-tonalite solidus (Lambert and Wyllie, 1974) during metamorphism.

Titanium-in-zircon thermometry (Ferry and Watson, 2007) records a temperature increase from ~800 to ~900 ˚C at 418 Ma in one intermediate granulite sample (D213B). A nearby tonalite sample yields a U-Pb zircon mean age of 419 Ma, indistinguishable from the timing of the temperature increase. Zircon REE patterns for the tonalite are scattered and exhibit a range of Eu anomalies and HREE patterns. Such variability is uncommon in igneous samples; typical igneous zircon growth is generally more uniform in REE patterns between grains. The range of REE patterns may be indicative of multiple zircon sources mixing together, suggesting that this sample is a partial melt from the granulites that has incorporated multiple zircon signatures from different source rocks. The timing indicates melting occurred a few million years after UHP metamorphism is interpreted to have stopped.

Zircons from granulite leucosome sample D136B and banded granulite D143 have similar REE patterns as tonalite sample D213A (Fig. 38 and 39, Mattinson, personal communication). This indicates the felsic granulites are partial melts derived form the mafic-intermediate granulites. The zircons from these two samples record mean U-Pb ages of 437 ± 3 Ma (D136B) and 412 ± 2 Ma (D143), with Ti-in-zircon temperatures of 575–789 ˚C and 589–815 ˚C. If these samples are partial melts, they indicate partial melting may have occurred at multiple points during the HP granulite history.

Tonalite sample D217C is also a partial melt from the Dulan granulite area, but represents a partial melt derived from the Grt-Ky gneiss, instead of the granulites. The Rt in this tonalite suggests melting of Ti-bearing minerals in the source rock. Titanium in the mafic-intermediate granulites is concentrated in Rt, which would not melt under the

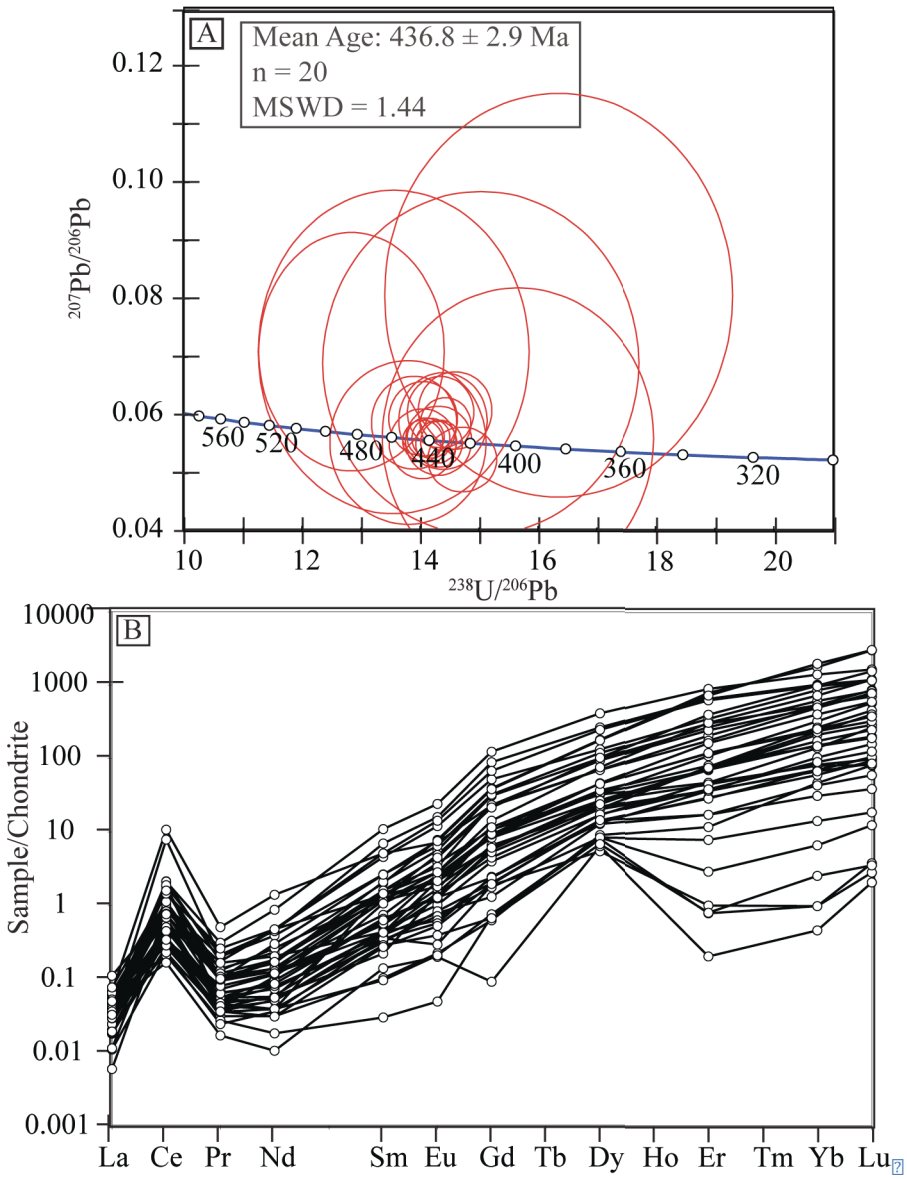

Figure 38. Previous results for SHRIMP-RG U-Pb and trace-element zircon analysis for granulite leucosome D136B (Mattinson, personal communication). A) U-Pb Terra-Wasserburg plot (Terra and Wasserburg, 1972) for sample D136B (error ellipses are 2 sigma). B) Zircon REE patterns for the granulite leucosome showing variability similar to sample D213A (see Fig. 29 and 30).

calculated temperatures. The Grt-Ky gneiss, however, contains Bt with 3.6-4.0 wt%

TiO_2, which would melt. This suggests the Rt-bearing tonalite was not derived from the

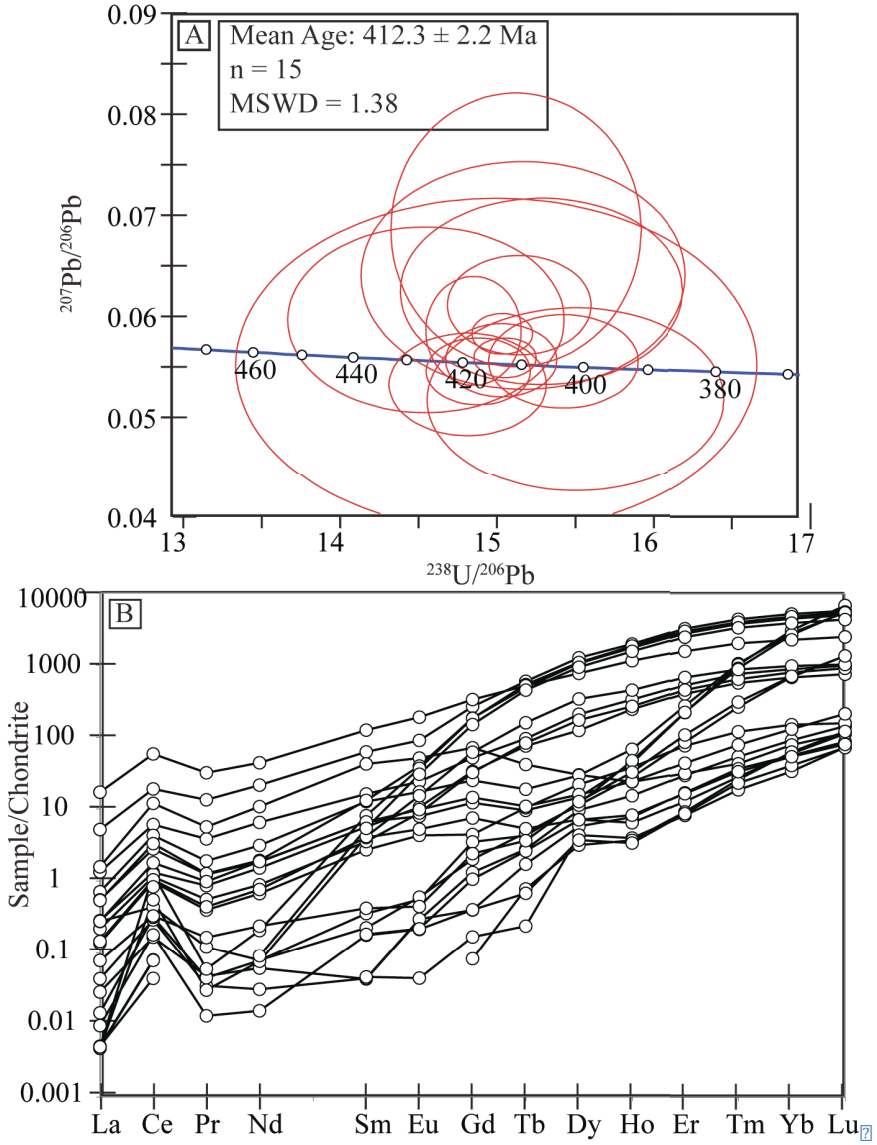

Figure 39. Previous results for SHRIMP-RG U-Pb and trace-element zircon analysis for banded granulite sample D143 (Mattinson, personal communication). A) U-Pb Terra-Wasserburg plot (Terra and Wasserburg, 1972) for sample D143 (error ellipses are 2 sigma). B) Zircon REE patterns for the banded granulite showing variability similar to sample D213A (see Fig. 29 and 30).

granulites but from the gneiss. Zircon U-Pb data from D217C yields an upper intercept age of 910 ± 52 Ma, indistinguishable from the metamorphic age of zircon rims seen in the Grt-Ky gneiss (938 ± 28 Ma). Younger zircons in sample D217C have REE patterns typical of HP-granulite conditions (negative Eu anomalies and depleted HREEs). Despite

the apparent lack of garnet in the tonalite sample, if it were derived from the Grt-Ky gneiss, the resulting melt would be HREE depleted. The lower intercept for sample D217C (412 ± 12 Ma) is indistinguishable from the age recorded by sample D143 and D213A, and may indicate continued melting in the Dulan granulites almost 10 million years after the UHP rocks began to exhume.

Though melting appears to have occurred throughout HP granulite formation, almost all of the partial melts studied here occurred after HP/UHP conditions were thought to have ended (Mattinson et al., 2006; Zhang et al., 2010). The proximity in time between UHP cessation and partial melting in the HP granulites may indicate partial melting in the granulites is related to exhumation of the UHP rocks (presumed to begin after ~422 Ma). Yu et al. (2010) suggested the exhumation of the HP granulites was related to slab break off or delamination of the lithospheric mantle, leading to crustal thinning (Arnold et al., 2001; Willner et al., 2002). Slab break off can also lead to mantle upwelling, which would supply significant amounts of heat to the overriding HP granulites, and may have caused the associated partial melting (Arnold et al., 2001). Partial melting also appears to be accompanied by rapid cooling. Sample D213B indicates temperature reached ~900 ˚C at 418 Ma, but at this same time tonalite sample D213A records zircon growth, suggesting temperatures were cool enough to crystallize the melt. This overlap between tonalite formation and temperatures ≥ 900 ˚C suggests rapid cooling of the tonalite melt may have occurred.

An amphibolite overprint can be seen in both the HP-granulites and UHP rocks, suggesting the two units might have come together prior to or during amphibolite facies

conditions. A metamorphic age of 419 Ma was attributed to amphibolite facies conditions from the Dulan UHP rocks, and if this is the case this means partial melting was still occurring in the HP-granulites during amphibolite-facies conditions (Mattinson, personal communication). Zircon U-Pb geochronology from a UHP paragneiss and Mu $^{40}Ar/^{39}Ar$ geochronology from an UHP orthogneiss yield ages of ~402 Ma (Song et al., 2006) and are interpreted to represent retrograde conditions for the UHP rocks. If the granulites and UHP rocks were juxtaposed prior to or during the amphibolite facies, the partial melting in the granulites must have ceased prior to ~402 Ma, as by this point they would have reached upper crustal levels.

Other North Qaidam Granulites

Though HP-granulites are not limited to the Dulan UHP exposure of the North Qaidam Terrane, the Dulan HP-granulites indicate a more rapid UHP exhumation for the Dulan UHP rocks compared to other North Qaidam UHP units. High-pressure granulites found in the Xitieshan and Lüliangshan exposures west of Dulan are indicative of overprinted eclogites. In the Xitieshan, overprinted eclogites record eclogite conditions at ~486 Ma (Zhang et al., 2005b). High-pressure granulite conditions are recorded in eclogite and paragneiss zircons with ages from 451–461 Ma in both the overprinted eclogite and surrounding paragneiss (Zhang et al., 2008a, 2009a). Further west, the Lüliangshan paragneiss and orthogneiss record HP-granulite facies metamorphism at ~450 Ma and a MP-granulite facies at ~425 Ma, and enclosed mafic granulite blocks may record a previous eclogite facies based on omphacite inclusions in garnet (Zhang et al., 2008a). These overprinted eclogites are different from the HP-HT granulites reported in

this study. The presence of overprinted eclogites west of Dulan, but not within the Dulan UHP exposure, suggests different portions of the North Qaidam have different exhumation histories. The timing between eclogite and granulite metamorphic events in other areas of the North Qaidam indicates 20-30 million years of exhumation from HP/UHP conditions to HP-HT conditions. Based on results from this study (see above sections), the Dulan UHP rocks did not experience a HP-granulite stage, and instead exhumed from UHP to shallow crustal levels in ~20 m.y., indicating a much faster rate of exhumation for the Dulan UHP rocks.

High-pressure granulites have also been reported in the South Altyn Terrane, thought to be a continuation of the North Qaidam Terrane now offset by the Altyn Tagh fault (see Fig. 2). In the Bashiwake region of the South Altyn exposures of felsic granulite enclose mafic granulite and garnet peridotite. Geothermobarometry for all three rock types yields peak conditions of 870–1020 ˚C, 18.5–27.3 kbar. Zircon U-Pb geochronology indicates metamorphic zircon growth from 493–501 Ma (Zhang et al., 2005a). The peak conditions suggest near eclogite facies conditions at this date. The HP-granulite assemblage found in these rocks is most likely a reflection of bulk rock composition and not HP-granulite conditions like those in this study. The Dulan HP-granulites are different from other North Qaidam and South Altyn granulites in that they represent non-eclogite facies conditions separate from the UHP rocks, and may indicate a different exhumation rate for the Dulan rocks relative to the rest of the North Qaidam Terrane.

CHAPTER VII

CONCLUSION AND FUTURE WORK

Conclusion

The Dulan HP granulites represent HP-HT rocks that reached peak conditions of 750–880 ˚C. Granulite metamorphism occurred between 449 and 418 Ma, at the same time as eclogite facies metamorphism in the nearby UHP gneiss unit (459–422 Ma). After UHP conditions ceased in the adjacent UHP rocks, temperatures within the HP-granulite unit increased to 900+ ˚C, beyond the wet tonalite solidus (Lambert and Wyllie, 1974), which caused partial melting to occur throughout the HP granulites. Partial melting continued in the HP granulites while the UHP rocks exhumed. The UHP rocks had reached amphibolite facies conditions by ~419 Ma, when the HP-granulites still show signs of partial melting. Tonalite from the HP-granulite unit suggests cooling to ~650 ˚C at ~419 Ma. This indicates a period of rapid heating and cooling within a few million years. There is no evidence of partial melting in the UHP rocks, therefore if the HP-granulites and UHP rocks had come together within the amphibolite facies, then the UHP rocks must have remained relatively cool. The UHP rocks and HP granulites must have joined before 402 Ma, when the UHP rocks are thought to have reached upper crustal levels. The P-T-t paths of the UHP rocks and HP granulites may indicate rapid exhumation of the UHP/HP granulite units from ~50 km to shallow crustal levels in < 10 million years.

Future Work

As previously stated the fault contact between the Dulan HP granulites and UHP rocks is only inferred and has not been mapped. Future work must include attempting to find this contact to fully understand the structural relationship between HP granulite and UHP rocks. A highly deformed amphibolite is found between the HP-granulites and UHP rocks, and geochronology for this sample would help constrain the timing for juxtaposition of the granulite and eclogite units.

Future work must also include expanded trace element analysis. Zircon REE patterns seen in this study are atypical of HP granulites. Because zircon REE patterns are affected by the presence of garnet (Rubatto, 2002), garnet trace element analysis would be very useful to fully interpret the zircon REE results.

This study has shown there to be prolonged partial melting in the Dulan granulites. Most partial melt samples analyzed here formed after presumed exhumation of the Dulan UHP rocks had begun. One sample, however, indicated melting might have occurred more than 10 million years before UHP exhumation. A more detailed geochronological study of partial melts from the Dulan HP granulite is required to determine the full extent of HT conditions in the North Qaidam.

REFERENCES

Arnold, J., Jacoby, W.R., Schmeling, H., and Schott, B., 2001, Continental collision and the dynamic and thermal evolution of the Variscan orogenic crustal root – numerical models: Journal of Geodynamics, v. 31, p. 273-291.

Ballard, J.R., Palin, J.M., and Campbell, I.H., 2002, Relative oxidation sates of magmas inferred from Ce(IV)/Ce(III) in zircon: application to porphyry copper deposits of northing Chile: Contributions to Mineralogy and Petrology, v. 144, p. 347-364.

Black, L.P., Kamo, S.L., Allen, C.M., Davis, D.W., Aleinikoff, J.N., Valley, J.W., Mundul, R., Campbell, I.H., Korsch, R.J., Williams, I.S., and Foudoulis, C., 2004, Improved $^{206}Pb/^{238}U$ microprobe geochronology by the monitoring of a trace-element-related matrix effect; SHRIMP, ID-TIMS, ELA-ICP-MS and oxygen isotope documentation for a series of zircon standards: Chemical Geology, v. 205, p. 115-140.

Chen, N., Gong, S., Sun, M., Li, X., Xia, X., Wang, Q., Wu, F., and Xu, P., 2009, Precambrian evolution of the Quanji Block, northeastern margin of Tibet: Insights from zircon U-Pb and Lu-Hf isotope compositions: Journal of Asian Earth Sciences, v. 35, p. 367-376.

Chopin, C., 2003, Ultrahigh-pressure metamorphism: tracing continental crust into the mantle: Earth and Planetary Science Letters, v. 212, p. 1-14.

Coryell, C.D., Chase, J.W., and Winchester, J.W., 1963, A procedure for geochemical interpretation of terrestrial rare-earth abundance patterns: Journal of Geophysical Research, v. 68, p. 559-566.

Ferry, J.M., and Watson, E.B., 2007, New thermodynamic models and revised calibrations for the Ti-in-zircon and Zr-in-rutile thermometers: Contributions to Mineralogy and Petrology, v. 154, p. 429-437.

Grimes, C.B., John, B.E., Cheadle, M.J., Mazdab, F.K., Wooden, J.L., Swapp, S., and Schwartz, J.J., 2009, On the occurrence, trace element geochemistry, and crystallization history of zircon from in situ ocean lithosphere: Contributions to Mineralogy and Petrology, v. 158, p. 757-783.

Harlow, G.E., 1999, Interpretation of Kcpx and CaEs components in clinopyroxene from diamond inclusions in mantle samples, *in* Gurney, G.G., Pascoe, M.D., and Richardson, S.H., eds., The J.B. Dawson Volume: Proceedings of the VIIth International Kimberlite Conference, v. 1.

Hodges, K.V., and Spear, F.S., 1982, Geothermometry, geobarometry and the Al_2SiO_5 triple point at Mt. Moosilauke, New Hampshire: American Mineralogist, v. 67, p. 1118-1134.

Holland, T.J.B., 1980, The reaction albite = jadeite + quartz determined experimentally in the range 600–1200 ˚C: American Mineralogist, v. 65, p. 129-134.

Holland, T.J.B., and Powell, R., 1998, An internally consistent thermodynamic data set for phases of petrological interest: Journal of Metamorphic Geology, v. 16, p. 309-343.

Indares, A.D., 2003, Metamorphic textures and P–T evolution of high-P granulites from the Lelukuau terrane, NE Grenville Province: Journal of Metamorphic Geology, v. 21, p. 35-48.

Johnson, D.M., Hooper, P.R., and Conrey, R.M, 1999, XRF analysis of rocks and minerals for major and trace elements on a single dilution Li-tetraborate fused bead: *in* Proceedings, Advances in X-ray Analysis, 41st, Denver, Colorado, International Center for Diffraction Data, p. 843-867.

Kretz, R., 1983, Symbols for rock-forming minerals: American Mineralogist, v. 68, p. 277-279.

Kohn, M.J., and Spear, F.S., 1990, Two new barometers for garnet amphibolites with application to southeastern Vermont: American Mineralogist, v. 75, p. 89-96

Krogh Ravna, E.J., and Paquin, J., 2003, Thermobarometric methodologies applicable to eclogites and garnet ultrabasites, *in* Carswell, D.A., and Compagnoni, R., eds., EMU Notes in Mineralogy, v. 5, p. 229-259.

Lambert, I.B., and Wyllie, P.J., 1974, Melting of tonalite and crystallization of andesite liquid with excess water to 30 kilobars: Journal of Geology, v. 82, p. 88-97.

Liou, J.G., Zhang, R.Y., Ernst, W.G., Rumble, D., and Maruyama, S., 1998, High-pressure minerals from deeply subducted metamorphic rocks: Reviews in Mineralogy, v. 37, p. 33-96.

Ludwig, K.R., 2001, Squid 1.02: A user's manual: Berkeley Geochronology Center Special Publication No. 2, 19 p.

Ludwig, K.R., 2003, User's manual for Isoplot 3.00: A geochronological toolkit for Microsoft Excell: Berkeley Geochronology Center Special Publication No. 04, 70 p.

Newton, R.C., and Perkins III, D., 1982, Thermodynamic calibration of geobarometers based on the assemblage garnet-plagioclase-orthopyroxene (clinopyroxene)-quartz: American Mineralogist, v. 67, p. 203-222.

Mass, R., Kinny, P.D., Williams, I.S., Froude, D.O., and Compston, W., 1992, The Earth's oldest known crust: A geochronological and geochemical study of 3900–4200 Ma detrital zircons from Mt. Narryer and Jack Hills, Western Australia: Geochimica et Cosmochimica Acta, v. 56, p. 1281-1300.

Mattinson, C.G., Menold, C.A., Zhang, J.X., and Bird, D.K., 2007, High- and ultrahigh-pressure metamorphism in the North Qaidam and South Altyn Terranes, Western China: International Geology Review, v. 49, p. 969-995.

Mattinson, C.G., Wooden, C.A., Zhang, J.X., and Bird, D.K., 2009, Paragneiss zircon geochronology and trace element geochemistry, North Qaidam HP/UHP, western China: Journal of Asian Earth Sciences, v. 35, p. 298-309.

Mattinson, C.G., Wooden, J.L., Liou, J.G., Bird, D.K., and Wu, C.L., 2006, Age and duration of eclogite-facies metamorphism, North Qaidam HP/UHP terrane, western China: American Journal of Science, v. 306, p. 683-711.

Mazdab, F.K., and Wooden, J.L., 2006, Trace element analysis in zircon by ion microprobe (SHRIMP-RG); technique and applications: Geochimica et Cosmochimica Acta, v. 70, p. 26.

McDonough, W.F., and Sun, S.S., 1995, The composition of the Earth: Chemical Geology, v. 120, p. 223-253.

O'Brien, P.J., and Rötzler, J., 2003, High-pressure granulites: formation, recovery of peak conditions and implications for tectonics: Journal of Metamorphic Geology, v. 21, p. 3-20.

Page, Z.F., Essene, E.J., and Mukasa, S.B., 2005, Quartz exsolution in clinopyroxene is not proof of ultrahigh pressures: Evidence from eclogites from the Eastern Blue Ridge, Southern Appalachians, U.S.A: American Mineralogist, v. 90, p. 1092-1099.

Pattison, D.R.M., 2003, Petrogenetic significance of orthopyroxene-free garnet + clinopyroxene + plagioclase ± quartz-bearing metabasites with respect to the amphibolite and granulite facies: Journal of Metamorphic Geology, v. 21, p. 21-34.

Pattison, D.R.M., and Newton, R.C., 1989, Reversed experimental calibration of the garnet-clinopyroxene Fe–Mg exchange thermometer: Contributions to Mineralogy and Petrology, v. 101, p. 87-103.

Powell, R., 1985, Regression diagnostics and robust regression in geothermometer/ geobarometer calibration; the garnet-clinopyroxene geothermometer revisited: Journal of Metamorphic Geology, v. 3, p. 231-243.

Rubatto, D., 2002, Zircon trace element geochemistry: partitioning with garnet and the link between U-Pb ages and metamorphism: Chemical Geology, v. 184, p. 123-138.

Shervais, W., 1982, Ti–V plots and the petrogenesis of modern and ophiolitic lavas: Earth and Planetary Science Letters, v. 59, p. 101-118.

Snow, C.A., 2006, A reevaluation of tectonic discrimination diagrams and a new probabilistic approach using large geochemical databases: Moving beyond binary and ternary plots: Journal of Geophysical Research, v. 111, doi. 10.1029/2005JB003799.

Song, S.G., Yang, J.S., Liou, J.G., Wu, C., Shi, R.D., and Xu, Z.Q., 2003a, Petrology, geochemistry and isotopic ages of eclogites from the Dulan UHPM Terrane, the North Qaidam, NW China: Lithos, v. 70, p. 195-211.

Song, S.G., Yang, J.S., Xu, Z.Q., Liou, J.G., and Shi, R.D., 2003b, Metamorphic evolution of the coesite-bearing ultrahigh-pressure terrane in the North Qaidam, Northern Tibet, NW China: Journal of Metamorphic Geology, v. 21, p. 631-644.

Song, S.G., Zhang, L., Niu, Y., Su, L., Song, B., and Liu, D., 2006, Evolution from oceanic subduction to continental collision: a case study from the Northern Tibetan Plateau based on geochemical and geochronological data: Journal of Petrology, v. 47, p. 435-455.

Spear, F.S., 1995, Metamorphic phase equilibria and pressure-temperature-time paths: Mineralogical Society of America Monograph, 799 p.

Spear, F.S., and Kohn, M.J., 1999, Program Thermobarometry: GTB Program Manual, 42 p.

Stacey, J.S., and Kramers, J.D., 1975, Approximation of terrestrial lead isotope evolution by a two-stage model: Earth and Planetary Science Letters, v. 26, p. 207-221.

Steiger, R.H., and Jäger, E., 1977, Subcommission on geochronology : Convention on the use of decay constants in geo- and cosmochemistry: Earth and Planetary Science Letters, v. 36, p. 359-362.

Terra, F., and Wasserburg, G.J., 1972, U-Th-Pb systematics in three Apollo 14 basalts and the problem of initial Pb in lunar rocks: Earth and Planetary Science Letters, v. 26, p. 205-222.

Williams, I.S., 1998, U-Th-Pb geochronology by ion microprobe, *in* McKibben, M.A., Shanks, W.C., III, and Williams, I.S., eds, Applications of microanalytical techniques to understanding mineralizing processes: Society of Economic Geologists, Reviews in Economic Geology, v. 7, p. 1-35.

Willner, A.P., Sebazungu, E., Gerya, T.V., Maresch, W.V., and Krohe, A., 2002, Numerical modeling of PT-paths related to rapid exhumation of high-pressure rocks from the crustal root in the Variscan Erzgebirge Dome (Saxony/Germany): Journal of Geodynamics, v. 33, p. 281-314.

Yang, J.S., Xu, Z., Song, S.G., Zhang, J.X., Wu, C., Shi, R., Li, H., and Brunel, M., 2001, Discovery of coesite in the North Qaidam Early Palaeozoic ultrahigh pressure (UHP) metamorphic belt, NW China: Sciences de la Terre et des planètes, v. 333, p. 719-724.

Yang, J.S., Xu, Z., Zhang, J.X., Song, S.G., Wu, C., Rendeng, S., Li, H., and Brunel, M., 2002, Early Palaeozoic North Qaidam UHP metamorphic belt on the north-eastern Tibetan Plateau and a paired subduction model: Terra Nova, v. 14, p. 397-404.

Yu, S.Y., Zhang, J.X., and García Del Real, P., 2010, Petrology and P–T path of high-pressure granulite from the Dulan area, North Qaidam Mountains, northwestern China: Journal of Asian Earth Sciences, v. 42, p. 641-660.

Zhang, J.X., Mattinson, C.G., Meng, F.C, and Wan, Y.S., 2005a, An early Paleozoic HP/HT granulite-garnet peridotite association in the south Altyn Tagh, NW China: P–T history and U-Pb geochronology: Journal of Metamorphic Geology, v. 23, p. 491-510.

Zhang, J.X., Mattinson, C.G., Meng, F.C., Wan, Y.S., and Tung, K., 2008a, Polyphase tectonothermal history recorded in granulitized gneisses from the north Qaidam HP/UHP metamorphic terrane, western China: Evidence from zircon U–Pb geochronology: Geological Society of America Bulletin, v.120, p. 732-749.

Zhang, J.X., Mattinson C.G., Meng, F.C., Yang, H.J., and Wan, Y.S., 2009a, U–Pb geochronology of paragneisses and metabasite in the Xitieshan area, north Qaidam Mountains, western China: constraints on the exhumation of HP/UHP metamorphic rocks: Journal of Asian Earth Sciences, v. 35, p. 245-258.

Zhang, J.X., Mattinson, C.G., Yu, S.Y., Li, J.P., and Meng, F.C., 2010, U–Pb zircon geochronology of coesite-bearing eclogites from the southern Dulan area of the North Qaidam UHP terrane, northwestern China: spatially and temporally extensive UHP metamorphism during continental collision: Journal of Metamorphic Geology, v. 28, p. 955-978.

Zhang, J.X., Meng, F.C., Li, J.P., and Mattinson, C.G., 2009b, Coesite in eclogite from the North Qaidam Mountains and its implications: Chinese Science Bulletin, v. 54, p. 1105-1110.

Zhang, G.B., Song, S.G., Zhang, L.F., and Niu, Y.L., 2008b, The subducted oceanic crust within continental-type UHP metamorphic belt in the North Qaidam, NW China: evidence from petrology, geochemistry and geochronology: Lithos, v. 104, p. 99-118.

Zhang, J.X., Yang, J.S., Mattinson, C.G., Xu, Z.Q., Meng, F.C., and Shi, R.D., 2005b, Two contrasting eclogite cooling histories, North Qaidam HP/UHP terrane, western China: petrological and isotopic constraints: Lithos, v. 84, p. 51-76.

Zhang, J.X., Yu, S.Y., Mattinson, C.G., Meng, F.C., and Li, J.P., 2009c, Relationship between high pressure granulite and eclogite in collision orogens and their geodynamic implications, *in* Programs & Abstracts: 8th International Eclogite Conference, p. 173-174.

Zhang, G.B., Zhang, J.X., Song, S.G., and Niu, Y., 2009d, UHP metamorphic evolution and SHRIMP geochronology of a coesite-bearing meta-ophiolitic gabbro in the North Qaidam, NW China: Journal of Asian Earth Sciences, v. 35, p. 310-322.

APPENDIXES

Appendix A

Field and Sample Descriptions

TABLE A1. LIST OF FOLIATIONS AND LINEATIONS, DULAN UHP EXPOSURE, NORTH QAIDAM, WESTERN CHINA.

Rock type	Sample	Location	Foliation/lineation	Strike/Trend	Dip/Plunge
Amphibolite	–	N36˚31.429' E98˚17.366'	Foliation	350˚	8O˚ NE
Paragneiss	–	– –	Foliation	310˚	Near Vertical
Grt-Paragneiss	D168	N36˚37.872' E98˚24.572'	Foliation	25˚	47˚ NW
Orthogneiss	–	– –	Foliation	66˚	70˚NW
Orthogneiss	–	– –	Foliation	255˚	74˚NW
Orthogneiss	–	– –	Foliation	358˚	42˚NE
Orthogneiss	–	– –	Foliation	350˚	56˚NE
Paragneiss	–	– –	Foliation Lineation	162˚ 131˚	20˚NE 18˚
Paragneiss	D169	N36˚37.767' E98˚25.306'	Foliation Lineation	104˚ 145˚	28˚SW 25˚
Paragneiss	–	– –	Foliation	348˚	38˚NE
Amphibolite	D174	N36˚41.739' E98˚21.432'	Lineation	95˚	23˚
Orthogneiss	–	– –	Foliation	100˚	55˚NE
Orthogneiss	D175	N36˚41.851' E98˚21.460'	Foliation Lineation	104˚ 82˚	50˚NE 26˚
Orthogneiss	–	– –	Foliation	90˚	58˚N
Grt-Orthogneiss	D176A	N36˚41.775' E98˚21.523'	Foliation Lineation	114˚ 301˚	37˚NE 8˚
Orthogneiss	–	– –	Foliation	100˚	50˚NE
Paragneiss	–	– –	Foliation	173˚	29˚NE
Greenschist	D179	N36˚32.328' E98˚20.339'	Foliation	95˚	74˚SW
Granulite	D180A,B	N36˚32.063' E98˚21.448'	Foliation	130˚	42˚NE

TABLE A1, CONTINUED

Rock type	Sample	Location	Foliation/lineation	Strike/Trend	Dip/Plunge
Amphibolite	–	–	Foliation	15˚	51˚SE
		–			
Amphibolite	–	–	Foliation	28˚	51˚NE
		–			
Grt-Paragneiss	D183	N36˚31.874'	Foliation	2˚	25˚SE
		E98˚22.270'			
Orthogneiss	–	N36˚39.510'	Foliation	138˚	49˚NE
		E98˚26.306'			
Paragneiss	–	N36˚40.712'	Foliation	132˚	46˚NE
		E98˚23.690'			
Amphibolite	D187B	N36˚40.716'	Foliation	120˚	43˚NE
		E98˚23.698'			
Orthogneiss	–	–	Foliation	120˚	46˚NE
		–	Lineation	99˚	12˚
Orthogneiss	D188A	N36˚40.883'	Foliation	140˚	52˚NE
		E98˚23.786'	Lineation	115˚	20˚
Orthogneiss	D189	N36˚40.916'	Foliation	132˚	56˚NE
		E98˚23.814'			
Ms-Quartzite	D190	N36˚26.702'	Foliation	94˚	28˚SW
		E98˚47.605'	Lineation	120˚	16˚
Gneiss	–	–	Foliation	85˚	11˚SE
		–			
Orthogneiss	–	–	Foliation	80˚	75˚NW
		–			
Orthogneiss	D193	N36˚27.450'	Foliation	45˚	81˚SE
		E98˚45.115'	Lineation	225˚	2˚
Amp-Gneiss	–	N36˚26.337'	Foliation	96˚	45˚NE
		E98˚43.939'	Lineation	62˚	38˚
Amphibolite	–	–	Foliation	105˚	43˚NE
		–	Lineation	50˚	26˚
Greenschist	–	N36˚26.895'	Foliation	155˚	55˚SW
		E98˚39.666'			
Greenschist	–	–	Foliation	105˚	62˚NE
		–			
Orthogneiss	–	N36˚29.032'	Foliation	155˚	32˚NE
		E98˚30.263'			
Greenschist	D200	N36˚28.985'	Foliation	0˚	43˚E
		E98˚30.357	Lineation	96˚	41˚
Orthogneiss	–	–	Foliation	150˚	48˚NE
		–	Lineation	95˚	56˚
Amphibolite	–	N36˚29.063'	Foliation	126˚	27˚NE
		E98˚30.580'			
Greenschist	D203	N36˚27.197'	Foliation	290˚	78˚NE
		E98˚30.015'			

TABLE A1, CONTINUED

Rock type	Sample	Location	Foliation/lineation	Strike/Trend	Dip/Plunge
Greenschist	–	N36˚27.345'	Foliation	30˚	25˚NW
		E98˚30.310'			
Amphibolite	–	N36˚27.408'	Foliation	330˚	65˚NE
		E98˚30.527'			
Greenschist	–	N36˚27.490'	Foliation	70˚	25˚NW
		E98˚30.847'			
Greenschist	–	N36˚27.572'	Foliation	80˚	45˚NW
		E98˚31.013'	Lineation	7˚	41˚
Greenschist	-	N36˚27.787'	Foliation	90˚	40˚N
		E98˚31.079'	Lineation	350˚	38˚
Greenschist	D206	N36˚28.213'	Foliation	100˚	56˚NE
		E98˚31.188'			
Greenschist	D207	N36˚28.423'	Lineation	101˚	30˚
		E98˚31.225'			
Mica-gneiss	D209	N36˚28.545'	Foliation	165˚	40˚
		E98˚31.296'			
Amphibolite	–	N36˚28.637'	Foliation	140˚	46˚NE
		E98˚31.343'			
Orthogneiss	–	N36˚28.994'	Foliation	100˚	Near Vertical
		E98˚41.575'			
Amphibolite	–	N36˚28.794'	Foliation	105˚	58˚NE
		E98˚41.098'			

TABLE A2. SUMMARY OF MINERAL ASSEMBLAGES FOR SAMPLES COLLECTED FROM THE DULAN HP-GRANULITE EXPOSURE, NORTH QAIDAM, WESTERN CHINA

Sample	Rock Type	Lat (N)	Long (E)	Qtz	Pl	Ksp	Grt	Cpx	Ky	Zo/Czo	Rt	Sph	Bt	Chl*	Amp*	Ep*	Zrc
D131A	Grt-Cpx-Hbl Granulite	36.5282	98.3975	+	+		+	Sym†	+	+	+				+?	–	
D131C	Grt Granulite	36.5282	98.3975	+	–	+	+	+		+	+				–	–	
D131D	HP Granulite w/ fresh Cpx	36.5282	98.3975	+	+		+	Sym†		+	+				–		
D131F	Grt-Czo Granulite	36.5282	98.3975		+		+	Sym†		+	+				–	–	
D135A	Grt-rich Granulite	36.5235	98.3913	+	+		+			+	+			–	–	–	
D135B	Grt-rich Cpx Granulite	36.5235	98.3913	+	+		+	Sym†		+	+			–	–		
D135C	Grt Granulite	36.5235	98.3913	+	+		+	+			+			–	–		
D136A	Grt-Ky Granulite	36.5232	98.3909	+	+		+	+	+	+	+				–		
D136B	Granulite Leucosome	36.5232	98.3909	+	+		+	+	+	+	+				–		
D136C	Ky Vein with Grt	36.5232	98.3909	+			+	+	+		+				–	–	MS§
D137C	Ky-bearing Melt Vein	36.5225	98.3906	+	+	+			+		+				–	–	
D141A	Czo-bearing Leucosome	36.5279	98.3903	+	+		+	Sym†		+	+			–	–	–	
D141B	Grt-Czo Granulite	36.5279	98.3903	+	+		+	+		+	+				–		
D141C	Grt-Ky Granulite	36.5279	98.3903	+	+		+	Sym†	+	+	+		+	–	–		
D141D	Grt Czo Granulite	36.5279	98.3903	+	+		+	Sym†		+	+				–	–	
D141E	Grt-Ky Granulite	36.5279	98.3903	+	+		+	+	+	+	+				–	–	
D141F	Grt-bearing Leucosome	36.5279	98.3903	+	+		+		+	+	+				–		
D142A§	Grt Granulite w/ Cpx	36.5265	98.3856	+	+		+	+			+				–		
D142B	Czo-rich Grt Granulite	36.5265	98.3856	+	+		+	+		+	+				–	–	
D142C	Grt-Czo Granulite	36.5265	98.3856				+	+		+	+				–	–	
D143	Banded Grt Granulite	36.5251	98.3846	+	+		+	+	+	+	+				–		MS§
D144	Czo-rich Grt Granulite	36.5268	98.3858		+		+	+		+	+				–	–	
D181	Amp-Zo Granulite	36.5334	98.3685	+	+		+	Sym†		+	+				+?		
D184	Cpx Granulite	36.5311	98.3711	+	+	+	+	+		+	+	+		–			
D211A	Zo-Grt Granulite	36.5248	98.3846	+	+		+	+		+	+				–		
D211B	Zo-Grt Granulite	36.5248	98.3846	+	+		+	+		+	+				–		
D211C	Grt Clinopyroxenite	36.5248	98.3846				+	+		+					+?		

TABLE A2. CONTINUED

Sample	Rock Type	Lat (N)	Long (E)	Qtz	Pl	Ksp	Grt	Cpx	Ky	Zo/Czo	Rt	Sph	Bt	Chl*	Amp*	Ep*	Zrc
D212A	Rt-bearing Tonalite	36.5260	98.3853	+	+						+		+	–		–	
D212B	Mafic Granulite	36.5260	98.3853	+	+		+	+	+	+	+				–	–	MS[§]
D213A	Tonalite	36.5258	98.3851	+	+									–		–	+
D213B	Intermediate Granulite	36.5258	98.3851	+	+		+	+	+	+	+			–	–	–	MS[§]
D213C	Amphibolite	36.5258	98.3851	+	+		+	+					–	–	–	–	
D214	Intermediate Granulite	36.5256	98.3850	+	+		+	+	+	+	+				–	–	
D216A	Rt-bearing Tonalite	36.5251	98.3846	+	+						+			–		–	
D216B	Garnet Granulite	36.5251	98.3846	+	+		+	+	+	+					–	–	
D217A	Grt-Ky Gneiss	36.5227	98.3848	+	+	+	+		+		+		+				MS[§]
D217B	Grt Amphibolite	36.5227	98.3848	+	+		+	+	+	+	+				–		
D217C	Rt-bearing tonalite	36.5227	98.3848	+	+						+			–		–	MS[§]
D217D	Grt-Ky Gneiss	36.5227	98.3848	+	+	+	+		+		+		+				

Note: Minerals identified in thin sections as part of the peak mineral assemblage are indicated by a +.

*Minerals identified in thin sections as replacement of peak assemblage minerals are indicated by a –.

[†]Sym: most or all of the Cpx exists as fine grained symplectite of Cpx + Pl or Amp + Pl.

[§]MS: mineral identified via mineral separation techniques.

[#]Sample D142A also contains Scp as part of the main assemblage.

Appendix B

Expanded Methods

Whole Rock analysis

Samples sent to WSU were analyzed for SiO_2, TiO_2, Al_2O_3, FeO, MnO, MgO, CaO, Na_2O, K_2O, P_2O_5, Ni, Cr, Sc, V, Ba, Rb, Sr, Zr, Y, Nb, Ga, Cu, Zn, Pb, La, Ce, Th, Nd and U.

Geochronology and Trace Elements

Samples selected for analysis at the Stanford/USGS SHRIMP-RG lab were first crushed and sieved to <250 μm. The two igneous samples, D213A and D217C, were run through a spiral panning machine to remove a large portion of quartz and feldspar, and to concentrate the heavier minerals such as zircon. Magnetic minerals such as clinopyroxene and garnet were removed with multiple runs of Frantz magnetic separation. Samples were first put through a vertical Frantz before being run through the horizontal Frantz at increasing magnet strength and a 10-5˚ side-slope. The remaining low-density, non-magnetic minerals were removed by two stages of heavy liquids: lithium polytungstate (density: 2.85 g/cm^3) and methylene iodide (density: 3.3 g/cm^3). Remaining grains (density > 3.3 g/cm^3) were dominantly rutile, kyanite and zircon, with some residual apatite (due to incomplete separation). Zircon abundances were very low, so samples D212B, D213B and D217A were run through the Frantz again at full power (~1.8 amp) and a 3˚ side-slope to partially remove rutile. Samples were then examined under a microscope and zircon grains were concentrated by hand picking. Zircon concentrations were still low for the three granulite samples, however, with D213B

providing the highest number of grains (~60). This larger yield is most likely due to the large sample size, given Zr concentrations in all three granulites were very low (≤10 ppm; see results).

Samples D212B, D213B, D214, D217A, D213A, and D217C were all analyzed for U-Pb and a limited number of trace elements. Samples were sputtered by a ~5 nA O_2^- primary beam focused to ~23 μm diameter, and the mass resolution was ~8000 at 10% peak height. Prior to analysis, the primary ion beam was rastered across the grain surface to remove the Au-coating and any surface contamination. Each analysis comprised 5 scans of peaks corresponding to ^{89}Y, ^{139}La, ^{140}Ce, ^{146}Nd, ^{147}Sm, ^{153}Eu, ^{155}Gd, $^{163}Dy^{16}O$, $^{166}Er^{16}O$, $^{172}Yb^{16}O$, HfO, $^{90}Zr_2{}^{16}O$, ^{204}Pb, background, ^{206}Pb, ^{207}Pb, ^{208}Pb, ^{232}Th, ^{238}U, $^{232}Th^{16}O$, $^{238}U^{16}O$, and $^{238}U^{16}O_2$, with count times of 1-16 seconds for each peak.

Samples D212B, D213B, D217A, and D213A were lightly re-polished and a new Au coating was added. These samples were then run through a separate, expanded trace element analyses. This expanded analysis had a smaller spot size and in some cases, multiple spots were analyzed on individual zircon grains. One isotope was selected to represent each element, based on abundance and absence of significant interferences, similar to the approach of Mattinson et al. (2009) and Mass et al. (1992). Each analysis comprised of one scan of peaks corresponding to ^{7}Li, ^{9}Be, ^{11}B, ^{19}F, ^{23}Na, ^{27}Al, ^{30}Si, ^{31}P, ^{39}K, ^{40}Ca, ^{45}Sc, ^{48}Ti, ^{49}Ti, ^{56}Fe, ^{89}Y, ^{93}Nb, ^{94}ZrH, ^{96}Zr, ^{139}La, ^{140}Ce, ^{146}Nd, ^{147}Sm, ^{153}Eu, ^{155}Gd, ^{165}Ho, $^{159}Tb^{16}O$, $^{163}Dy^{16}O$, $^{166}Er^{16}O$, $^{169}Tm^{16}O$, $^{172}Yb^{16}O$, $^{175}Lu^{16}O$, $^{90}Zr_2{}^{16}O$, $^{180}Hf^{16}O$, ^{206}Pb, ^{207}Pb, $^{232}Th^{16}O$, and $^{238}U^{16}O$. Count times were 2-10 seconds with a mass resolution of 10000–11000 at 10% peak height. The primary beam current was

~1.5 nA and beam diameter was ~17 μm. The raw data were converted to ppm by normalizing average count rates to ^{30}Si, and calibrating concentrations to trace element values for zircon standard MAD (Mazdab and Wooden, 2006). Conversion of these concentrations to chondrite-normalized patterns (Coryell et al., 1963) uses the recommended Cl carbonaceous chondrite composition of McDonough and Sun (1995).

Mineral Chemistry

TABLE B1. STANDARD SETTINGS FOR ELECTRON MICROPROBE ANALYSIS

Standard	Minerals Analyzed	Elements Analyzed	Spot Size (μm)	Beam current (nA)
Plagioclase	Pl, Kfs	Si, Al, Ti, Al, Fe*, Mg, Ca, Na, K	10	15
Amphibole	Amp, Bt, Ms	Si, Al, Ti, Al, Fe*, Mn, Mg, Ca, Na, K, P, F, Cl	5	30
Pyroxene	Cpx, Czo	Si, Al, Ti, Al, Fe*, Cr, Mn, Mg, Ca, Na, K	1	15
Chromite/Fe-Ti oxide	$FeTiO_3$	Si, Al, Ti, Al, Fe*, Cr, Mn, Mg, Ca, Na, K	1	30
Garnet	Grt	Si, Al, Ti, Al, Fe*, Cr, Mn, Mg, Ca, Na, K	1	30

Note: All Standards run at 15 keV accelerating voltage.
*All Fe initially calculated as FeO.

Pressure–Temperature Estimates

TABLE B2. EQUATIONS USED BY THE PROGRAM THERMOCALC (v3.33)

Equation	Number
Grs* + 2Ky + Qtz = 3An	1
2Czo = Grs + An + H_2O + Ky	2
Grs + 3Di + 6Ky = Prp + 6An	3
Grs + 3Hd + 6Ky = Alm + 6An	4
3Di + 4Ky = Prp + 3An + Qtz	5
3Di + 2Czo + 5Ky = Prp + 7An + H_2O	6
15Di + 12Czo = 5Prp + 13Grs + 6H_2O + 12Qtz	7
2Czo + Qtz + Ky = 4An + H_2O	8
Prp + 8Czo + 5Qtz = 3Di + 13An + 4H_2O	9
Alm + *Czo + 5Qtz = 3Hed + 13An + 4H_2O	10
3Hd + 2Czo + 5Ky = Alm + 7An + H_2O	11
Prp + 2Grs + 3Qtz = 3Di + 3An	12
3Di + 2Ky = Prp + Grs + 2Qtz	13
3East* + 6Qtz = 2Phl + Sa + H_2O + 3Ky	14
Ann + 6An = 2Grs + Alm + Sa + H_2O +3Ky	15
7Phl + 12An = 5Prp + 4Grs + 3East + 4Sa +4H_2O	16
Phl + 3East + 12Qtz = 3Py +4Sa +4H2O	17

TABLE B2. CONTINUED

Equation	Number
$2Ann + 3An + 3Qtz = Grs + 2Alm + 2Sa + 2H_2O$	18
$Prp + Ann = Alm + Phl$	19
$Ann + 2Qtz + Ky = Alm + Sa + H_2O$	20
$5Phl + 6Ky = 3Prp + 3East + 2Sa + 2H_2O$	21
$3Phl + 4Ky = Prp + 3East + 4Qtz$	22
$Phl + 2Qtz + Ky = Prp + Sa + H_2O$	23
$4Grs + 3Phl + 12Ky = Prp + 3East + 12An$	24
$Prp + 2Grs + 3East + 6Qtz = 3Phl + 6An$	25
$3Hed + 4Ky = Alm + 3An + Q$	26
$Alm + 12Czo = 7Grs + 3Hed + 6H_2O + 12Ky$	27
$Phl + 6An = Prp + 2Grs + Sa + H_2O + 3Ky$	28
$3East + 10Qtz = 3Prp + 4Sa + 4H_2O$	29

Note: Mineral abbreviation after Kretz (1983) except eastonite (East).

Appendix C

Continued Zircon SHRIMP-RG Results

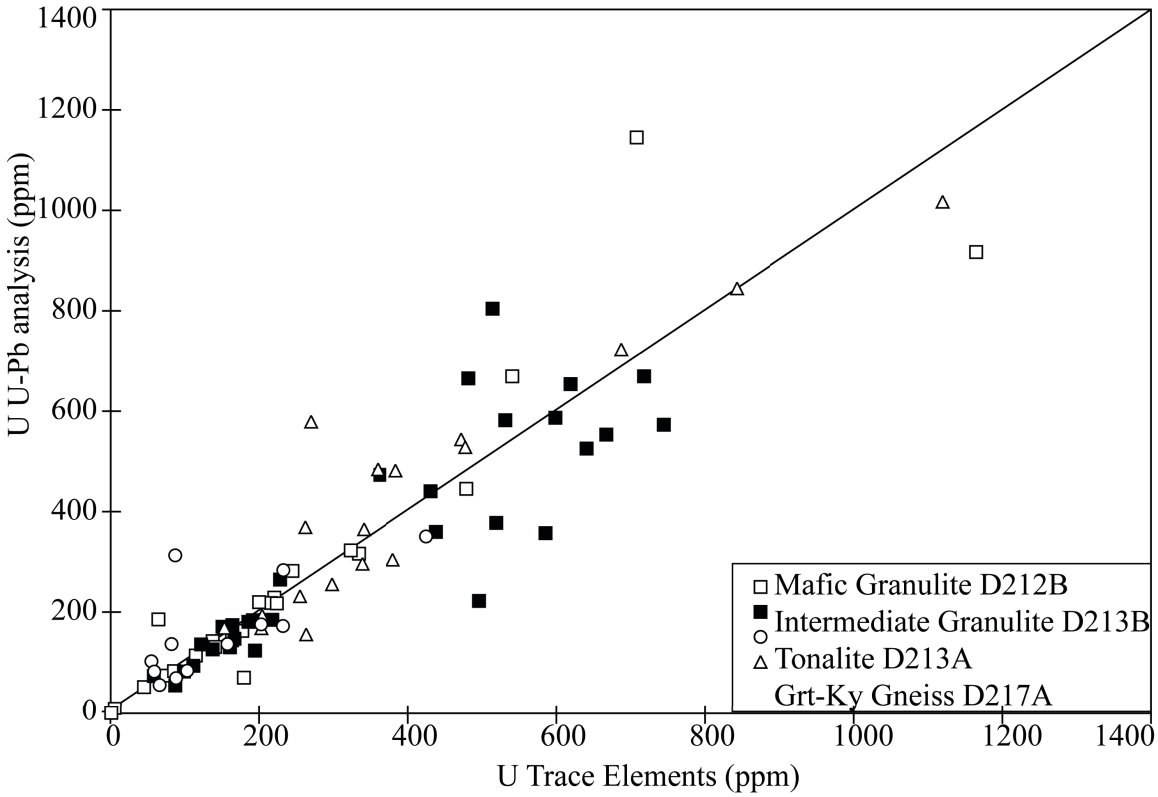

Figure C1. Plot of uranium vs. uranium concentrations between separate U-Pb and trace element analyses for samples from the Dulan HP-granulite exposure. Diagonal line follows the ideal trend of Y = X.

TABLE C1. ZIRCON U-Pb ISOTOPIC DATA, INTERMEDIATE GRANULITE SAMPLE D214, NORTH QAIDAM, WESTERN CHINA

Analysis	$^{206}Pb_c$ %	U (ppm)	Th (ppm)	$^{232}Th/^{238}U$	^{207}Pb-corr $^{206}Pb/^{239}U$ age (Ma ± 1σ err)	Total $^{238}U/^{206}Pb$ (± % err)	Total $^{207}Pb/^{206}Pb$ (± % err)
D214-1	–	4696	4097	0.90	474.5 ± 0.9	13.10 ± 0.2	0.0564 ± 0.5
D214-2	–	411	43	0.11	496.5 ± 9.0	13.10 ± 0.2	0.0178 ± 88.1
D214-3*	0.10	2943	2522	0.89	438.0 ± 0.9	14.21 ± 0.2	0.0564 ± 0.6
D214-4*	0.13	1633	202	0.13	438.9 ± 1.2	14.18 ± 0.3	0.0567 ± 0.8
D214-5*	0.05	2414	745	0.32	448.5 ± 1.0	13.87 ± 0.2	0.0563 ± 0.6
D214-6*	0.09	827	80	0.10	419.3 ± 1.8	14.87 ± 0.4	0.0559 ± 1.1
D214-7*	0.08	3468	3149	0.94	442.8 ± 1.0	14.05 ± 0.2	0.0564 ± 0.5
D214-8*	0.26	1317	294	0.23	399.8 ± 1.2	15.59 ± 0.3	0.0568 ± 0.8

Note: Anaysis D214-2 is only a partial run due to instrument shut down during analysis.
*Analyses used in calculation of intercept ages.

TABLE C2. ZIRCON TRACE-ELEMENT RESULTS (ppm) FOR INTERMEDIATE GRANULITE SAMPLE D214, NORTH QAIDAM, WESTERN CHINA

Sample	Y	La	Ce	Nd	Sm	Eu	Gd	Dy	Er	Yb	Hf	Yb/Gd	Ce/Ce*	Eu/Eu*
D214-1	4902	0.011	226	4.3	13.5	3.37	124	469	899	1682	22023	13.5	1371	0.25
D214-2*	1599	0.000	11	0.7	3.1	1.60	46	162	228	347	17372	7.5	–	0.41
D214-3	3479	0.856	169	7.1	11.2	3.40	87	318	610	1121	15840	13.0	47	0.33
D214-4	1544	0.532	27	7.0	13.4	4.39	88	188	156	162	18544	1.8	10	0.39
D214-5	1193	0.038	28	1.8	6.1	2.30	54	133	135	172	17001	3.2	99	0.38
D214-6	1231	0.563	12	1.0	2.4	1.18	33	126	167	243	14080	7.5	8	0.41
D214-7	4085	0.029	201	4.3	11.5	3.53	104	397	746	1340	16235	12.8	628	0.31
D214-8	1693	0.456	16	1.7	5.4	1.87	60	186	223	286	15200	4.8	11	0.31

Note: Results are based on limited analysis during zircon U-Pb analysis
*Anaysis D214-2 is only a partial run due to instrument shut down during analysis.

TABLE C3. ZIRCON U-Pb ISOTOPIC DATA, RT-BEARING TONALITE SAMPLE D217C, NORTH QAIDAM, WESTERN CHINA

Analysis	$^{206}Pb_c$ %	U (ppm)	Th (ppm)	$^{232}Th/^{238}U$	^{207}Pb-corr $^{206}Pb/^{239}U$ age (Ma ± 1σ err)	Total $^{238}U/^{206}Pb$ (± % err)	Total $^{207}Pb/^{206}Pb$ (± % err)
D217C-1	0.30	206	89	0.45	451.5 ± 3.4	13.74 ± 0.8	0.0584 ± 2.0
D217C-2	0.13	1282	132	0.11	407.8 ± 1.3	15.29 ± 0.3	0.0560 ± 0.8
D217C-3	0.36	1103	742	0.69	414.4 ± 1.3	15.01 ± 0.3	0.0579 ± 1.2
D217C-4	–	288	66	0.24	439.9 ± 2.8	14.19 ± 0.6	0.0541 ± 1.8
D217C-5	0.29	1366	105	0.08	825.8 ± 2.3	7.30 ± 0.3	0.0690 ± 0.5
D217C-6	0.15	252	1	0.004	415.5 ± 2.9	15.00 ± 0.7	0.0563 ± 2.2
D217C-7	–	251	6	0.02	426.5 ± 3.1	14.63 ± 0.7	0.0551 ± 1.9
D217C-8	0.01	435	21	0.05	422.3 ± 2.3	14.77 ± 0.5	0.0533 ± 1.4
D217C-9	0.14	996	231	0.24	421.4 ± 1.6	14.78 ± 0.4	0.0564 ± 1.0
D217C-10	0.02	385	16	0.04	407.4 ± 2.3	15.32 ± 0.6	0.0551 ± 1.5
D217C-11	–	549	19	0.04	409.3 ± 1.9	15.26 ± 0.5	0.0549 ± 1.3
D217C-12	–	145	29	0.20	396.1 ± 3.4	15.82 ± 0.9	0.0528 ± 2.4
D217C-13	5.80	431	8	0.02	268.0 ± 2.1	22.19 ± 0.6	0.0981 ± 4.4
D217C-14	0.15	950	70	0.08	388.3 ± 1.3	16.08 ± 0.3	0.0556 ± 1.0
D217C-15	0.0	225	11	0.05	413.3 ± 3.1	15.10 ± 0.7	0.0550 ± 2.0

Note: * indicate analysis used in calculation of intercept ages.

TABLE C4. ZIRCON TRACE-ELEMENT RESULTS FOR RT-BEARING TONALITE SAMPLE D217C, NORTH QAIDAM, WESTERN CHINA

Sample	Y	La	Ce	Nd	Sm	Eu	Gd	Dy	Er	Yb	Hf	Yb/Gd	Ce/Ce*	Eu/Eu*
D217C-1	1037	0.017	15	0.4	1.2	0.45	14	78	206	488	9783	35.9	153	0.35
D217C-2	785	0.339	13	3.4	9.7	7.00	64	111	100	125	9767	2.0	8	0.86
D217C-3	1285	110.308	271	51.9	20.0	4.67	63	138	221	354	9584	5.6	2	0.40
D217C-4	259	1.352	12	1.3	1.6	0.70	10	26	39	66	7459	6.9	4	0.54
D217C-5	1769	3.319	19	4.6	5.7	1.94	37	173	326	640	11997	17.5	3	0.41
D217C-6	33	0.621	8	4.5	1.9	0.62	3	5	4	4	12001	1.5	3	0.82
D217C-7	42	0.008	1	0.0	0.2	0.20	2	6	5	5	11469	2.4	34	0.99
D217C-8	58	0.316	4	0.8	0.8	0.41	4	8	8	10	11528	2.8	4	0.76
D217C-9	674	0.071	24	6.1	13.7	7.59	74	98	82	100	10091	1.4	38	0.72
D217C-10	47	0.016	1	0.1	0.3	0.24	3	7	6	7	10950	2.5	25	0.89
D217C-11	1885	0.020	1	0.2	1.0	0.10	18	168	398	877	13448	47.6	7	0.07
D217C-12	64	0.301	9	1.2	2.1	1.27	10	12	7	6	8022	0.6	9	0.85
D217C-13	92	13.167	116	33.1	31.1	7.27	47	18	8	6	10541	0.1	3	0.58
D217C-14	278	1.219	13	1.8	3.0	2.07	18	36	38	51	7664	2.8	5	0.84
D217C-15	37	0.006	2	0.0	0.3	0.29	3	7	5	6	11433	2.1	63	1.02

Note: Results are based on limited analysis during zircon U-Pb analysis.

Appendix D

Continued Pressure-Temperature Results

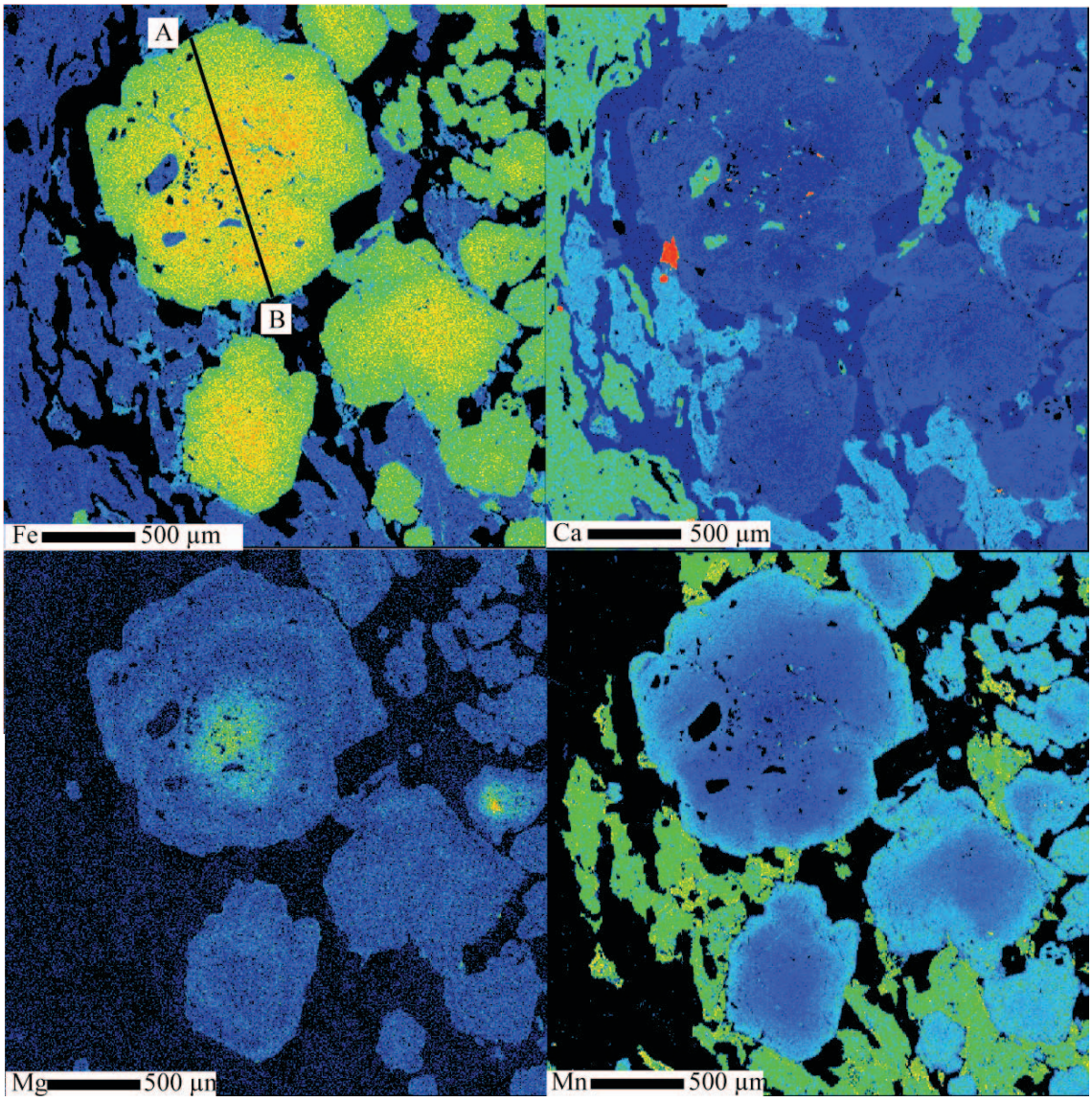

Figure D1. X-ray map showing the compositional change in garnet from mafic granulite sample D212B (transect Grt2). Dark line indicates the location of EMP transect, this specific garnet was not used for P-T calculations of the mafic granulite sample (see text). Colors are relative with compositions increasing from black-blue-yellow-orange-red.

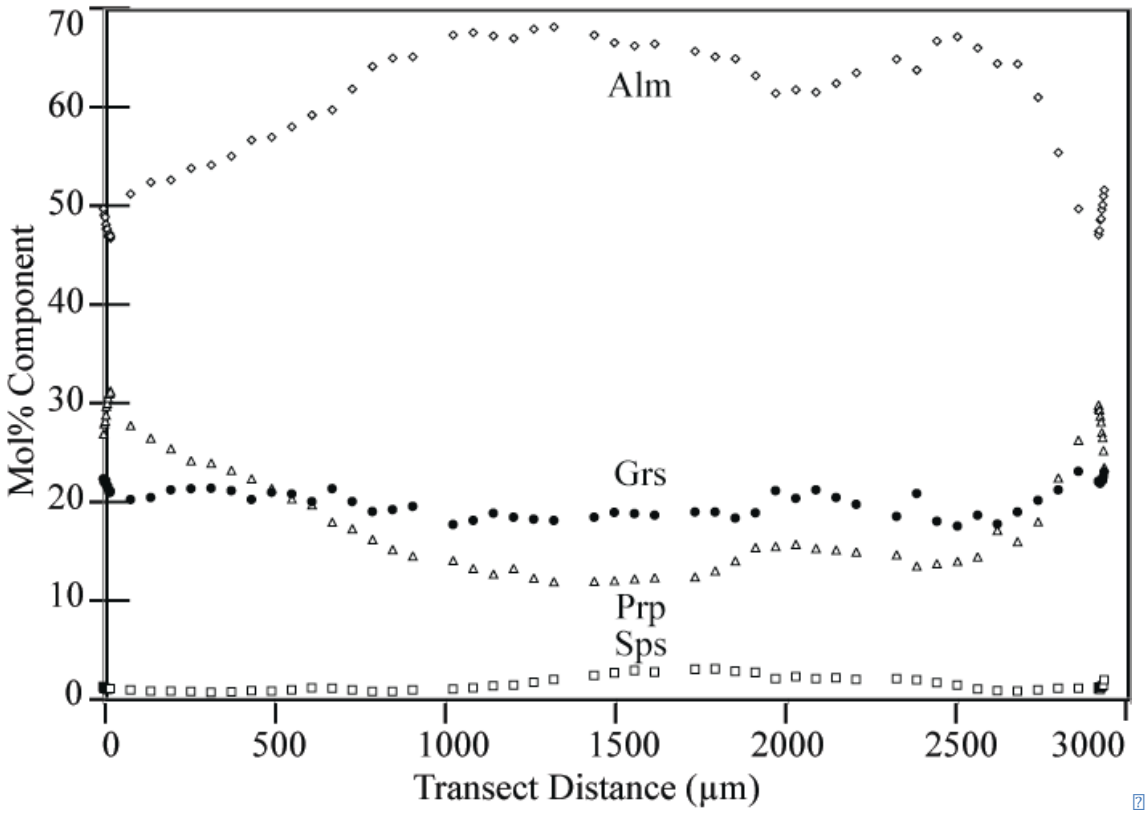

Figure D2. Compositional trend for mafic granulite sample transect Grt2 (see Fig. D1).

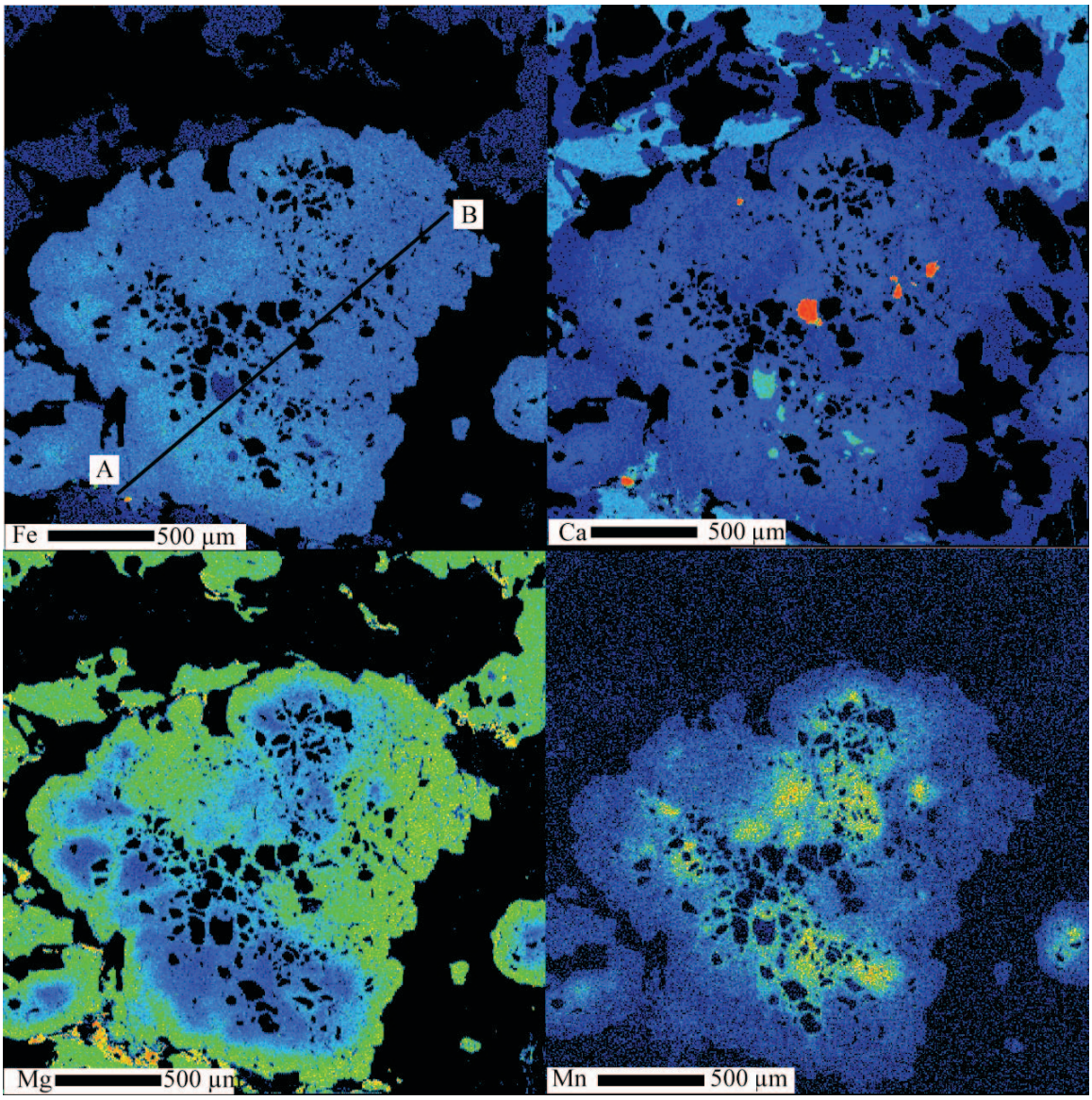

Figure D3. X-ray map showing the compositional change in garnet from intermediate granulite sample D213B (transect Grt3). Dark line indicates the location of EMP transect, this specific garnet was not used for P-T calculation on the intermediate granulite sample (see text). Colors are relative with compositions increasing from black-blue-yellow-orange-red.

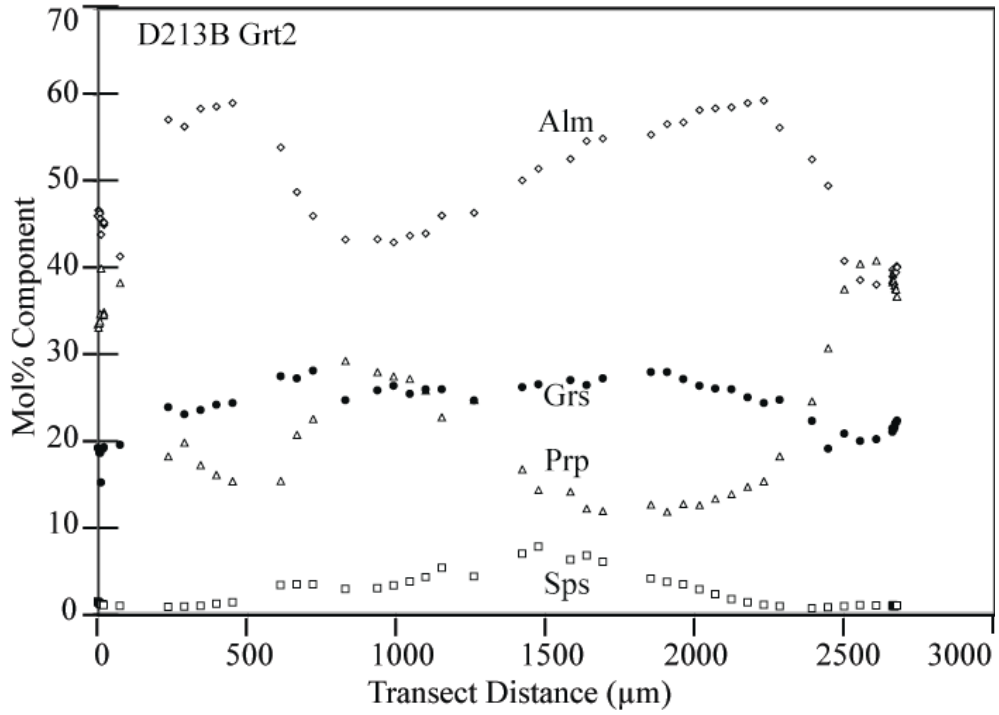

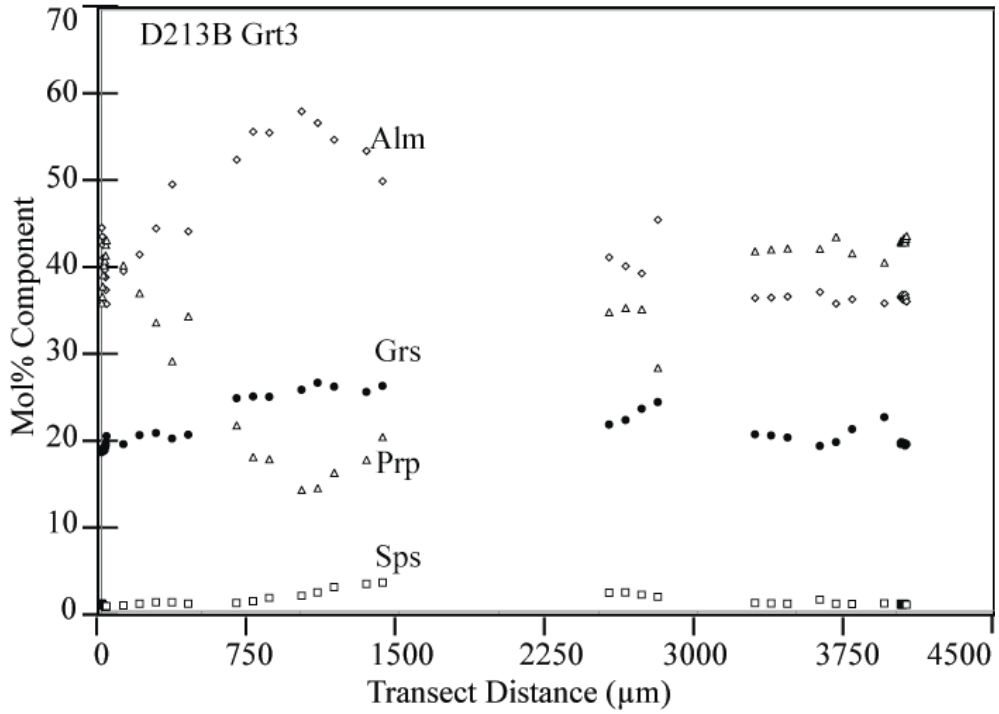

Figure D4. Compositional profile of intermediate granulite sample D213B transects Grt2 (See Fig. 17) and Grt3 (see Fig. D3).

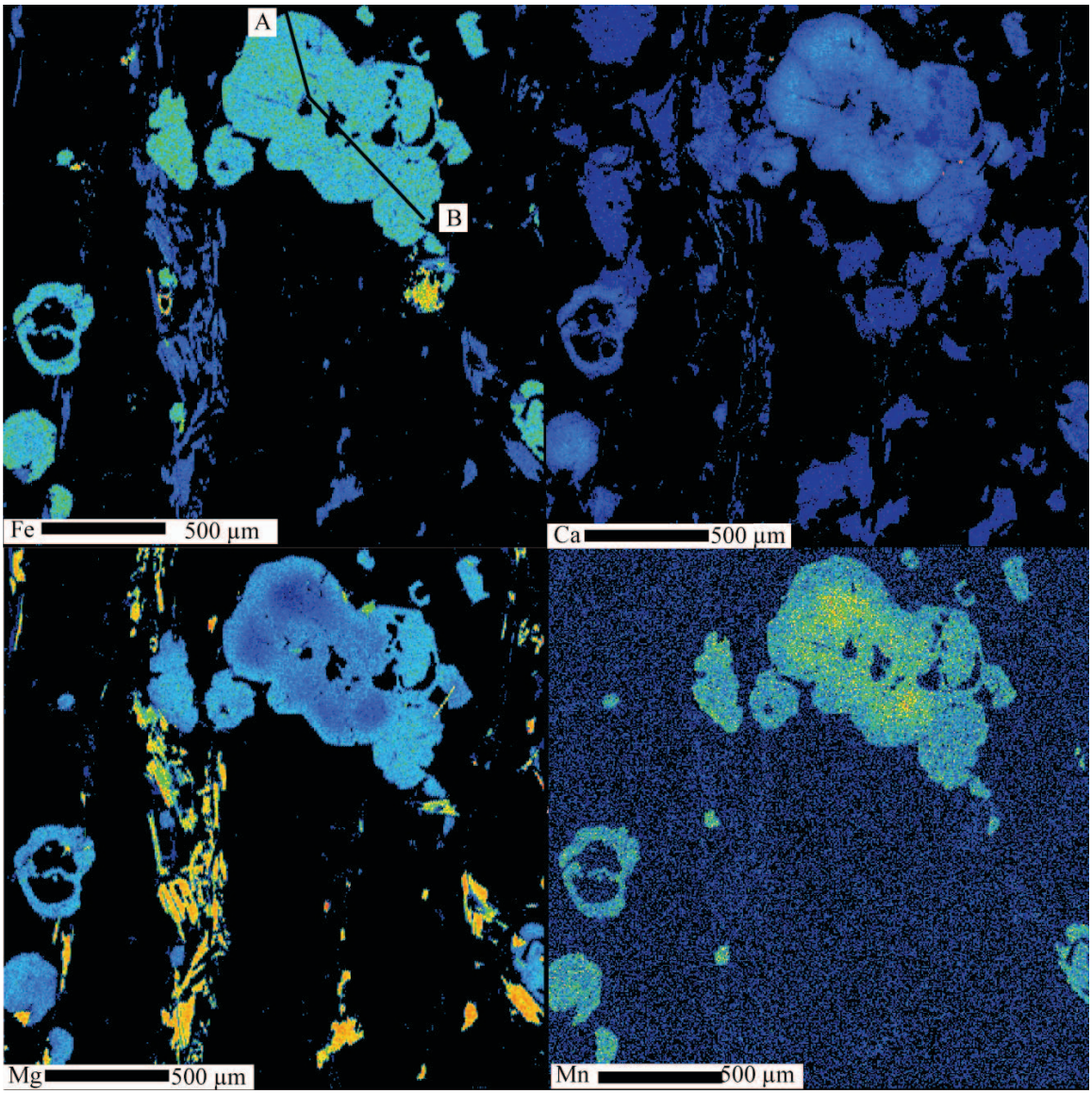

Figure D5. X-ray map showing the compositional change in garnet from Grt-Ky gneiss sample D217A (transect Grt2). Dark line indicates the location of EMP transect. Colors are relative with compositions increasing from black-blue-yellow-orange-red.

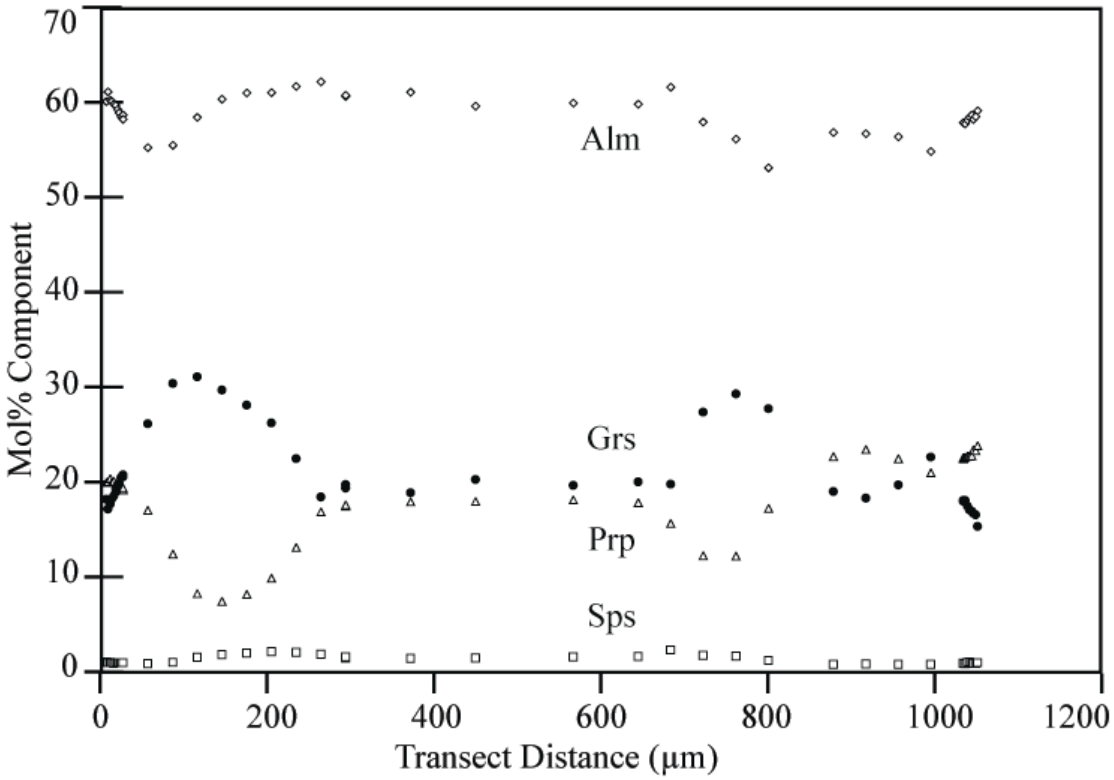

Figure D6. Compositional profile for Grt-Ky gneiss transect Grt2 (see Fig. D5).

TABLE D1. EXPANDED LIST OF MINERAL COMPOSITIONS USED IN P-T ESTIMATES, NORTH QAIDAM, WESTERN CHINA

Sample	D212B											
No.	Grt1A	Grt1B	Cpx1min	Cpx1max	Cpx1avg	Cpx2min	Cpx2max	Cpx2avg	Pl1min	Pl1max	Pl1avg	Czo1min
SiO_2	39.28	38.04	49.98	51.06	50.50	49.81	49.67	49.53	61.54	61.62	61.45	38.29
TiO_2	0.09	0.06	0.61	0.50	0.54	0.68	0.57	0.64	0.00	0.00	0.01	0.23
Al_2O_3	22.96	22.03	9.95	8.67	9.57	10.43	8.88	10.08	24.14	24.30	24.11	28.64
Cr_2O_3	0.00	0.01	0.03	0.00	0.00	0.00	0.01	0.00	0.00	0.00	0.00	0.00
FeO*	21.25	21.73	6.98	6.59	6.84	7.07	7.73	7.26	0.09	0.04	0.07	5.65
MnO	0.43	0.50	0.04	0.03	0.03	0.07	0.07	0.06	0.00	0.00	0.00	0.01
MgO	7.77	7.14	9.78	10.66	10.07	9.43	10.05	9.69	0.00	0.00	0.01	0.26
CaO	9.02	9.57	18.46	18.48	18.57	18.69	18.89	18.70	5.85	5.75	5.78	23.28
Na_2O	0.03	0.06	3.04	3.03	3.04	2.99	2.44	2.82	8.09	8.25	8.24	0.00
K_2O	0.00	0.02	0.00	0.00	0.00	0.01	0.02	0.01	0.06	0.05	0.05	0.00
Totals	100.83	99.16	98.87	99.02	99.16	99.18	98.33	98.79	99.78	100.01	99.73	96.38
Oxygens	12	12	6	6	6	6	6	6	8	8	8	12.5
Si	2.969	2.935	1.846	1.878	1.858	1.837	1.856	1.835	2.735	2.732	2.733	2.992
Ti	0.005	0.003	0.017	0.014	0.015	0.019	0.016	0.018	0.000	0.000	0.000	0.014
Al	2.046	2.004	0.433	0.376	0.415	0.453	0.391	0.440	1.265	1.270	1.264	2.639
Cr	0.000	0.001	0.001	0.000	0.000	0.000	0.000	0.000	0.000	0.000	0.000	0.000
Fe^{3+}	0.011	0.130	0.058	0.057	0.056	0.050	0.043	0.057	0.003	0.001	0.003	0.362
Fe^{2+}	1.332	1.272	0.157	0.146	0.154	0.168	0.198	0.167	0.000	0.000	0.000	0.007
Mn	0.028	0.033	0.001	0.001	0.001	0.002	0.002	0.002	0.000	0.000	0.000	0.001
Mg	0.875	0.821	0.538	0.584	0.552	0.518	0.560	0.535	0.000	0.000	0.001	0.030
Ca	0.730	0.791	0.730	0.728	0.732	0.738	0.756	0.742	0.279	0.273	0.275	1.949
Na	0.004	0.009	0.218	0.216	0.217	0.214	0.177	0.203	0.697	0.709	0.711	0.000
K	0.000	0.002	0.000	0.000	0.000	0.000	0.001	0.000	0.003	0.003	0.003	0.000
Sum	8.000	8.000	4.000	4.000	4.000	4.000	4.000	4.000	4.982	4.988	4.990	7.996

Note: FeO* assumes all Fe is assumed FeO.

TABLE D1. CONTINUED

Sample	D212B		D213B									
No.	Czo1max	Czo1avg	Grt1A	Grt1B	Cpx1min	Cpx1max	Cpx1avg	Cpx2min	Cpx2max	Cpx2avg	Pl1min	Pl1max
SiO_2	38.24	38.05	39.30	38.7	50.67	50.75	50.72	50.60	49.56	50.35	60.98	61.63
TiO_2	0.12	0.12	0.05	0.05	0.51	0.50	0.52	0.49	0.66	0.54	0.01	0.02
Al_2O_3	27.90	27.82	22.64	22.30	9.66	9.66	9.63	9.66	9.51	9.49	24.38	23.79
Cr_2O_3	0.02	0.01	0.03	0.01	0.03	0.00	0.02	0.00	0.05	0.03	0.00	0.00
FeO*	7.11	6.43	19.19	19.54	6.59	6.51	6.48	6.35	6.98	6.57	0.06	0.09
MnO	0.03	0.02	0.36	0.33	0.06	0.03	0.02	0.04	0.00	0.02	0.00	0.00
MgO	0.19	0.21	10.71	10.63	10.71	10.78	10.46	10.13	10.82	10.49	0.00	0.00
CaO	23.14	23.08	7.31	7.36	18.38	18.39	18.27	17.90	18.48	18.40	5.98	5.74
Na_2O	0.02	0.01	0.04	0.01	2.97	2.81	3.08	3.17	2.62	2.96	7.97	8.45
K_2O	0.00	0.00	0.00	0.00	0.04	0.01	0.01	0.00	0.00	0.00	0.09	0.08
Totals	97.55	96.46	99.63	98.93	99.62	99.44	99.21	98.34	98.68	98.85	99.48	99.81
Oxygens	12.5	12.5	12	12	6	6	6	6	6	6	8	8
Si	2.987	2.999	2.958	2.937	1.851	1.859	1.860	1.872	1.833	1.855	2.720	2.741
Ti	0.007	0.007	0.003	0.003	0.014	0.014	0.014	0.014	0.018	0.015	0.000	0.001
Al	2.569	2.585	2.009	1.995	0.416	0.417	0.416	0.421	0.415	0.412	1.282	1.247
Cr	0.001	0.001	0.002	0.001	0.001	0.000	0.001	0.000	0.001	0.001	0.000	0.000
Fe^{3+}*	0.460	0.420	0.073	0.125	0.065	0.038	0.054	0.035	0.069	0.058	0.002	0.003
Fe^{2+}	0.005	0.004	1.135	1.115	0.136	0.161	0.145	0.161	0.147	0.144	0.000	0.000
Mn	0.002	0.001	0.023	0.021	0.002	0.001	0.001	0.001	0.000	0.001	0.000	0.000
Mg	0.022	0.025	1.201	1.202	0.583	0.588	0.572	0.559	0.596	0.576	0.000	0.000
Ca	1.937	1.949	0.590	0.599	0.719	0.722	0.718	0.710	0.732	0.726	0.286	0.274
Na	0.003	0.002	0.006	0.001	0.210	0.200	0.219	0.227	0.188	0.211	0.689	0.729
K	0.000	0.000	0.000	0.000	0.002	0.000	0.000	0.000	0.000	0.000	0.005	0.005
Sum	7.993	7.992	8.000	8.000	4.000	4.000	4.000	4.000	4.000	4.000	4.985	4.999

Note: FeO* assumes all Fe is assumed FeO.

TABLE D1. CONTINUED

Sample	D213B				D217A							
No.	Pl1avg	Pl2min	Pl2max	Pl2avg	Czo1min	Czo1max	Czo1avg	Grt1	Bt1min	Bt1max	Bt1avg	Bt2min
SiO_2	61.35	61.43	60.55	61.68	37.9	38.16	38.13	37.90	37.24	36.47	36.89	37.01
TiO_2	0.01	0.02	0.01	0.00	0.20	0.12	0.17	0.05	3.72	3.60	3.72	3.73
Al_2O_3	24.10	23.93	23.56	23.91	27.69	27.51	27.64	22.34	18.35	17.98	18.22	18.5
Cr_2O_3	0.00	0.00	0.00	0.00	0.05	0.02	0.02	0.02	0.00	0.00	0.00	0.00
FeO*	0.05	0.00	0.06	0.09	6.42	7.45	6.84	27.92	14.44	15.3	14.67	14.64
MnO	0.00	0.00	0.00	0.00	0.04	0.11	0.06	0.53	0.03	0.03	0.02	0.07
MgO	0.00	0.00	0.01	0.01	0.28	0.24	0.29	5.15	12.54	13.07	12.77	12.57
CaO	5.87	5.78	5.62	5.68	23.11	22.67	22.89	6.18	0.13	0.15	0.15	0.18
Na_2O	8.11	7.97	8.22	8.19	0.00	0.00	0.02	0.03	0.11	0.11	0.12	0.10
K_2O	0.08	0.09	0.08	0.09	0.00	0.01	0.00	0.02	9.10	8.72	9.11	9.20
Totals	99.58	99.22	98.12	99.66	95.71	97.11	96.81	100.14	95.67	95.44	95.68	96.01
Oxygens	8	8	8	8	12.5	12.5	12.5	12	11	11	11	11
Si	2.733	2.743	2.738	2.744	2.996	2.996	2.998	2.959	2.743	2.705	2.723	2.722
Ti	0.000	0.001	0.000	0.000	0.012	0.007	0.010	0.003	0.206	0.201	0.207	0.206
Al	1.266	1.260	1.256	1.254	2.580	2.546	2.562	2.056	1.593	1.572	1.586	1.604
Cr	0.000	0.000	0.000	0.000	0.003	0.001	0.001	0.001	0.000	0.000	0.000	0.000
Fe^{3+}*	0.002	0.000	0.002	0.003	0.386	0.484	0.445	0.025	0.000	0.000	0.000	0.000
Fe^{2+}	0.000	0.000	0.000	0.000	0.038	0.005	0.004	1.798	0.889	0.949	0.906	0.901
Mn	0.000	0.000	0.000	0.000	0.003	0.007	0.004	0.035	0.002	0.002	0.001	0.004
Mg	0.000	0.000	0.001	0.001	0.033	0.028	0.034	0.599	1.376	1.445	1.405	1.378
Ca	0.280	0.277	0.272	0.271	1.957	1.907	1.928	0.517	0.010	0.012	0.012	0.014
Na	0.700	0.69	0.721	0.706	0.000	0.000	0.003	0.005	0.016	0.016	0.017	0.014
K	0.005	0.005	0.005	0.005	0.000	0.001	0.000	0.002	0.855	0.825	0.858	0.863
Sum	4.986	4.974	4.995	4.984	8.010	7.982	7.990	8.000	7.691	7.729	7.715	7.708

Note: FeO* assumes all Fe is assumed FeO.

TABLE D1. CONTINUED

Sample	D217A										
No.	Bt2max	Bt2avg	Pl1min	Pl1max	Pl1avg	Pl2min	Pl2max	Pl2avg	Ksp1min	Ksp1max	Ksp1avg
SiO_2	37.17	36.90	61.80	62.28	62.95	62.48	63.65	63.04	64.59	64.64	64.74
TiO_2	3.70	3.84	0.03	0.01	0.01	0.01	0.00	0.00	0.02	0.01	0.01
Al_2O_3	18.24	18.18	22.68	22.24	22.67	22.81	22.73	22.73	18.52	18.37	18.5
Cr_2O_3	0.00	0.00	0.00	0.00	0.00	0.00	0.00	0.00	0.00	0.00	0.00
FeO	14.50	14.69	0.24	0.10	0.08	0.10	0.03	0.05	0.12	0.04	0.07
MnO	0.02	0.03	0.00	0.00	0.00	0.00	0.00	0.00	0.00	0.00	0.00
MgO	12.76	12.64	0.08	0.00	0.01	0.10	0.00	0.03	0.01	0.01	0.02
CaO	0.13	0.16	4.50	4.38	4.43	4.45	4.24	4.46	0.21	0.23	0.23
Na_2O	0.13	0.12	8.37	8.71	8.66	8.38	8.83	8.60	1.11	0.87	1.07
K_2O	9.18	9.45	0.27	0.28	0.28	0.38	0.23	0.32	14.82	15.28	14.99
Totals	95.84	96.02	98.00	98.01	99.10	98.72	99.71	99.24	99.43	99.47	99.65
Oxygens	11	11	8	8	8	8	8	8	8	8	8
Si	2.736	2.721	2.789	2.809	2.806	2.797	2.817	2.806	2.989	2.995	2.991
Ti	0.205	0.213	0.001	0.000	0.000	0.000	0.000	0.000	0.001	0.000	0.000
Al	1.583	1.58	1.207	1.183	1.192	1.204	1.186	1.193	1.010	1.003	1.008
Cr	0.000	0.000	0.000	0.000	0.000	0.000	0.000	0.000	0.000	0.000	0.000
Fe^{3+}*	0.000	0.000	0.009	0.004	0.003	0.004	0.001	0.002	0.005	0.002	0.003
Fe^{2+}	0.893	0.906	0.000	0.000	0.000	0.000	0.000	0.000	0.000	0.000	0.000
Mn	0.001	0.002	0.000	0.000	0.000	0.000	0.000	0.000	0.000	0.000	0.000
Mg	1.400	1.389	0.005	0.000	0.001	0.007	0.000	0.002	0.001	0.001	0.001
Ca	0.010	0.013	0.218	0.212	0.212	0.213	0.201	0.213	0.010	0.011	0.011
Na	0.019	0.017	0.732	0.762	0.749	0.727	0.758	0.742	0.100	0.078	0.096
K	0.862	0.889	0.016	0.016	0.016	0.022	0.013	0.018	0.875	0.903	0.883
Sum	7.709	7.730	4.976	4.986	4.978	4.974	4.975	4.976	4.991	4.994	4.994

Note: FeO* assumes all Fe is assumed FeO.

TABLE D2. COMPLETE P-T CONDITIONS CALCULATED USING THE PROGRAM GTB V2.1

Sample	Mineral Combination	Temperature (˚C) at:		
	Fe-Mg Exchange	14 kbar	15kbar	16kbar
D212B	Grt1A+Cpx1min	827	833	838
	Grt1A+Cpx1avg	802	807	813
	Grt1A+cpx1max	750	755	761
	Grt1A+Cpx2min	855	861	866
	Grt1A+Cpx2avg	855	861	866
	Grt1A+cpx2max	870	876	881
	Grt1B+Cpx1min	814	819	825
	Grt1B+Cpx1avg	790	795	801
	Grt1B+cpx1max	742	747	753
	Grt1B+Cpx2min	839	845	850
	Grt1B+Cpx2avg	839	844	850
	Grt1B+cpx2max	853	858	864
D213B	Grt1A+Cpx1min	823	829	834
	Grt1A+Cpx1avg	831	836	842
	Grt1A+cpx1max	812	817	823
	Grt1A+Cpx2min	838	843	849
	Grt1A+Cpx2avg	835	841	846
	Grt1A+cpx2max	858	864	869
	Grt1B+Cpx1min	812	817	823
	Grt1B+Cpx1avg	819	824	830
	Grt1B+cpx1max	800	806	811
	Grt1B+Cpx2min	826	831	837
	Grt1B+Cpx2avg	823	829	834
	Grt1B+cpx2max	846	851	857
D217A	Grt1+Bt1min	747	751	755
	Grt1+Bt1avg	746	750	754
	Grt1+Bt1max	754	758	762
	Grt1+Bt2min	751	755	759
	Grt1+Bt2avg	750	754	758
	Grt1+Bt2max	741	745	749
	Grt2+Bt3min	796	801	805
	Grt2+Bt3avg	784	788	792
	Grt2+Bt3max	770	774	778
		Pressure (kbar) at:		
	GADS*	750 ˚C	800˚C	850 ˚C
D212B	Grt1A+Cpx1min+Pl1min	14	15	15
	Grt1A+Cpx1min+Pl1avg	14	15	15
	Grt1A+Cpx1min+Pl1max	14	15	15
	Grt1A+Cpx1avg+Pl1min	14	14	15
	Grt1A+Cpx1avg+Pl1avg	14	15	15
	Grt1A+Cpx1avg+Pl1max	14	15	15
	Grt1A+Cpx1max+Pl1min	14	14	15
	Grt1A+Cpx1max+Pl1avg	14	14	15
	Grt1A+Cpx1max+Pl1max	14	14	15

TABLE D2. CONTINUED

Sample	Mineral Combination	Pressure (kbar) at:		
	GADS*	750 ˚C	800˚C	850 ˚C
D212B	Grt1A+Cpx2min+Pl1min	14	15	15
	Grt1A+Cpx2min+Pl1avg	14	15	15
	Grt1A+Cpx2min+Pl1max	14	15	15
	Grt1A+Cpx2avg+Pl1min	14	15	15
	Grt1A+Cpx2avg+Pl1avg	14	15	15
	Grt1A+Cpx2avg+Pl1max	14	15	15
	Grt1A+Cpx2max+Pl1min	14	14	15
	Grt1A+Cpx2max+Pl1avg	14	14	15
	Grt1A+Cpx2max+Pl1max	14	14	15
	Grt1B+Cpx1min+Pl1min	14	15	15
	Grt1B+Cpx1min+Pl1avg	14	15	15
	Grt1B+Cpx1min+Pl1max	14	15	15
	Grt1B+Cpx1avg+Pl1min	14	14	15
	Grt1B+Cpx1avg+Pl1avg	14	15	15
	Grt1B+Cpx1avg+Pl1max	14	15	15
	Grt1B+Cpx1max+Pl1min	14	14	15
	Grt1B+Cpx1max+Pl1avg	14	14	15
	Grt1B+Cpx1max+Pl1max	14	14	15
	Grt1B+Cpx2min+Pl1min	14	15	15
	Grt1B+Cpx2min+Pl1avg	14	15	15
	Grt1B+Cpx2min+Pl1max	14	15	15
	Grt1B+Cpx2avg+Pl1min	14	15	15
	Grt1B+Cpx2avg+Pl1avg	14	15	15
	Grt1B+Cpx2avg+Pl1max	14	15	15
	Grt1B+Cpx2max+Pl1min	14	14	15
	Grt1B+Cpx2max+Pl1avg	14	14	15
	Grt1B+Cpx2max+Pl1max	14	14	15
D213B	Grt1A+Cpx1min+Pl1min	14	14	15
	Grt1A+Cpx1min+Pl1avg	14	14	15
	Grt1A+Cpx1min+Pl1max	14	14	15
	Grt1A+Cpx1min+Pl2min	14	14	15
	Grt1A+Cpx1min+Pl2avg	14	14	15
	Grt1A+Cpx1min+Pl2max	14	14	15
	Grt1A+Cpx1avg+Pl1min	14	14	15
	Grt1A+Cpx1avg+Pl1avg	14	14	15
	Grt1A+Cpx1avg+Pl1max	14	14	15
	Grt1A+Cpx1avg+Pl2min	14	14	15
	Grt1A+Cpx1avg+Pl2avg	14	14	15
	Grt1A+Cpx1avg+Pl2max	14	14	15
	Grt1A+Cpx1max+Pl1min	13	14	15
	Grt1A+Cpx1max+Pl1avg	14	14	15
	Grt1A+Cpx1max+Pl1max	14	14	15
	Grt1A+Cpx1max+Pl2min	14	14	15
	Grt1A+Cpx1max+Pl2avg	14	14	15

TABLE D2. CONTINUED

Sample	Mineral Combination	Pressure (kbar) at:		
	GADS*	750 ˚C	800˚C	850 ˚C
D213B	Grt1A+Cpx1max+Pl2max	14	14	15
	Grt1A+Cpx2min+Pl1min	14	14	15
	Grt1A+Cpx2min+Pl1avg	14	14	15
	Grt1A+Cpx2min+Pl1max	14	15	15
	Grt1A+Cpx2min+Pl2min	14	14	15
	Grt1A+Cpx2min+Pl2avg	14	15	15
	Grt1A+Cpx2min+Pl2max	14	15	15
	Grt1A+Cpx2avg+Pl1min	14	14	15
	Grt1A+Cpx2avg+Pl1avg	14	14	15
	Grt1A+Cpx2avg+Pl1max	14	14	15
	Grt1A+Cpx2avg+Pl2min	14	14	15
	Grt1A+Cpx2avg+Pl2avg	14	14	15
	Grt1A+Cpx2avg+Pl2max	14	14	15
	Grt1A+Cpx2max+Pl1min	13	14	14
	Grt1A+Cpx2max+Pl1avg	13	14	15
	Grt1A+Cpx2max+Pl1max	14	14	15
	Grt1A+Cpx2max+Pl2min	13	14	15
	Grt1A+Cpx2max+Pl2avg	14	14	15
	Grt1A+Cpx2max+Pl2max	14	14	15
	Grt1B+Cpx1min+Pl1min	13	14	15
	Grt1B+Cpx1min+Pl1avg	14	14	15
	Grt1B+Cpx1min+Pl1max	14	14	15
	Grt1B+Cpx1min+Pl2min	14	14	15
	Grt1B+Cpx1min+Pl2avg	14	14	15
	Grt1B+Cpx1min+Pl2max	14	14	15
	Grt1B+Cpx1avg+Pl1min	14	14	15
	Grt1B+Cpx1avg+Pl1avg	14	14	15
	Grt1B+Cpx1avg+Pl1max	14	14	15
	Grt1B+Cpx1avg+Pl2min	14	14	15
	Grt1B+Cpx1avg+Pl2avg	14	14	15
	Grt1B+Cpx1avg+Pl2max	14	14	15
	Grt1B+Cpx1max+Pl1min	13	14	14
	Grt1B+Cpx1max+Pl1avg	14	14	15
	Grt1B+Cpx1max+Pl1max	14	14	15
	Grt1B+Cpx1max+Pl2min	14	14	15
	Grt1B+Cpx1max+Pl2avg	14	14	15
	Grt1B+Cpx1max+Pl2max	14	14	15
	Grt1B+Cpx2min+Pl1min	14	14	15
	Grt1B+Cpx2min+Pl1avg	14	14	15
	Grt1B+Cpx2min+Pl1max	14	15	15
	Grt1B+Cpx2min+Pl2min	14	14	15
	Grt1B+Cpx2min+Pl2avg	14	14	15
	Grt1B+Cpx2min+Pl2max	14	15	15
	Grt1B+Cpx2avg+Pl1min	13	14	15

TABLE D2. CONTINUED

Sample	Mineral Combination	Pressure (kbar) at:		
	GADS*	750 ˚C	800 ˚C	850 ˚C
D213B	Grt1A+Cpx1max+Pl2max	14	14	15
	Grt1A+Cpx2min+Pl1min	14	14	15
	Grt1A+Cpx1max+Pl2max	14	14	15
	Grt1B+Cpx2avg+Pl2avg	14	14	15
	Grt1B+Cpx2avg+Pl2max	14	14	15
	Grt1B+Cpx2max+Pl1min	13	14	14
	Grt1B+Cpx2max+Pl1avg	13	14	14
	Grt1B+Cpx2max+Pl1max	14	14	15
	Grt1B+Cpx2max+Pl2min	13	14	14
	Grt1B+Cpx2max+Pl2avg	14	14	15
	Grt1B+Cpx2max+Pl2max	14	14	15
		Pressure (kbar) at:		
	GASP†	750 ˚C	800 ˚C	850 ˚C
D212B	Grt1A+Pl1min	13	14	15
	Grt1A+Pl1avg	14	15	16
	Grt1A+Pl1max	14	15	16
	Grt1B+Pl1min	14	15	16
	Grt1B+Pl1avg	14	15	16
	Grt1B+Pl1max	14	15	16
D213B	Grt1A+Pl1min	13	14	15
	Grt1A+Pl1avg	13	14	15
	Grt1A+Pl1max	13	14	15
	Grt1A+Pl2min	13	14	15
	Grt1A+Pl2avg	13	14	15
	Grt1A+Pl2max	13	14	15
	Grt1B+Pl1min	13	14	15
	Grt1B+Pl1avg	13	14	15
	Grt1B+Pl1max	13	14	15
	Grt1B+Pl2min	13	14	15
	Grt1B+Pl2avg	13	14	15
	Grt1B+Pl2max	13	14	15
D217A	Grt1+Pl1min	13	14	15
	Grt+Pl1avg	13	14	15
	Grt1+P1max	13	15	16
	Grt1+Pl2min	13	14	15
	Grt1+Pl2avg	13	14	15
	Grt1+Pl2max	13	15	16
		Pressure (kbar) at:		
	Ab-Jd-Qtz§	750 ˚C	800 ˚C	850 ˚C
D212B	Cpx1min+Pl1min	15	16	16
	Cpx1min+Pl1avg	15	16	16
	Cpx1min+Pl1max	15	16	16
	Cpx1avg+Pl1min	15	16	16
	Cpx1avg+Pl1avg	15	16	16

TABLE D2. CONTINUED

Sample	Mineral Combination	Pressure (kbar) at:		
	Ab-Jd-Qtz§	750 ˚C	800 ˚C	850 ˚C
D212B	Cpx1avg+Pl1max	15	16	16
	Cpx1max+Pl1min	15	16	16
	Cpx1max+Pl1avg	15	16	16
	Cpx1max+Pl1max	15	16	16
	Cpx2min+Pl1min	15	16	16
	Cpx2min+Pl1avg	15	16	16
	Cpx2min+Pl1max	15	16	16
	Cpx2avg+Pl1min	15	15	16
	Cpx2avg+Pl1avg	15	15	16
	Cpx2avg+Pl1max	14	15	16
	Cpx2max+Pl1min	14	14	15
	Cpx2max+Pl1avg	14	14	15
	Cpx2max+Pl1max	14	14	15
D213B	Cpx1min+Pl1min	15	15	16
	Cpx1min+Pl1avg	15	15	16
	Cpx1min+Pl1max	15	15	16
	Cpx1min+Pl2min	15	15	16
	Cpx1min+Pl2avg	15	15	16
	Cpx1min+Pl2max	15	15	16
	Cpx1avg+Pl1min	15	16	16
	Cpx1avg+Pl1avg	15	16	16
	Cpx1avg+Pl1max	15	16	16
	Cpx1avg+Pl2min	15	16	16
	Cpx1avg+Pl2avg	15	16	16
	Cpx1avg+Pl2max	15	16	16
	Cpx1max+Pl1min	15	15	16
	Cpx1max+Pl1avg	15	15	16
	Cpx1max+Pl1max	15	15	16
	Cpx1max+Pl2min	15	15	16
	Cpx1max+Pl2avg	15	15	16
	Cpx1max+Pl2max	15	15	16
	Cpx2min+Pl1min	15	16	17
	Cpx2min+Pl1avg	15	16	17
	Cpx2min+Pl1max	15	16	17
	Cpx2min+Pl2min	15	16	17
	Cpx2min+Pl2avg	15	16	17
	Cpx2min+Pl2max	15	16	17
	Cpx2avg+Pl1min	15	15	16
	Cpx2avg+Pl1avg	15	15	16
	Cpx2avg+Pl1max	15	15	16
	Cpx2avg+Pl2min	15	15	16
	Cpx2avg+Pl2avg	15	15	16
	Cpx2avg+Pl2max	15	15	16
	Cpx2max+Pl1min	14	15	15

TABLE D2. CONTINUED

Sample	Mineral Combination	Pressure (kbar) at:		
	Ab-Jd-Qtz§	750 ˚C	800 ˚C	850 ˚C
D213B	Cpx2max+Pl1avg	14	14	15
	Cpx2max+Pl1max	14	14	15
	Cpx2max+Pl2min	14	14	15
	Cpx2max+Pl2avg	14	14	15
	Cpx2max+Pl2max	14	14	15

Note: Iron-magnesium exchange after Pattison and Newton (1989; Grt-Cpx) and Hodges and Spear (1982; Grt-Bt).

*GADS barometer after Newton and Perkins (1985).

†GASP barometer after Hodges and Spear (1982).

§Ab-Jd-Qtz barometer after Holland (1980).

TABLE D3. AVERAGE P-T CONDITIONS CALCULATED BY THE PROGRAM THERMOCALC V3.33

Sample	Mineral Combination	Temp (˚C)	Error (˚C)	Pressure (kbar)	Error (kbar)	Error Correlation	Significance of Fit	Iterations	Reactions
D212B	Grt1A+cpx1min+pl1min+czo1min	735	63	15.0	1.9	0.956	0.83	3	1,2,3,4
	Grt1A+cpx1min+pl1min+czo1avg	760	56	15.5	1.8	0.956	0.89	3	3,4,8,9
	Grt1A+cpx1min+pl1min+czo1max	777	57	16.0	1.8	0.953	0.95	3	1,3,4,7
	Grt1A+cpx1min+pl1max+czo1min	735	63	15.1	1.9	0.954	0.83	2	1,3,4,8
	Grt1A+cpx1min+pl1max+czo1avg	759	56	15.6	1.8	0.954	0.88	3	1,3,4,9
	Grt1A+cpx1min+pl1max+czo1max	776	57	16.1	1.8	0.951	0.96	3	3,5,11,26
	Grt1A+cpx1avg+pl1min+czo1min	734	63	15.0	1.9	0.956	0.86	4	1,2,3,4
	Grt1A+cpx1avg+pl1min+czo1avg	760	56	15.5	1.8	0.956	0.93	1	3,4,8,9
	Grt1A+cpx1avg+pl1min+czo1max	778	58	16.0	1.8	0.954	1.01	3	5,4,11,26
	Grt1A+cpx1avg+pl1max+czo1min	734	63	15.1	1.9	0.954	0.86	2	3,5,8,9
	Grt1A+cpx1avg+pl1max+czo1avg	760	56	15.6	1.8	0.954	0.94	2	1,2,3,4
	Grt1A+cpx1avg+pl1max+czo1max	777	58	16.1	1.9	0.951	1.02	2	1,3,8,10
	Grt1A+cpx1max+pl1min+czo1min	726	63	14.7	1.8	0.958	0.82	3	4,5,11,26
	Grt1A+cpx1max+pl1min+czo1avg	755	56	15.4	1.8	0.956	0.93	2	3,4,8,9
	Grt1A+cpx1max+pl1min+czo1max	772	61	15.9	1.9	0.954	1.06	3	1,3,4,8
	Grt1A+cpx1max+pl1max+czo1min	725	63	14.8	1.8	0.956	0.82	2	1,3,8,10
	Grt1A+cpx1max+pl1max+czo1avg	754	56	15.5	1.8	0.954	0.93	2	1,3,4,8
	Grt1A+cpx1max+pl1max+czo1max	772	61	15.9	1.9	0.954	1.06	4	1,3,4,8
	Grt1A+cpx2min+pl1min+czo1min	742	64	15.7	1.8	0.956	1.00	5	3,4,8,9
	Grt1A+cpx2min+pl1min+czo1avg	767	57	15.7	1.8	0.956	1.02	3	3,4,8,9
	Grt1A+cpx2min+pl1min+czo1max	784	61	16.2	1.9	0.953	1.06	3	1,3,8,10
	Grt1A+cpx2min+pl1max+czo1min	741	65	15.3	1.9	0.954	1.01	3	1,3,4,8
	Grt1A+cpx2min+pl1max+czo1avg	766	57	15.8	1.8	0.953	1.02	3	3,4,8,9
	Grt1A+cpx2min+pl1max+czo1max	781	63	16.2	2.0	0.951	1.09	3	1,3,4,8
	Grt1A+cpx2avg+pl1min+czo1min	743	64	15.2	1.9	0.955	1.00	3	1,3,8,9
	Grt1A+cpx2avg+pl1min+czo1avg	768	59	15.8	1.9	0.956	1.05	3	2,3,4,8
	Grt1A+cpx2avg+pl1min+czo1max	785	63	16.3	2.0	0.953	1.10	3	1,3,8,10
	Grt1A+cpx2avg+pl1max+czo1min	739	66	15.2	1.9	0.954	1.03	3	1,3,4,8
	Grt1A+cpx2avg+pl1max+czo1avg	763	58	15.8	1.9	0.953	1.05	3	1,3,4,8

TABLE D3. CONTINUED

Sample	Mineral Combination	Temp (˚C)	Error (˚C)	Pressure (kbar)	Error (kbar)	Error Correlation	Significance of Fit	Iterations	Reactions
D212B	Grt1A+cpx2avg+pl1max+czo1max	784	64	16.4	2.0	0.951	1.11	4	1,3,8,10
	Grt1A+cpx2max+pl1min+czo1min	756	90	15.6	2.7	0.956	1.39	3	3,8,9,10
	Grt1A+cpx2max+pl1min+czo1avg	781	81	16.3	2.6	0.953	1.44	4	1,3,8,9
	Grt1A+cpx2max+pl1min+czo1max	801	89	16.8	2.8	0.954	1.52	3	1,3,8,10
	Grt1A+cpx2max+pl1max+czo1min	756	90	15.8	2.6	0.954	1.37	3	1,3,8,10
	Grt1A+cpx2max+pl1max+czo1avg	780	81	16.4	2.6	0.951	1.45	2	3,4,8,9
	Grt1A+cpx2max+pl1max+czo1max	800	89	16.8	2.9	0.951	1.53	1	1,3,4,8
	Grt1B+cpx1min+pl1min+czo1min	751	63	15.5	1.9	0.954	0.86	3	1,3,4,8
	Grt1B+cpx1min+pl1min+czo1avg	773	55	16.1	1.7	0.951	0.92	3	1,3,8,10
	Grt1B+cpx1min+pl1min+czo1max	793	59	16.5	1.9	0.952	1.03	3	1,3,8,10
	Grt1B+cpx1min+pl1max+czo1min	751	63	15.6	1.9	0.952	0.87	2	1,3,8,10
	Grt1B+cpx1min+pl1max+czo1avg	773	54	16.2	1.9	0.949	0.93	2	3,4,8,9
	Grt1B+cpx1min+pl1max+czo1max	795	58	16.2	1.9	0.949	1.04	3	1,3,8,10
	Grt1B+cpx1avg+pl1min+czo1min	750	63	15.5	1.9	0.954	0.90	1	1,3,4,8
	Grt1B+cpx1avg+pl1min+czo1avg	774	55	16.1	1.8	0.951	0.97	2	1,3,8,10
	Grt1B+cpx1avg+pl1min+czo1max	794	63	16.6	2.0	0.952	1.10	2	1,3,8,10
	Grt1B+cpx1avg+pl1max+czo1min	750	63	15.6	1.9	0.952	0.90	2	1,3,8,10
	Grt1B+cpx1avg+pl1max+czo1avg	773	55	16.2	1.8	0.949	0.98	2	1,3,8,10
	Grt1B+cpx1avg+pl1max+czo1max	793	63	16.7	2.0	0.949	1.10	3	1,8,9,10
	Grt1B+cpx1max+pl1min+czo1min	742	62	15.3	1.8	0.954	0.89	2	1,3,4,8
	Grt1B+cpx1max+pl1min+czo1avg	769	55	16.0	1.7	0.952	0.98	3	1,3,4,8
	Grt1B+cpx1max+pl1min+czo1max	791	64	16.5	2.0	0.952	1.12	3	1,3,4,8
	Grt1B+cpx1max+pl1max+czo1min	741	62	15.4	1.9	0.952	0.90	3	1,3,4,8
	Grt1B+cpx1max+pl1max+czo1avg	769	55	16.0	1.7	0.952	0.98	1	1,3,4,8
	Grt1B+cpx1max+pl1max+czo1max	790	64	16.6	2.0	0.949	1.13	2	1,8,9,10
	Grt1B+cpx2min+pl1min+czo1min	759	65	15.7	1.9	0.954	1.01	3	1,3,8,10
	Grt1B+cpx2min+pl1min+czo1avg	780	57	16.3	1.8	0.951	1.05	2	1,3,8,10
	Grt1B+cpx2min+pl1min+czo1max	800	64	16.7	2.1	0.951	1.13	2	1,3,8,10
	Grt1B+cpx2min+pl1max+czo1min	758	65	15.8	1.9	0.952	1.02	2	1,3,8,10
	Grt1B+cpx2min+pl1max+czo1avg	779	58	16.4	1.9	0.948	1.05	2	1,3,8,10

TABLE D3. CONTINUED

Sample	Mineral Combination	Temp (˚C)	Error (˚C)	Pressure (kbar)	Error (kbar)	Error Correlation	Significance of Fit	Iterations	Reactions
D212B	Grt1B+cpx2min+pl1max+czo1max	800	65	16.8	2.1	0.949	1.13	3	1,3,8,10
	Grt1B+cpx2avg+pl1min+czo1min	758	65	15.7	1.9	0.954	1.03	2	1,3,8,10
	Grt1B+cpx2avg+pl1min+czo1avg	781	59	16.3	1.9	0.951	1.08	2	1,3,8,10
	Grt1B+cpx2avg+pl1min+czo1max	801	67	16.8	2.1	0.951	1.18	2	1,3,8,10
	Grt1B+cpx2avg+pl1max+czo1min	757	66	15.8	2.0	0.952	1.04	2	1,3,8,10
	Grt1B+cpx2avg+pl1max+czo1avg	780	59	16.4	1.9	0.948	1.09	2	1,3,8,10
	Grt1B+cpx2avg+pl1max+czo1max	800	67	16.9	2.2	0.949	1.18	2	1,3,8,10
	Grt1B+cpx2max+pl1min+czo1min	771	92	16.2	2.7	0.953	1.43	3	3,4,8,27
	Grt1B+cpx2max+pl1min+czo1avg	795	84	16.8	2.7	0.951	1.51	2	1,3,8,10
	Grt1B+cpx2max+pl1min+czo1max	817	89	17.4	2.9	0.949	1.54	3	1,3,8,10
	Grt1B+cpx2max+pl1max+czo1min	771	92	16.2	2.7	0.953	1.43	1	3,4,8,27
	Grt1B+cpx2max+pl1max+czo1avg	795	84	16.9	2.7	0.949	1.51	3	1,3,8,10
	Grt1B+cpx2max+pl1max+czo1max	816	89	17.5	2.9	0.946	1.55	3	1,3,8,10
D213B	Grt1A+cpx1min+pl1min+czo1min	725	69	14.2	2.0	0.964	1.03	3	1,2,4,12
	Grt1A+cpx1min+pl1min+czo1avg	738	59	14.6	1.8	0.962	0.98	5	1,8,10,12
	Grt1A+cpx1min+pl1min+czo1max	755	61	14.9	1.9	0.962	0.89	4	1,3,4,8
	Grt1A+cpx1min+pl1avg+czo1min	724	69	14.3	2.0	0.962	1.03	2	1,4,8,12
	Grt1A+cpx1min+pl1avg+czo1avg	737	59	14.6	1.8	0.960	0.98	3	1,6,10,12
	Grt1A+cpx1min+pl1avg+czo1max	754	61	15.0	1.9	0.961	0.90	2	1,3,8,10
	Grt1A+cpx1min+pl1max+czo1min	723	70	14.5	2.1	0.959	1.06	2	1,8,10,12
	Grt1A+cpx1min+pl1max+czo1avg	737	59	14.8	1.8	0.958	0.95	2	1,8,10,12
	Grt1A+cpx1min+pl1max+czo1max	753	61	15.2	1.9	0.956	0.91	2	1,8,10,12
	Grt1A+cpx1min+pl2avg+czo1min	724	69	14.4	2.0	0.961	1.04	2	1,4,8,12
	Grt1A+cpx1min+pl2avg+czo1avg	737	59	14.8	1.8	0.958	0.95	1	1,8,10,12
	Grt1A+cpx1min+pl2avg+czo1max	754	61	15.1	1.9	0.959	0.90	3	1,8,10,12
	Grt1A+cpx1avg+pl1min+czo1min	733	85	14.5	2.5	0.962	1.25	3	1,8,10,12
	Grt1A+cpx1avg+pl1min+czo1avg	745	68	14.8	2.1	0.962	1.15	2	1,8,10,12
	Grt1A+cpx1avg+pl1min+czo1max	761	68	15.1	2.1	0.962	1.10	3	1,6,10,12
	Grt1A+cpx1avg+pl1avg+czo1min	732	85	14.6	2.5	0.961	1.26	3	1,8,10,12
	Grt1A+cpx1avg+pl1avg+czo1avg	744	69	14.9	2.1	0.960	1.16	2	1,8,10,12

TABLE D3. CONTINUED

Sample	Mineral Combination	Temp (˚C)	Error (˚C)	Pressure (kbar)	Error (kbar)	Error Correlation	Significance of Fit	Iterations	Reactions
D213B	Grt1A+cpx1avg+pl1avg+czo1max	761	68	15.2	2.1	0.960	1.11	2	1,8,10,12
	Grt1A+cpx1avg+pl1max+czo1min	732	85	14.7	2.5	0.959	1.27	2	1,8,10,12
	Grt1A+cpx1avg+pl1max+czo1avg	743	69	14.9	2.1	0.958	1.16	3	1,8,10,12
	Grt1A+cpx1avg+pl1max+czo1max	760	69	15.4	2.1	0.956	1.12	2	1,8,10,12
	Grt1A+cpx1avg+pl2avg+czo1min	732	85	14.7	2.5	0.959	1.26	2	1,8,10,12
	Grt1A+cpx1avg+pl2avg+czo1avg	743	69	14.9	2.1	0.958	1.16	2	1,8,10,12
	Grt1A+cpx1avg+pl2avg+czo1max	760	68	15.3	2.1	0.958	1.11	2	1,8,10,12
	Grt1A+cpx1max+pl1min+czo1min	743	101	14.8	2.9	0.963	1.47	2	1,8,10,12
	Grt1A+cpx1max+pl1min+czo1avg	754	83	15.1	2.6	0.962	1.39	2	1,3,8,10
	Grt1A+cpx1max+pl1min+czo1max	772	83	15.6	2.6	0.961	1.34	3	1,3,8,10
	Grt1A+cpx1max+pl1avg+czo1min	743	101	14.9	2.9	0.961	1.48	3	1,8,10,12
	Grt1A+cpx1max+pl1avg+czo1avg	754	83	15.1	2.6	0.961	1.40	2	1,3,8,10
	Grt1A+cpx1max+pl1avg+czo1max	772	84	15.7	2.6	0.959	1.35	2	1,3,8,10
	Grt1A+cpx1max+pl1max+czo1min	742	101	15.0	3.0	0.959	1.48	2	1,2,4,12
	Grt1A+cpx1max+pl1max+czo1avg	753	84	15.3	2.6	0.956	1.41	3	1,8,10,12
	Grt1A+cpx1max+pl1max+czo1max	771	84	15.8	2.6	0.956	1.36	3	1,8,10,12
	Grt1A+cpx1max+pl2avg+czo1min	742	101	15.0	3.0	0.959	1.48	2	1,4,8,12
	Grt1A+cpx1max+pl2avg+czo1avg	753	84	15.2	2.6	0.958	1.40	2	1,8,10,12
	Grt1A+cpx1max+pl2avg+czo1max	771	84	15.8	2.6	0.956	1.36	2	1,8,10,12
	Grt1A+cpx2min+pl1min+czo1min	746	107	14.8	3.1	0.963	1.56	2	1,6,10,12
	Grt1A+cpx2min+pl1min+czo1avg	753	88	15.0	2.7	0.962	1.47	3	1,8,10,12
	Grt1A+cpx2min+pl1min+czo1max	771	87	15.5	2.7	0.961	1.40	2	1,8,10,12
	Grt1A+cpx2min+pl1avg+czo1min	745	108	14.9	3.1	0.961	1.57	2	1,4,8,12
	Grt1A+cpx2min+pl1avg+czo1avg	752	88	15.1	2.7	0.961	1.48	2	1,8,10,12
	Grt1A+cpx2min+pl1avg+czo1max	770	87	15.6	2.7	0.959	1.41	2	1,8,10,12
	Grt1A+cpx2min+pl1max+czo1min	744	109	15.1	3.2	0.958	1.58	3	1,8,10,12
	Grt1A+cpx2min+pl1max+czo1avg	751	89	15.3	2.8	0.956	1.49	3	1,8,10,12
	Grt1A+cpx2min+pl1max+czo1max	770	87	15.7	2.7	0.956	1.41	2	1,8,10,12
	Grt1A+cpx2min+pl2avg+czo1min	744	108	15.0	3.2	0.959	1.58	3	1,4,8,12
	Grt1A+cpx2min+pl2avg+czo1avg	752	88	15.2	2.7	0.958	1.48	2	1,8,10,12

TABLE D3. CONTINUED

Sample	Mineral Combination	Temp (˚C)	Error (˚C)	Pressure (kbar)	Error (kbar)	Error Correlation	Significance of Fit	Iterations	Reactions
D213B	Grt1A+cpx2min+pl2avg+czo1max	770	87	15.7	2.7	0.956	1.41	1	1,8,10,12
	Grt1A+cpx2avg+pl1min+czo1min	733	85	14.5	2.5	0.962	1.25	3	1,8,10,12
	Grt1A+cpx2avg+pl1min+czo1avg	744	67	14.7	2.1	0.962	1.13	3	1,8,10,12
	Grt1A+cpx2avg+pl1min+czo1max	762	66	15.1	2.0	0.962	1.08	3	1,4,8,12
	Grt1A+cpx2avg+pl1avg+czo1min	732	85	14.6	2.5	0.961	1.26	3	1,8,10,12
	Grt1A+cpx2avg+pl1avg+czo1avg	743	67	14.8	2.1	0.960	1.14	2	1,8,10,12
	Grt1A+cpx2avg+pl1avg+czo1max	761	66	15.2	2.0	0.961	1.08	2	1,3,8,10
	Grt1A+cpx2avg+pl1max+czo1min	732	85	14.7	2.5	0.959	1.26	1	1,8,10,12
	Grt1A+cpx2avg+pl1max+czo1avg	743	68	14.9	2.1	0.958	1.14	2	1,8,10,12
	Grt1A+cpx2avg+pl1max+czo1max	760	67	15.4	2.1	0.957	1.10	3	1,8,10,12
	Grt1A+cpx2avg+pl2avg+czo1min	732	85	14.7	2.5	0.959	1.26	2	1,8,10,12
	Grt1A+cpx2avg+pl2avg+czo1avg	743	68	14.9	2.1	0.958	1.14	1	1,8,10,12
	Grt1A+cpx2avg+pl2avg+czo1max	761	67	15.3	2.1	0.959	1.09	2	1,4,9,11
	Grt1A+cpx2max+pl1min+czo1min	730	77	14.3	2.2	0.964	1.14	3	1,4,9,10
	Grt1A+cpx2max+pl1min+czo1avg	743	61	14.7	1.9	0.962	1.03	3	1,8,10,12
	Grt1A+cpx2max+pl1min+czo1max	761	61	15.1	1.9	0.963	1.00	2	1,4,8,12
	Grt1A+cpx2max+pl1avg+czo1min	729	77	14.4	2.2	0.962	1.15	2	1,8,10,12
	Grt1A+cpx2max+pl1avg+czo1avg	742	62	14.8	1.9	0.960	1.04	2	1,3,8,10
	Grt1A+cpx2max+pl1avg+czo1max	760	62	15.2	1.9	0.961	1.01	2	1,3,8,10
	Grt1A+cpx2max+pl1max+czo1min	728	78	14.6	2.3	0.959	1.16	2	1,8,10,12
	Grt1A+cpx2max+pl1max+czo1avg	741	62	14.9	1.9	0.958	1.05	2	1,8,10,12
	Grt1A+cpx2max+pl1max+czo1max	759	62	15.4	1.9	0.957	1.02	2	1,8,10,12
	Grt1A+cpx2max+pl2avg+czo1min	728	78	14.6	2.3	0.959	1.16	1	1,8,10,12
	Grt1A+cpx2max+pl2avg+czo1avg	741	62	14.9	1.9	0.958	1.05	1	1,8,10,12
	Grt1A+cpx2max+pl2avg+czo1max	759	62	15.3	1.9	0.959	1.01	2	1,3,8,10
	Grt1B+cpx1min+pl1min+czo1min	729	73	14.3	2.1	0.964	1.08	2	4,8,9,12
	Grt1B+cpx1min+pl1min+czo1avg	741	60	14.7	1.9	0.962	1.02	3	1,8,10,12
	Grt1B+cpx1min+pl1min+czo1max	759	61	15.0	1.9	0.962	0.93	3	1,3,4,8
	Grt1B+cpx1min+pl1avg+czo1min	729	73	14.4	2.1	0.962	1.09	3	1,3,8,12
	Grt1B+cpx1min+pl1avg+czo1avg	741	60	14.8	1.9	0.960	1.03	1	1,6,8,10

TABLE D3. CONTINUED

Sample	Mineral Combination	Temp (˚C)	Error (˚C)	Pressure (kbar)	Error (kbar)	Error Correlation	Significance of Fit	Iterations	Reactions
D213B	Grt1B+cpx1min+pl1avg+czo1max	758	61	15.1	1.9	0.960	0.94	2	1,8,10,12
	Grt1B+cpx1min+pl1max+czo1min	728	73	14.6	2.2	0.959	1.10	2	1,8,10,12
	Grt1B+cpx1min+pl1max+czo1avg	740	61	14.8	1.9	0.958	1.03	2	1,8,10,12
	Grt1B+cpx1min+pl1max+czo1max	757	61	15.3	1.9	0.956	0.95	3	1,8,10,12
	Grt1B+cpx1min+pl2avg+czo1min	728	73	14.6	2.2	0.959	1.10	2	1,8,10,12
	Grt1B+cpx1min+pl2avg+czo1avg	740	61	14.8	1.9	0.958	1.03	2	1,8,10,12
	Grt1B+cpx1min+pl2avg+czo1max	757	61	15.2	1.9	0.958	0.95	2	1,8,10,12
	Grt1B+cpx1avg+pl1min+czo1min	737	88	14.6	2.5	0.962	1.30	3	1,8,10,12
	Grt1B+cpx1avg+pl1min+czo1avg	747	73	14.8	2.3	0.962	1.24	2	1,8,10,12
	Grt1B+cpx1avg+pl1min+czo1max	765	70	15.2	2.2	0.962	1.14	2	1,6,8,10
	Grt1B+cpx1avg+pl1avg+czo1min	736	88	14.7	2.6	0.961	1.30	2	1,8,10,12
	Grt1B+cpx1avg+pl1avg+czo1avg	747	74	14.9	2.3	0.960	1.24	1	1,8,10,12
	Grt1B+cpx1avg+pl1avg+czo1max	764	71	15.3	2.2	0.960	1.15	3	1,3,8,10
	Grt1B+cpx1avg+pl1max+czo1min	736	89	14.8	2.6	0.959	1.31	2	1,8,10,12
	Grt1B+cpx1avg+pl1max+czo1avg	746	74	15.1	2.3	0.956	1.26	4	1,8,10,12
	Grt1B+cpx1avg+pl1max+czo1max	763	71	15.5	2.2	0.956	1.16	2	1,8,10,12
	Grt1B+cpx1avg+pl2avg+czo1min	736	89	14.8	2.6	0.959	1.31	2	1,8,10,12
	Grt1B+cpx1avg+pl2avg+czo1avg	746	74	15.0	2.3	0.958	1.25	2	1,8,10,12
	Grt1B+cpx1avg+pl2avg+czo1max	763	71	15.4	2.2	0.956	1.16	3	1,8,10,12
	Grt1B+cpx1max+pl1min+czo1min	747	104	14.9	3.0	0.963	1.51	3	1,4,8,12
	Grt1B+cpx1max+pl1min+czo1avg	758	85	15.2	2.6	0.962	1.43	2	1,4,8,12
	Grt1B+cpx1max+pl1min+czo1max	777	85	15.7	2.6	0.960	1.38	4	1,4,8,12
	Grt1B+cpx1max+pl1avg+czo1min	747	104	15.0	3.0	0.961	1.52	2	1,4,8,12
	Grt1B+cpx1max+pl1avg+czo1avg	757	86	15.3	2.7	0.960	1.44	2	1,4,8,12
	Grt1B+cpx1max+pl1avg+czo1max	777	85	15.7	2.6	0.960	1.38	3	1,4,8,12
	Grt1B+cpx1max+pl1max+czo1min	746	105	15.2	3.1	0.958	1.54	2	1,8,10,12
	Grt1B+cpx1max+pl1max+czo1avg	756	86	15.4	2.7	0.956	1.45	2	1,8,10,12
	Grt1B+cpx1max+pl1max+czo1max	775	87	15.9	2.7	0.956	1.40	4	1,8,10,12
	Grt1B+cpx1max+pl2avg+czo1min	746	105	15.1	3.1	0.959	1.53	2	1,8,10,12
	Grt1B+cpx1max+pl2avg+czo1avg	757	86	15.3	2.7	0.958	1.44	3	1,8,10,12

TABLE D3. CONTINUED

Sample	Mineral Combination	Temp (˚C)	Error (˚C)	Pressure (kbar)	Error (kbar)	Error Correlation	Significance of Fit	Iterations	Reactions
D213B	Grt1B+cpx1max+pl2avg+czo1max	775	87	15.9	2.7	0.956	1.40	2	1,8,10,12
	Grt1B+cpx2min+pl1min+czo1min	750	111	15.0	3.2	0.963	1.61	3	1,4,8,12
	Grt1B+cpx2min+pl1min+czo1avg	756	91	15.1	2.8	0.962	1.51	2	1,4,8,12
	Grt1B+cpx2min+pl1min+czo1max	775	89	15.6	2.7	0.960	1.44	3	1,4,8,12
	Grt1B+cpx2min+pl1avg+czo1min	749	111	15.1	3.2	0.961	1.61	3	1,4,8,12
	Grt1B+cpx2min+pl1avg+czo1avg	756	91	15.2	2.8	0.960	1.52	2	1,4,8,12
	Grt1B+cpx2min+pl1avg+czo1max	774	90	15.7	2.8	0.958	1.45	2	1,8,10,12
	Grt1B+cpx2min+pl1max+czo1min	748	112	15.2	3.3	0.958	1.63	2	1,8,10,12
	Grt1B+cpx2min+pl1max+czo1avg	755	92	15.4	2.9	0.956	1.53	2	1,8,10,12
	Grt1B+cpx2min+pl1max+czo1max	773	90	15.8	2.8	0.956	1.46	2	1,8,10,12
	Grt1B+cpx2min+pl2avg+czo1min	749	111	15.1	3.3	0.959	1.62	3	1,8,10,12
	Grt1B+cpx2min+pl2avg+czo1avg	755	91	15.3	2.8	0.958	1.53	2	1,8,10,12
	Grt1B+cpx2min+pl2avg+czo1max	773	90	15.8	2.8	0.956	1.46	2	1,8,10,12
	Grt1B+cpx2avg+pl1min+czo1min	737	88	14.6	2.5	0.962	1.30	3	1,4,8,12
	Grt1B+cpx2avg+pl1min+czo1avg	748	70	14.9	2.1	0.962	1.17	3	1,8,10,12
	Grt1B+cpx2avg+pl1min+czo1max	766	69	15.3	2.1	0.962	1.11	3	1,8,10,12
	Grt1B+cpx2avg+pl1avg+czo1min	736	88	14.7	2.6	0.961	1.30	2	1,8,10,12
	Grt1B+cpx2avg+pl1avg+czo1avg	747	70	14.9	2.2	0.960	1.18	2	1,8,10,12
	Grt1B+cpx2avg+pl1avg+czo1max	765	69	15.3	2.1	0.960	1.12	1	1,6,10,12
	Grt1B+cpx2avg+pl1max+czo1min	736	89	14.8	2.6	0.959	1.31	2	1,8,10,12
	Grt1B+cpx2avg+pl1max+czo1avg	745	71	15.1	2.2	0.956	1.20	3	1,8,10,12
	Grt1B+cpx2avg+pl1max+czo1max	764	70	15.5	2.2	0.956	1.14	2	1,8,10,12
	Grt1B+cpx2avg+pl2avg+czo1min	736	89	14.8	2.6	0.959	1.31	2	1,8,10,12
	Grt1B+cpx2avg+pl2avg+czo1avg	746	71	15.0	2.2	0.958	1.19	2	1,8,10,12
	Grt1B+cpx2avg+pl2avg+czo1max	764	70	15.5	2.2	0.956	1.14	2	1,8,10,12
	Grt1B+cpx2max+pl1min+czo1min	733	79	14.5	2.3	0.962	1.17	4	1,8,10,12
	Grt1B+cpx2max+pl1min+czo1avg	746	64	14.8	2.0	0.962	1.08	2	1,3,8,10
	Grt1B+cpx2max+pl1min+czo1max	763	62	15.2	1.9	0.962	1.02	3	1,8,10,12
	Grt1B+cpx2max+pl1avg+czo1min	732	79	14.6	2.3	0.961	1.18	2	1,8,10,12
	Grt1B+cpx2max+pl1avg+czo1avg	745	64	14.9	2.0	0.960	1.09	1	1,8,10,12

TABLE D3. CONTINUED

Sample	Mineral Combination	Temp (˚C)	Error (˚C)	Pressure (kbar)	Error (kbar)	Error Correlation	Significance of Fit	Iterations	Reactions
D213B	Grt1B+cpx2max+pl1avg+czo1max	763	63	15.3	1.9	0.960	1.02	2	1,3,8,10
	Grt1B+cpx2max+pl1max+czo1min	732	80	14.7	2.3	0.959	1.19	1	1,8,10,12
	Grt1B+cpx2max+pl1max+czo1avg	744	65	15.1	2.0	0.956	1.10	2	1,8,10,12
	Grt1B+cpx2max+pl1max+czo1max	763	65	15.5	2.0	0.956	1.06	2	1,8,10,12
	Grt1B+cpx2max+pl2avg+czo1min	732	80	14.7	2.3	0.959	1.19	2	1,8,10,12
	Grt1B+cpx2max+pl2avg+czo1avg	745	65	15.0	2.0	0.958	1.09	2	1,8,10,12
	Grt1B+cpx2max+pl2avg+czo1max	763	64	15.4	2.0	0.958	1.05	3	1,3,8,10
D217A	Grt1+ksp1avg+pl1min+bt1min	803	47	15.4	1.4	0.669	0.14	3	1,17,18,19
	Grt1+ksp1avg+pl1min+bt1avg	799	47	15.3	1.3	0.665	0.11	2	1,17,20,28
	Grt1+ksp1avg+pl1min+bt1max	792	45	15.2	1.3	0.658	0.15	2	1,18,21,22
	Grt1+ksp1avg+pl1min+bt2min	801	47	15.4	1.3	0.666	0.16	2	1,16,20,28
	Grt1+ksp1avg+pl1min+bt2avg	798	46	15.3	1.3	0.664	0.11	2	1,16,17,18
	Grt1+ksp1avg+pl1min+bt2max	801	47	15.4	1.4	0.667	0.13	3	1,16,18,28
	Grt1+ksp1avg+pl1avg+bt1min	803	47	15.6	1.4	0.666	0.16	2	1,17,18,19
	Grt1+ksp1avg+pl1avg+bt1avg	799	47	15.5	1.4	0.663	0.13	3	1,16,20,28
	Grt1+ksp1avg+pl1avg+bt1max	792	45	15.3	1.3	0.656	0.16	4	1,18,21,22
	Grt1+ksp1avg+pl1avg+bt2min	800	47	15.5	1.4	0.663	0.18	3	1,16,20,28
	Grt1+ksp1avg+pl1avg+bt2avg	798	46	15.5	1.4	0.661	0.13	2	1,16,17,18
	Grt1+ksp1avg+pl1avg+bt2max	801	47	15.5	1.4	0.665	0.14	2	1,16,18,28
	Grt1+ksp1avg+pl2max+bt1min	802	47	15.7	1.4	0.664	0.18	3	1,17,18,19
	Grt1+ksp1avg+pl2max+bt1avg	798	46	15.6	1.4	0.660	0.15	2	1,16,20,28
	Grt1+ksp1avg+pl2max+bt1max	791	45	15.5	1.3	0.654	0.17	2	1,18,21,22
	Grt1+ksp1avg+pl2max+bt2min	800	47	15.6	1.4	0.661	0.20	3	1,16,20,24
	Grt1+ksp1avg+pl2max+bt2avg	797	46	15.6	1.4	0.659	0.15	2	1,16,17,18
	Grt1+ksp1avg+pl2max+bt2max	800	47	15.6	1.4	0.662	0.16	2	1,16,18,28
	Grt1+ksp1max+pl1min+bt1min	806	48	15.5	1.4	0.670	0.14	3	1,16,18,29
	Grt1+ksp1max+pl1min+bt1avg	802	47	15.4	1.4	0.666	0.11	2	1,17,18,19
	Grt1+ksp1max+pl1min+bt1max	795	46	15.3	1.3	0.660	0.14	3	1,17,18,21
	Grt1+ksp1max+pl1min+bt2min	803	47	15.4	1.4	0.667	0.15	3	1,16,17,18
	Grt1+ksp1max+pl1min+bt2avg	801	47	15.4	1.3	0.665	0.10	2	1,17,18,29

TABLE D3. CONTINUED

Sample	Mineral Combination	Temp (˚C)	Error (˚C)	Pressure (kbar)	Error (kbar)	Error Correlation	Significance of Fit	Iterations	Reactions
D217A	Grt1+ksp1max+pl1min+bt2max	802	47	15.4	1.3	0.667	0.06	3	1,17,18,29
	Grt1+ksp1max+pl1avg+bt1min	806	47	15.6	1.4	0.668	0.15	2	1,17,18,29
	Grt1+ksp1max+pl1avg+bt1avg	802	47	15.5	1.4	0.664	0.12	3	1,16,17,18
	Grt1+ksp1max+pl1avg+bt1max	794	46	15.4	1.3	0.657	0.14	2	1,17,18,21
	Grt1+ksp1max+pl1avg+bt2min	803	47	15.5	1.4	0.665	0.17	3	1,16,17,18
	Grt1+ksp1max+pl1avg+bt2avg	801	47	15.5	1.4	0.662	0.12	3	1,17,18,29
	Grt1+ksp1max+pl1avg+bt2max	804	47	15.6	1.4	0.667	0.11	3	1,17,18,29
	Grt1+ksp1max+pl2max+bt1min	805	47	15.8	1.4	0.665	0.17	3	1,17,18,29
	Grt1+ksp1max+pl2max+bt1avg	801	47	15.7	1.4	0.661	0.14	2	1,16,17,18
	Grt1+ksp1max+pl2max+bt1max	794	46	15.5	1.4	0.655	0.15	3	1,17,18,21
	Grt1+ksp1max+pl2max+bt2min	802	47	15.7	1.4	0.662	0.19	3	1,16,17,18
	Grt1+ksp1max+pl2max+bt2avg	800	47	15.6	1.4	0.660	0.14	2	1,17,18,29
	Grt1+ksp1max+pl2max+bt2max	803	47	15.7	1.4	0.664	0.13	3	1,17,18,29

TABLE D4. AVERAGE P-T CALCULATIONS USING THE PROGRAM THERMOCALC v3.33 AND DEACREASING WATER ACTIVITY

Mineral Combination	Water Activity	Temp (˚C)	Error (˚C)	Pressure (kbar)	Error (kbar)	Error Correlation	Significance of Fit	Iterations	Reactions
D212B-Mafic Granulite	1	760	56	15.6	1.8	0.954	0.94	2	1,2,3,4
Grt1A+cpx1avg+pl1max+czo1avg	0.9	750	55	15.4	1.8	0.954	0.94	2	1,2,3,8
	0.8	743	54	15.3	1.7	0.953	0.92	2	1,2,3,8
	0.7	739	54	15.2	1.7	0.953	0.87	3	1,2,3,4
D213B-Intermediate Granulite	1	744	69	14.9	2.1	0.960	1.16	2	1,8,10,12
Grt1A+cpx1avg+pl1avg+czo1avg	0.9	735	70	14.7	2.2	0.96	1.2	3	1,4,8,12
	0.8	729	71	14.4	2.2	0.962	1.23	3	1,4,8,12
	0.7	723	74	14.3	2.3	0.962	1.29	3	1,4,8,12
D217A-Grt-Ky Gneiss	1	799	47	15.5	1.4	0.663	0.13	3	1,16,20,25
Grt1+Ksp1avg+Pl1avg+Bt1avg	0.9	790	46	15.3	1.3	0.658	0.17	3	1,16,18,25
	0.8	782	45	15.1	1.3	0.653	0.2	2	1,16,18,21
	0.7	775	43	14.8	1.3	0.649	0.24	3	16,18,25,28